UNIVERSITÀ
DEGLI STUDI
FIRENZE

DOTTORATO DI RICERCA IN
SCIENZE CHIMICHE

CICLO XXVII

COORDINATORE Prof. Andrea Goti

TOWARDS MICROROBOTICS: NEW LIQUID CRYSTALLINE ELASTOMER BASED PHOTOACTIVE MICROSTRUCTURES

Settore Scientifico Disciplinare CHIM/06

Dottorando
Daniele Martella

Tutore
Prof. Andrea Goti

Coordinatore
Prof. Andrea Goti

Anni 2012/2014

Summary

Preface and objectives

A robot is an automatically controlled, programmable machine able to replace a human work: it can modify the surrounding environment in response to an input command. Modern robots are usually electro-mechanical devices guided by a computer program or electronic circuits and they often resemble human or animal appearance and behavior. The limbs of animals or insects, typically based on rigid segments connected by joints with constrained range of motion, often serve as model for robotic elements.
Robotics has witnessed a great grown substantially until the 20th century due to the possibility of these machines to perform repetitive or dangerous tasks which humans prefer not to do or are unable to do due to size limitations. Moreover they can work in extreme conditions where humans could not survive such as in outer space or at the bottom of the sea. This branch of technology is currently dominated by devices having hard body construction largely made of metal structural elements. Robots have a broad impact on different types of industry like manufacturing, logistics, medicine, healthcare, military, agriculture and consumer product.[1]

Unfortunately, traditional robots are not suitable to handle fragile objects, from the ordinary (like fruit) to more important (like internal organs), and a new class of "soft robots" has been attracted researchers' attention. These structures, made by polymers or other soft materials, offer new model for manipulation of objects allowed by the continuous deformations permitted by the material.[1]

This thesis work is part of a research project in the Prof. Diederik Wiersma research group at the European Laboratory for non Linear Spectroscopy (LENS). The project concerns the development of microscopic structures able to perform robotic tasks entirely powered and controlled by light. It brings a lot of challenges both from the point of view of the physics involved as well as the chemistry needed to create the appropriate material. The moving idea is to create photonic microrobots of various kinds that can, for example, swim in liquids, walk or crawl, and when at destination perform specific tasks which could have different possible application areas. For example such robots could

[1] F. Ilievski, A. D Mazzeo, R. F. Sheperd, X. Chen, G. M. Whitesides, *Angew. Chem. Int. Ed.* **2011**, *20*, 18900.

be able to penetrate microscopic environments and perform tasks like sensing or sampling. Within the human body, one could envision also tasks as drug delivery, local modifications and repairs, and artificial functionalities on a microscopic scale. Light to drive them could be delivered by optical fibers or via the skin.

The two main aspects addressed in the project are the constituent material as well as the technique used for its microstructuring. The materials chosen for the fabrication are **Liquid Crystalline Elastomers** (**LCEs**), a type of shape-changing polymers that have attracted scientists and engineers for their ability to translate small molecular movement, triggered by an external stimulus, into large mechanical motion. Regarding the fabrication of microstructures, we chose the **Direct Laser Writing** (**DLW**), a technique based on a point-by-point polymerization induced by two photon absorption in the focus of a laser beam, where a tiny voxel is polymerized with high precision. Direct Laser Writing allows a rapid, cheap and flexible fabrication of microscale objects with nanoscale precision.

The objectives of this thesis are summarized below:

- the synthesis of suitable molecules for the preparation of different LCEs and the optimization of their mechanical properties;
- the examination of different architectures for LC networks, starting from synthetic approaches already used by other research groups but also extending to new ones;
- the determination of the real possibility to pattern LCEs in the microscale by DLW also studying the best process conditions and material for this type of fabrication;
- the application of the knowledge from the previous points to build truly photoactive robotic microactuators.

Chapter 1 reports a brief introduction on Liquid Crystalline Elastomers describing the material structures and properties. Relevant examples of LCE preparation, selected from literature, are reported and, in the last part, DLW main features are described.
Chapter 2 shows the synthesis and the characterizations of different molecules which allow to prepare LCEs by acrylate free radical polymerization. This small library of LC components is mandatory to create new materials and to study

the influence of different molecular parameters on the liquid crystalline and mechanical properties of the final polymeric network.

Chapter 3 presents some example of LCE microstructures created by DLW, showing also how it is possible to control the alignment in the microscale. Deformation of the LCE microstructures by irradiation is shown. Moreover, examples of different mixtures are studied to try the optimization of the material.

Chapter 4 reports the application of thiol-yne click chemistry to obtain LCEs with different architecture. Such materials, which incorporate part of mesogens in the main-chain of the polymer, are able to undergo bigger deformation with respect to the acrylate based one. The work described in the chapter was realized at the University of Zaragoza in the Liquid Crystals and Polymers group, under the supervision of Dr. Luis Oriol and Dr. Milagros Piñol.

Chapter 1

Introduction

1.1 Liquid Crystals: general concepts

Liquid Crystals (LCs) are partially ordered, anisotropic fluids, thermodynamically located between the three-dimensional ordered solid state crystal and the isotropic liquid (**Figure 1**).[2] Like crystals, a liquid crystal exhibits anisotropy in its optical, electrical and magnetic properties, however maintaining many of the mechanical properties of liquids as a high fluidity and formation and coalescence of droplets. The main feature of LCs is the presence of a long range orientational order of molecules and sometimes of one- or two- dimensional long-range positional orders.[3]

Figure 1 States of matter

Liquid crystals can be catalogued into two main categories.

The lyotropic LCs are two or more component systems in which amphiphilic compounds, with a hydrophilic polar head and a hydrophobic non polar tail, are dissolved in a solvent (typically water). Well-known examples of lyotropic LCs are solutions of soap and various related detergents.

The thermotropic LCs are organic molecules (mesogens) that exhibit a phase transition into a liquid crystalline phase (mesophase) at a certain temperature, ranging between the melting temperature (T_m) and the clearing temperature ($T_{LC\text{-}I}$), when it transforms into an isotropic liquid. Mesogenic molecules usually have an anisotropic shape, either elongated or disk-like, with a central rigid core and a flexible tail. The rod-like molecules form *calamitic* LCs while the

[2] I. Dierking, *Textures of Liquid Crystals*, Wiley-VCH Verlag GmbH & Co **2003**.
[3] J. Collings, M. Hirde, *Introduction to Liquid Crystals. Chemistry and Physics*, Taylor and Francis Ltd. London **1997**.

disk-like ones form *discotic* LCs. Banana-shape molecules are another example of building block able to form more exotic LC phases (**Figure 2**).[4]

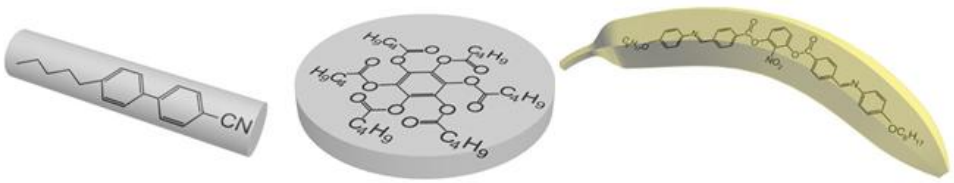

Figure 2 Structural examples of thermotropic mesogens: rod-like, disk-like and banana-shape molecules.

Regarding the work of this thesis, we focused our attention on *calamitic* LCs: considerations and results described below are all referred to this type of compounds.

The most common mesophases are shown in **Figure 3**. Among these the nematic phase (**N**) is the less ordered and presents only an orientational order: the long molecular axes are preferentially oriented in one direction, defined as director. Nematic LCs possess a relative low viscosity so they can deform under even small external forces. In smectic phases molecules lay parallel one to the others and they are arranged in layers with the long axis perpendicular (smectic A phase, **SmA**) or tilted (smectic C phase, **SmC**) to the layer plane. Many variations of smectic phases have been identified.

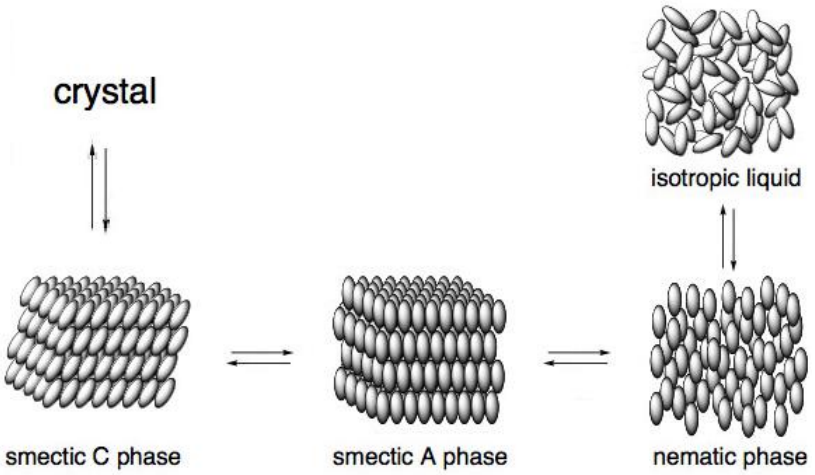

Figure 3 Example of calamitic mesophases.

[4] J. W. Goodby, J. Collings, T. Kato, C. Tschierske, H. F Gleeson, P. Raynes, *Handbook of Liquid Crystals: 8 Volume Set*, Second Edition, Wiley-VCH Verlag GmbH &Co. **2014**.

Chiral mesogens can give rise to more complex chiral phases as the cholesteric (or chiral nematic, **N***) one (**Figure 4**), which exhibits a twisting of the molecules perpendicular to the director, with the molecular axis parallel to the director. The finite twist angle between adjacent molecules is due to their asymmetric packing which results in a long-range chiral order. This phase is characterised by the chiral pitch defined as the distance over which the molecules undergo a full 360° twist.

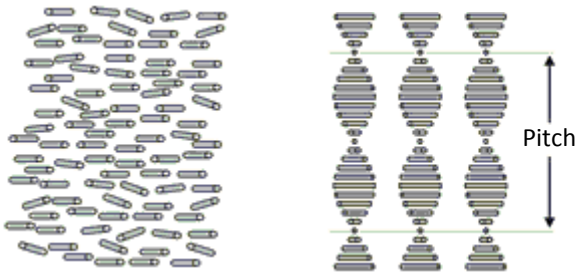

Figure 4 Comparison between nematic and cholesteric phases.

A thermotropic phase is defined as enantiotropic or monotropic referring to its thermal stability with respect to the crystalline phase. An enatiotropic phase is thermodynamically stable forms by heating the crystalline material above T_m or by cooling the isotropic liquid. A monotropic phase is a metastable phase that occurs only by cooling the isotropic liquid below T_m and is due to hysteresis in the crystallization process.[4]

Liquid crystals are widely used in different areas of science and engineering. Their most common application is for display devices exploiting the different optical properties of selected mesophases in the presence or absence of an electric field. A twisted liquid crystalline layer is placed between two crossed polarizer obtaining a transparent device: the light passes through the first polarizer and is reoriented by the LC layer allowing its transmission through the second polarizer. By application of an electric field, the LC layer loses gradually its twisting and the light polarized by the first polarizer is not reoriented: the device loses the transparency for the absorption of light on the second polarizer. This process results in the switching on or off of the pixels.
Chiral liquid crystalline phases reflect light with a wavelength equal to the pitch which is strongly dependent from the temperature. Exploiting such property, thermometers for aquariums and pools as well as thermometers for

infants or industrial sensors were developed: just looking at the color of the devices it is possible to accurately determine the temperature.
Lasers can use liquid crystals as lasing medium: the emission of the photonic bandgap created by the periodic dielectric structure of the LC gives a low-threshold high-output device with stable monochromatic emission. These examples are only a small part of a world of materials that is still being developed to provide effective solutions to different problems.

The easiest way to study the phase transitions of a compound is the Differential Scanning Calorimetry (DSC) that measures the heat capacity of a material as function of temperature with reference to a standard. However, this technique cannot identify the type of liquid crystal phase, the level of enthalpy change gives some information about the degree of molecular order within the phase. Typically, a melting transition from a crystalline solid (**Cr**) to LC phase or isotropic phase generates an enthalpy change of around 30 to 50 $kJmol^{-1}$. Transitions between different **LC** phases or between **LC** and **I** phase are characterized by much smaller enthalpy changes. Typically, the **SmA** to **I** transition involves an enthalpy changes of 4 to 6 $kJmol^{-1}$ and **N** to **I** transition involves only 1-2 $kJmol^{-1}$. Transition energy between different liquid crystal phases can be extremely small: the **SmC** to **SmA** transition, for example, is generally difficult to be detected by DSC because the enthalpy change involved is less than 300 $Jmol^{-1}$.[3]
The identification of the type of mesophase requires the observation of the sample with the Polarized Optical Microscopy (POM): the optical texture which appears by observing an anisotropic material between two polarizers, crossed at 90° to each other, gives information relating to the arrangement of the molecules within the medium. The texture depends on the structural defects of the LC phase and it provides a valuable diagnostic tool for the identification of mesophase type.[3]

An example of application of these techniques is described below. The compound shown in **Figure 5** was synthesized and characterized during this thesis. The DSC trace shows an enantiotropic LC phase: the material melts in a mesophase at 84 °C that is present up to 157 °C (**Figure 5a**). The transition to the isotropic phase involves an enthalpy change of 1.8 $kJmol^{-1}$, typical of a **N** phase. The nature of the mesophase is confirmed by the Schlieren texture

observed by POM (**Figure 5b**). During the cooling stage the crystalline phase appears at a lower temperature (54 °C) due to supercooling of the sample.

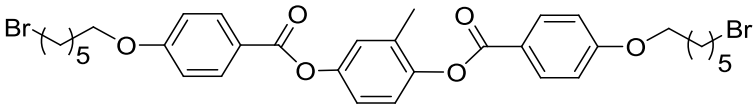

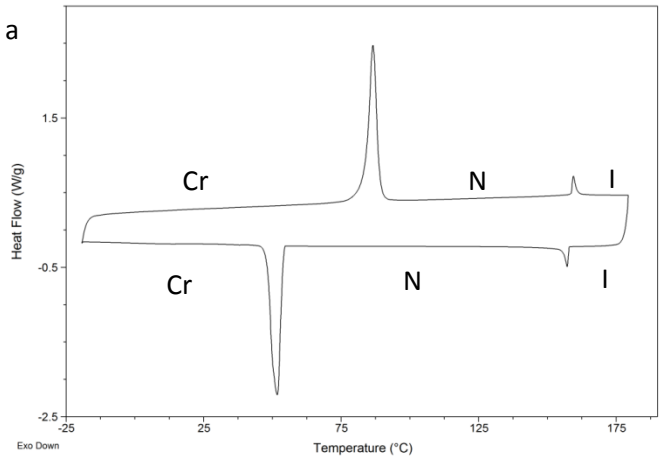

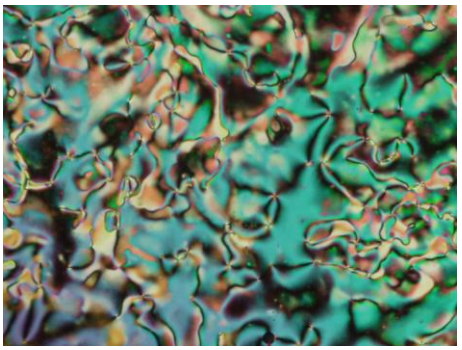

Figure 5 Example of study of LC properties. a) DSC traces corresponding to the second cycle of heating and cooling; b) POM image of the mesophase at 140 °C on cooling.

1.2 Liquid Crystalline Elastomers: definition and preparation

Liquid Crystalline Elastomers (LCEs) are unique materials that combine the entropy elasticity of polymeric networks (elastomers) with the ability of liquid crystals to self-organize into liquid crystalline phases.[5]

They are among the best candidates for smart artificial materials, in particular for their capability to perform a reversible shape-change in response to external stimuli like temperature, electric field, or light.[6,7,8]

The concept of LCEs was firstly exposed by de Gennes in 1975. He recognized that the interplay between the liquid crystalline order and the macromolecular network structure generates new physical properties that also resemble those of some biological systems.[9] Like muscles, able to convert chemical energy into mechanical motion, some soft materials can accept different types of energy and convert them in several ways. Among artificial muscles, LCEs may present a distortion, as a contraction, generated by the liquid crystalline to isotropic phase transition. A big impulse in the study of LCEs followed the Küpfer and Finkelmann pioneering method of preparation of a monodomain LCE in 1991.[10]

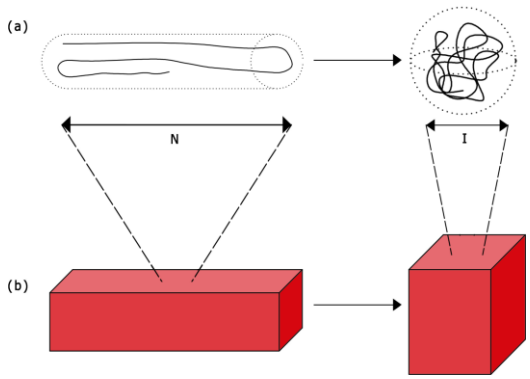

Figure 6 Polymer conformations in N and I phases (a) and macroscopic change of a sample during the N to I phase transition (b).

[5] C. Ohm, M. Brehmer, R. Zentel, *Adv. Mater.* **2010**, *22*, 3366 and reference cited herein.
[6] H. Finkelmann, H.-J. Kock, G. Rehage, *Makromol. Chem. Rapid Commun.* **1981**, *2*, 317.
[7] R. Kishi, Y. Suzuki, H. Ichijo, O. Hirasa, *Chem. Lett.* **1994**, 2257.
[8] M. Li, P. Keller, B. Li, X. Wang, M. Brunet, *Adv. Mater.* **2003**, *15*,569.
[9] P. G. de Gennes, *C. R. Hebd. Séances Acad. Sci. B* **1975**, *281*, 101.
[10] J. Küpfer, H. Finkelmann, *Macromol. Chem. Rapid Commun.* **1991**, *12*, 717.

At a certain temperature, a LCE exhibits LC behavior and when heated above its LC to isotropic phase transition temperature (T_{LC-I}) it shows a contraction along the direction of alignment of the mesogens and an expansion in the perpendicular direction. On cooling below its T_{LC-I}, a LCE reverts to its initial shape (**Figure 6**). de Gennes' theory predicts that the shape-change is brought by changing the alignment of mesogens. Due to the coupling with the LC parts, the polymer chains present an anisotropic conformation but if the LC order is lost, for example by heating above T_{LC-I}, the isotropic chain conformation is adopted and the sample as a whole has to change its shape.[5]

LC polymers can be built by chemically linking mesogenic groups to polymer chains. Different structures can be obtained depending on how the mesogens are linked to the backbone: either the mesogens can be attached with a flexible spacer to the network (side-chain polymers, **Figure 7a** and **b**) or directly linked together within the chain (main-chain polymers, **Figure 7c** and **d**). Another structural modification is given connecting the mesogenic groups in different geometries: for example rod-like mesogens could be attached via their long axis ("end-on" type polymers, **Figure 7a** and **c**) or via their short axis ("side-on" type polymers, **Figure 7b** and **d**).[11]

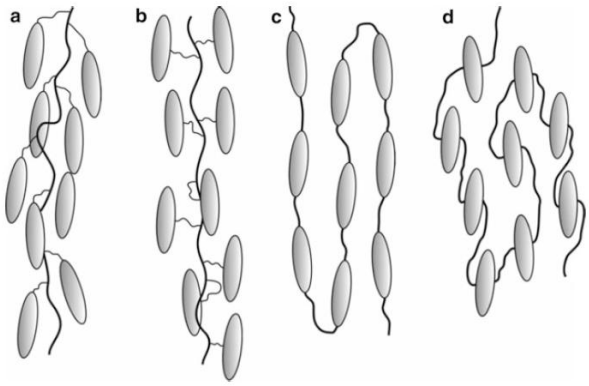

Figure 7 Architectures for liquid crystalline elastomers.

Main-chain LCEs have generally enhanced mechanical and optical properties compared to side-chain LCEs due to the stronger coupling of the mesogenic units with the polymer backbone;[5] however, the former are more difficult to be prepared, and therefore less studied and developed for applications.

[11] F. Brömmel, D. Kramer, H. Finkelmann, *Adv. Polym. Sci.* **2012**, *250*, 1.

Preparation of LCEs requires two synthetic tasks: the build-up of the liquid crystalline polymer and the crosslinking of the different chains.
A first approach, commonly used to prepare side-chain elastomers, consists in the formation of the network in a single step by a free radical polymerization. A LC monomer, functionalized with a polymerizable unit, is mixed with a multifunctional crosslinker, which may or may not be liquid crystalline, and then polymerized after the alignment in nematic phase. This method has the advantage that the monomeric materials can be oriented much easier than a liquid crystalline polymer allowing the use of many orientation techniques known from low-molecular-weight LCs. Acrylates and metacrylates monomers are the most used as starting material (**Scheme 1**);[12] however, other polymerizable units, as vinyl or allyl carbonates groups, were studied for this aim.[13]

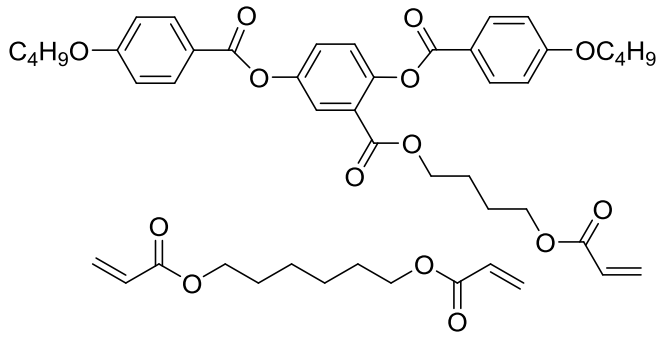

Scheme 1 Example of monomers for LCE preparation with radical polymerization.

In a second strategy, a preformed LC polymer, containing proper additional functional groups, is crosslinked using a multifunctional crosslinker that reacts selectively with them. Reactions used in this field are the coupling of isocyanates to alcohols,[14] click chemistry of azides to acetylenes[15] or coupling between active esters and amines.[16]

Another synthesis was introduced by Komp et al., who attached a photo-crosslinkable benzophenone side-group to the polymer backbone: this group can attach any weak C-H σ-bond after UV irradiation in an H-abstraction

[12] D. L. Thomsen III, P. Keller, J. Naciri, R. Pink, H. Jeon, D. Shenoy, B. R. Ratna, *Macromolecules* **2001**, *34*, 5868.
[13] Z. L. Wu, A. Buguin, H. Yang, J.-M. Taulemesse, N. Le Moigne, A. Bergeret, X. Wang, P. Keller, *Adv. Funct. Mater.* **2013**, *23*, 3070.

mechanism (**Scheme 2**) allowing the crosslinking to an aliphatic part of the polymer.[17]

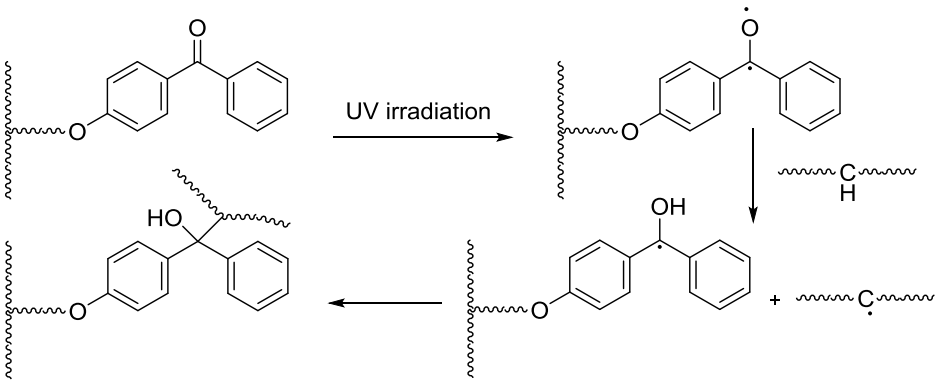

Scheme 2 Mechanism of photo-crosslinking using the benzophenone.

To prepare the suitable linear polymers, a polycondensation of mesogenic diols and malonic acid esters can be used (**Scheme 3**): the ester component is partially functionalized with a benzophenone derivative, which allowed the subsequent crosslinking, by UV irradiation.[18]

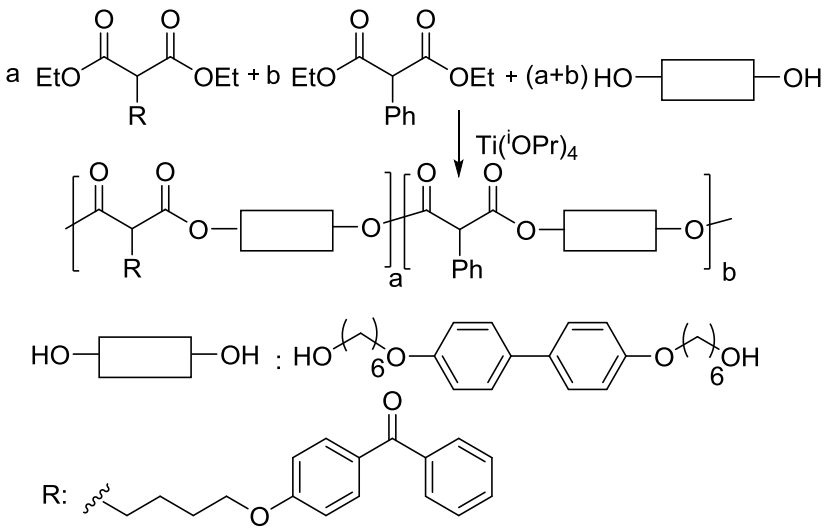

Scheme 3 Synthesis of a linear copolymer containing benzophenone moieties.

---

[14] J. Naciri, A. Srinivasan, H. Jeon, N. Nikolov, P. Keller, B. Ratna, *Macromolecules* **2003**, *36*, 8499.
[15] Y. Xia, R. Verduzco, R, H. Grubbs, J. A. Kornfield, *J. Am. Chem. Soc.* **2008**, *130*, 1735.
[16] X. J. Li, R. B. Wen, Y. Zhang, L. R. Zhu, B. L. Zhang, H. Q. Zhang, *J. Mater. Chem.* **2009**, *19*, 236.
[17] A. Komp, J. Rühe, H. Finkelmann, *Macromol. Rapid. Commun.* **2005**, *26*, 813.
[18] P. Beyer, L. Braun, R. Zentel, *Macromol. Chem. Phys.* **2007**, *208*, 2439.

Finkelmann and co-workers developed a synthesis based on silicone chemistry exploiting the platinum-catalyzed addition of terminal C=C double bonds to Si-H bonds to attach mesogens and crosslink different chains to a polyhydrosiloxane backbone (**Scheme 4**).[10]

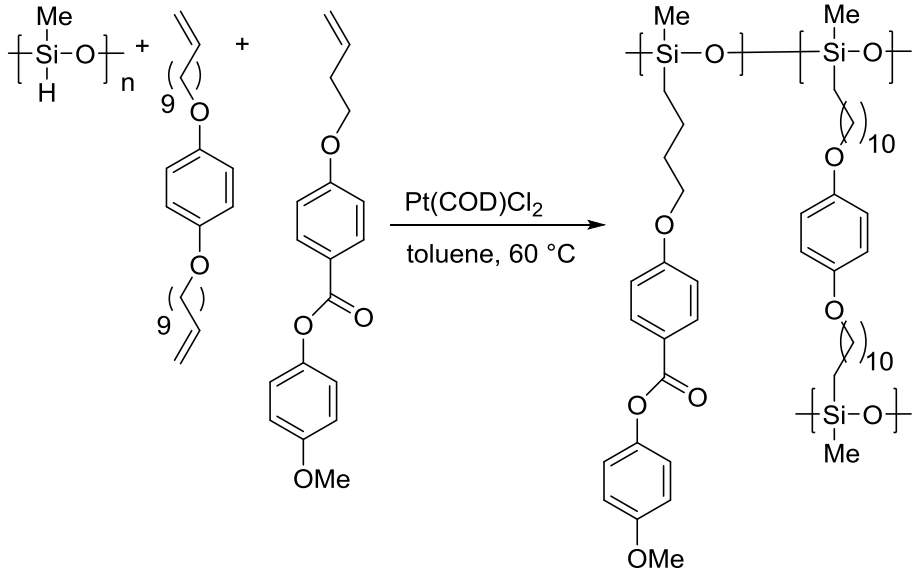

Scheme 4 Synthesis of a LCE by using the Pt-catalyzed hydrosilylation reaction.

A modification of this method consists in the use of a monomer functionalised with a vinyl group and a crosslinker with both vinyl and methacryloyl groups: kinetic studies show that vinyl group reacts two order of magnitude faster than the methacrylate one, allowing a crosslinking process in two steps. This concept was used in the preparation of highly oriented samples: after reaction of the vinyl groups, the weakly crosslinked polymer was mechanically stretched uniaxially and then the second-slower-crosslinking reaction is driven to completion obtaining a monodomain LCE.

Silicone chemistry results useful also to prepare main-chain LCEs: a divinylic monomer is reacted with a mixture of 1,1,3,3-tetramethyldisiloxane and 2,4,6,8-tetramethylcyclotetrasiloxane in a poly-condensation reaction. The disiloxane acts as chain extender while the tetrasiloxane allows the crosslinking of different chains.[19]

[19] B. Donnio, H. Wermter, H. Finkelmann, *Macromolecules* **2000**, *33*, 7724.

1.3 Photoactive Liquid Crystalline Elastomers

Among all possible external stimuli able to modulate the LC behavior, light enables a rapid punctual wireless control of the material properties and it is a clean, cheap and environmental friendly energy source. Different strategies could be used to obtain photoactive LCEs.

A first approach concerns the preparation of composite materials through the doping of LCEs with structures able to absorb light and to transform it into thermal energy. They act as nanoscale heaters able to induce the N to I transition. Chen et al. reported that carbon nanotube-LCE composite films exhibit a significant and reversible contraction upon IR irradiation.[20] The same authors prepared films doped with a commercial near IR dye (Dye 1002, **Scheme 5**) and laser irradiation at 980 nm successfully allowed the contraction of the structures. Using different types of near IR dyes it is possible to select the desired IR wavelength for the actuation of the structure. After switching off the laser irradiation, the film returns in the initial position. To prepare a composite material, a solution of carbon nanotubes or dyes was added to the monomer mixture, concentrated and then used for the film preparation.[21]

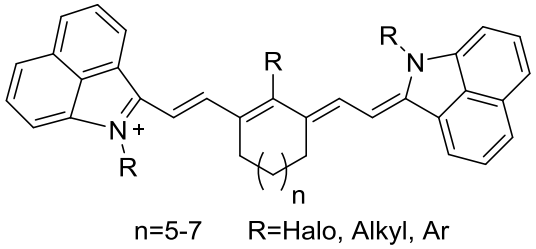

Scheme 5 Structure of Dye 1002.

Infiltration of metallic nanoparticles can also be used to obtain a light sensitive material: Smalyukh and Keller prepared some cylindrical LCE micropillars which where infiltrated with gold nanocrystals able to mediate the energy transfer from laser light to heat in a submicrometer region of the micropillars. Different 3D deformations os the structures were possible by scanning in different way the laser spot. The wavelength of the laser used (1064 nm) was far from the gold nanospheres absorption peak (530 nm) suggesting that two-photon

[20] L. Yang, K. Setyowati, A. Li, S. Gong, J. Chen, *Adv. Mater.* **2008**, *20*, 2271.
[21] M. Moua, R. R. Kohlmeyer, J. Chen, *Angew. Chem. Int. Ed.* **2013**, *52*, 1.

absorption process and particle aggregates play an important role in the actuation of LCEs.[22]

A different approach is based on the use of photocromic molecules, such as azobenzenes, stilbenes, spiropyrans and fulgides, to trigger the N to I phase transition. When a small amount of these molecules is incorporated and the resulting guest/host mixture is irradiated to cause photochemical reaction of the photocromic guest molecules, a LC to I transition can be induced isothermally.[23]

Among these molecules, azobenzenes are the most used due to the possibility of a totally and reversible isomerization process between their two geometric isomers: both isomers can be switched back and forward with light of appropriate wavelength.

The *trans* isomer is 10–12 Kcalmol^{-1} more stable than *cis*; consequently, in the dark at the equilibrium, the *trans* is the dominant isomer (99.99%). The *trans* conformation is near planar and has a dipole moment close to zero, while the *cis* conformation presents an angular geometry and a dipole moment. The isomerization process involves a decrease in the distance between the two carbon atoms in position 4 of the aromatic rings, from 9.0 Å in the *trans* to 5.5 Å in the *cis* isomer (**Figure 8a**).[24]

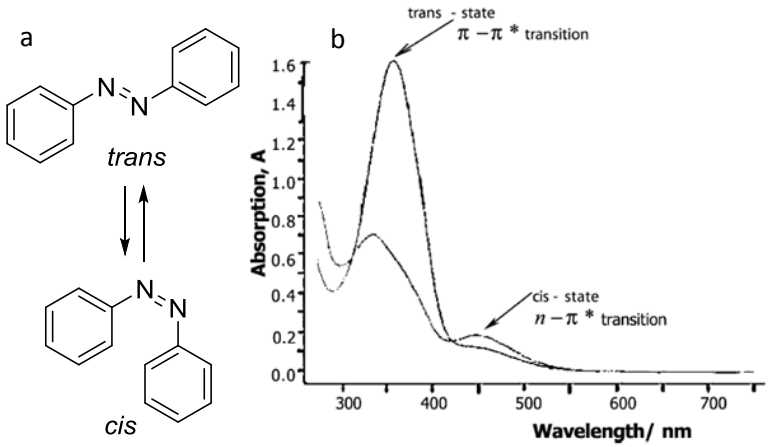

Figure 8 Structure (a) and absorption spectra (b) of *trans* and *cis* azobenzene.

[22] Y. Sun, J. S. Evans, T. Lee, B. Senyuk, P. Keller, S. He, I. I. Smalyukh, *Appl. Phys. Lett.* **2012**, *100*, 241901.
[23] T. Ikeda, *J. Mater. Chem.* **2003**, *13*, 2037.
[24] A. A. Beharry, G. A, Woolley, *Chem. Soc. Rev.* **2011**, *40*, 4422.

The absorption spectra of the two isomers are distinct but overlapping (**Figure 8b**): *trans* azobenzene shows a weak n–π* band near 440 nm and a strong π-π* transition near 320 nm, while the *cis* azobenzene has a stronger n–π* band also near 440 nm and two weaker bands in the UV region.
Exploiting the differences in the absorption properties, the isomerization process could be addressed with UV light, for *trans* to *cis* conversion, and visible light, for the reverse process. Moreover, *cis* isomer can also relax back spontaneously to the thermodynamically more stable *trans* form in the dark isothermally. The two photochemical conversions occur in the scale of picoseconds, while the thermal relaxation is much slower (milliseconds to day).[25] The substituents on the aromatic ring can modify strongly both the absorption spectrum and the time life of the *cis* state.

The photochemical phase transition behaviour of mixtures of azobenzenes and nematic LCs has been systematically explored. The *trans* form of azobenzene has a rod-like shape which can stabilize the LC phase, whereas its *cis* form tends to destabilize the phase order of the mixture. As a result, the LC to I phase transition temperature of the mixture with the *cis* form (T_{cc}) is much lower than that with the *trans* azobenzenes (T_{ct}) (**Figure 9**).[26]

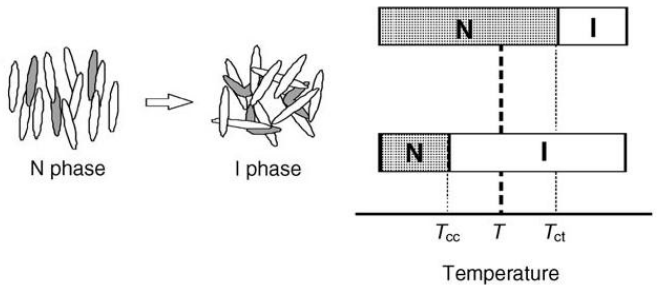

Figure 9 Phase diagram of the photochemical phase transition of a LC system doped with azobenzenes.

If the temperature of the sample (T) is set at a temperature between T_{ct} and T_{cc} and the sample is irradiated to cause the *trans* to *cis* isomerization of the azobenzene guest molecules, the LC to I phase transition of the sample is induced.
In the field of LCE, this concept has been firstly applied by Finkelmann and co-workers who prepared nematic LCEs with polysiloxane main chain and an

[25] E. Merino, M. Ribagorda, *Beilstein J. Org.Chem*. **2012**, *8*, 1071.
[26] C. H. Legge, G. R. Mitchell, *J. Phys. D: Appl. Phys.* **1992**, *25*, 492.

azobenzene chromophore as crosslinker: under exposure to UV light, the structures were contracted of 20% of their length.[27]
Photopolymerization methods present some problems due to the azobenzene isomerization during the irradiation: an unsuccessful initiation and absence or defects in the alignment of the mixture could be observed. Keller and co-workers synthesized a side-on elastomer by photopolymerization with a near-infrared photoiniatior avoiding the previously mentioned drawbacks.[28]

Several parameters affected the contraction in azobenzene containing LCEs as the photochemical properties of the chromophore, its percentage and location in the polymeric structure (in the side chain or in the crosslinker). Ikeda and co-workers studied all these parameters demonstrating different three-dimensional movements of LCE films.[29]
Bending of a film could be more advantageous to construct artificial hands and robots with respect to the two-dimensional movements of contraction and expansion. UV irradiation of a crosslinked LC polymer composed only by azobenzene mesogens induces the bending of the film (**Figure 10**).[30]

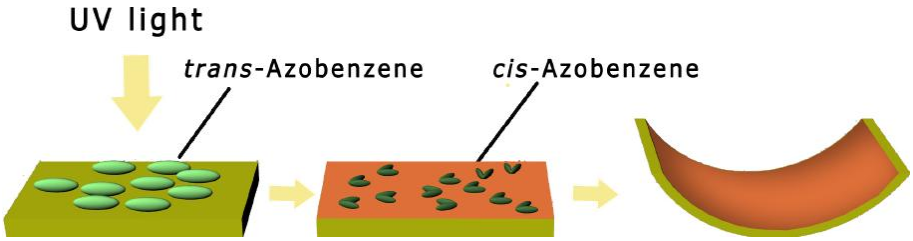

Figure 10 Mechanism of the photoinduced bending of a LCE film.

Due to the large extinction coefficient of azobenzenes, during the irradiation more than 99% of the incident photons are absorbed within 1 μm surface, and the *trans to cis* isomerization occurs only in this region. As the thickness of the film is 20 μm the contraction was generated only on the surface layer causing the bending of the film toward the light source. Irradiation of the bent film with visible light causes the *cis to trans* isomerisation with the return to its initial flat shape.

[27] H. Finkelmann, E. Nishikawa, G. G. Pereira, M. Warner, *Phys. Rev. Lett.* **2001**, *87*, 015501.
[28] M.-H Li, P. Keller, B. Li, X. Wang, M. Brunet, *Adv. Mater.* **2003**, *15*, 569.
[29] H. Yu, T. ikeda, *Adv. Mater.* **2011**, *23*, 2149.
[30] T. Ikeda, M. Nakano, Y. Yu, O. Tzutzumi, A. Kanazawa, *Adv. Mater.* **2005**, *15*, 201.

1.4 Liquid Crystalline Elastomers for robotic applications

Combining LCEs with different materials and exploring new fabrication techniques allow the development of many devices, attracting the interest of researchers to create structures able to actuate mechanical work without using of any batteries or electric wire.

A model of motor was prepared using a plastic belt of a LCE film laminated with polyethylene on a homemade pulley system (**Figure 11**). The device converts the energy of the simultaneous irradiation with UV and visible light in different parts of the belt into a continuous rotation. A contraction force, acting on the right pulley by exposure to UV light, and an expansion force, on the left pulley irradiated with visible light, cooperate and drive a counterclockwise rotation of the belt. This rotation brings new parts of LCE film to be exposed to light, which enables the motor to rotate continuously.[31]

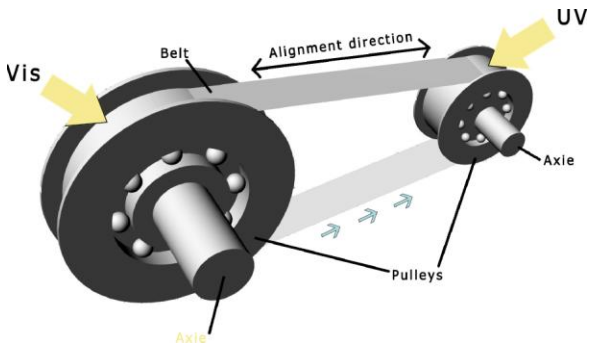

Figure 11 Example of light driven plastic motor.

Laminated films can be used also to fabricate other types of devices in arbitrary shapes and sizes. The motion of a robotic arm is shown in **Figure 12**. A plastic film without photoresponsive properties was only partially covered with a crosslinked liquid crystalline polymer (CLCP); controlling the irradiation position and intensity of the light, it is possible to drive this composite film in a chosen manner, which enables to use the system to manipulate object just by light irradiation.[32]

[31] M. Yamada, M. Kondo, J. Mamiya, Y. Yu, M. Kinoshita, C. J. Barrett, T. Ikeda, *Angew. Chem.* **2008**, *120*, 5064.

[32] M. Yamada, M. Kondo, R. Miyasato, Y. Naka, J. Mamiya, M. Kinoshita, A. Shishido, Y. L. Yu, C. J. Barrett, T. Ikeda, *J. Mater.Chem.* **2009** , *19* , 60 .

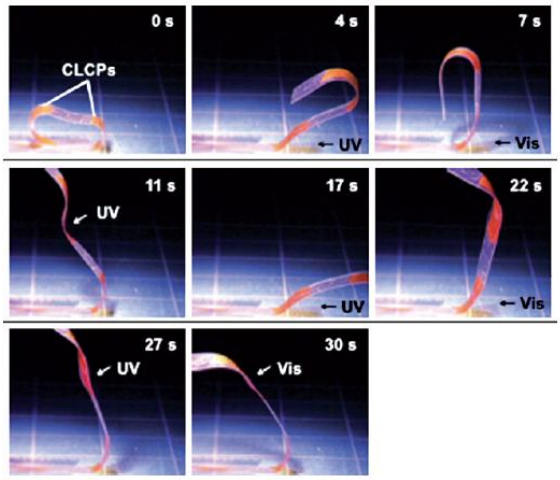

Figure 12 Movement of a flexible robotic arm by irradiation with UV and visible light.

More complex bending movements were obtained by Ikeda et al. by means of the selective absorption of linearly polarized light in a polydomain LCE film. Azobenzenes have an absorption transition moment nearly parallel to its long molecular axis: only those with their transition moments parallel to the polarization direction of light absorb incident photons, undergoing the *trans to cis* isomerization. This means that only determined microdomains give a contraction of surface layers and the film bent toward the irradiation source in a direction parallel to the light polarization.[33]

Furthermore, LCEs have recently attracted attention for application in microfluidics and microrobotics and recent examples include work on artificial cilia,[34] fibers,[35] surface topologies,[36] and switchable microarrays.[37] Turning to sub-millimeter dimensions or even further, calls for new fabrication technologies, capable of simple, repeatable structuring of the LCE media in terms of the overall shape as well as the molecular orientation within the object volume.

[33] Y. Yanlei, M. Nakano, T. Ikeda, *Nature* **2003**, *425*, 145.
[34] C. L. van Oosten, C. W. M. Bastiaansen, D. J. Broer, *Nat. Mater.* **2009**, 8, 677.
[35] T. Yoshino, M. Kondo, J. Mamiya, M. Kinoshita, Y. Yu, T. Ikeda, *Adv Mater.* **2010**, *22*, 1361.
[36] D. Liu, C. W. M. Bastiaansen, J. M. J. den Toonder, D. J. Broer, *Macromolecules* **2012**, *45*, 8005 .
[37] Z. Yan, X. Ji, W. Wu, J. Wei, Y. Yu, *Macromol. Rapid Commun.* **2012**, *33*, 1362 .

1.5 Direct Laser Writing

The term stereolithography historically refers to the technology of creating 3D objects from computer-aided design (CAD) pattern by polymerization of a resin layer by layer: by scanning the laser beam, one slice of the 3D structure is created according to the desired pattern and then a thin-layer of liquid resin is added and a new pattern slice is created. This technique, originally developed by Kodama in 1981 using UV light, has been also applied by Ikuta for the fabrication of microstructures as 3D micro coil of 70 µm diameter with 10 µm resolution.[38] However, the obtained resolution does not satisfy the modern requirements for device miniaturization. In 1997, Maruo et al. developed a two photon polymerization system opening the way to develop this technique for micro and nanofabrication.[39] Rather than the use of the UV light, photoresist was polymerized by the two-photon absorption at longer wavelength, usually in the red-infrared (IR) spectral region.

Two-photon absorption is the simultaneous absorption of two photons of identical or different frequencies in order to excite a molecule from one state (usually the ground state) to a higher energy electronic state. This process is mediated by a virtual state, which has an extremely short lifetime (several femtoseconds), and two-photon absorption occurs only if a second photon is absorbed before the decay of this virtual state (**Figure 13**).[40]

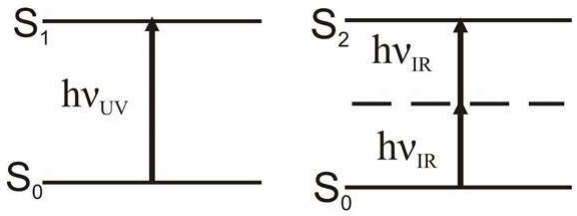

Figure 13 One-photon and two-photon absorption energy levels.

In principle, using the two-photon absorption is possible to activate the same reactions induced by the linear absorption of UV light: two-photon polymerization was already reported in 1965 by Pao and Rentzepis by focusing a 694 nm laser into a sample of styrene. After developing in methanol, the

[38] S. Maruo, J. T. Fourkas, *Laser & Photon. Rev.* **2008**, *2*, 100.
[39] S. Maruo, O. Nakamura, S. Kawata, *Opt.Lett.* **1997**, *22*, 132.
[40] H.-Bo Sun, S. Kawata, APS **2004**, *170*, 169.

solid precipitate was extracted and confirmed to be polystyrene through IR absorption studies.[41]

The system designede by Maruo and co-workers is the first example of direct laser writing: the laser was directly focused inside a liquid resin droplet and the two-photon absorption occurred only around the focal point volume, affording the polymerization of the material. This technology eliminates the requirement for the sequentially addition of liquid film and it does not require any mask or mold allowing a rapid turnaround time for fabrication and modification of structures design in an easy way. Denk et al. applied the two-photon excitation to laser scanning microscopes[42] and several modification of their experimental setup have been developed. One example of modern direct laser writing system is represented by the workstation Photonic Professional of Nanoscribe GmbH currently available in our laboratories. A scheme of the system is shown in **Figure 14**.

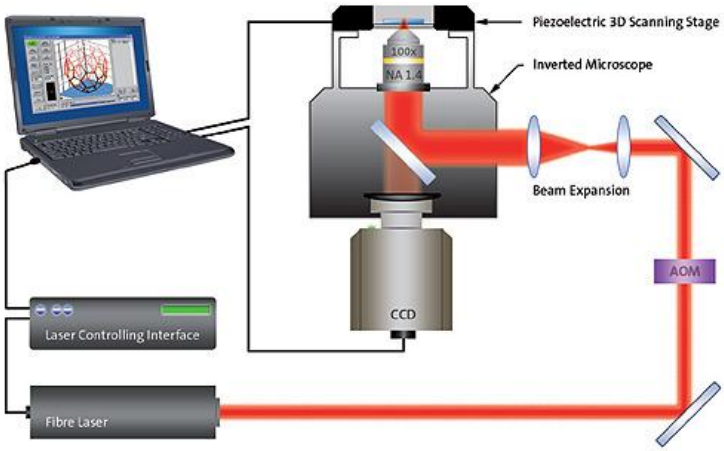

Figure 14 Scheme of a Direct Laser Writing fabrication system.

By tightly focusing the light of the laser using a microscopic objective lens, the intensity within the focal volume is sufficiently high to expose the photoresist by multiphoton absorption. This absorption initiates the polymerization within a small volumetric pixel (a "voxel") that is typically ellipsoidal in shape and represents the basic building block for the fabrication of 3D structures. Subsequently, the laser focal spot is scanned by moving the sample in all three

[41] Y. H. Pao, P. M. Rentzepis, *Appl. Phys. Lett.* **1965**, *6*, 93.
[42] W. Denk, J. H. Strickler, W. W. Webb, *Science* **1990**, *248*, 843.

dimensions by a piezo electric translation stage, thus creating point by point the computer designed 3D structure. The laser wavelength is chosen so that the photoresist is perfectly transparent, as the one-photon energy lies well below the two-photon absorption edge of the material, allowing the penetration of light deeply into the monomer mixture. At the end of the writing process, the unpolymerized remainder of the mixture is washed away by means of an organic solvent, leaving only the newly fabricated microstructures on the substrate (**Figure 15**).

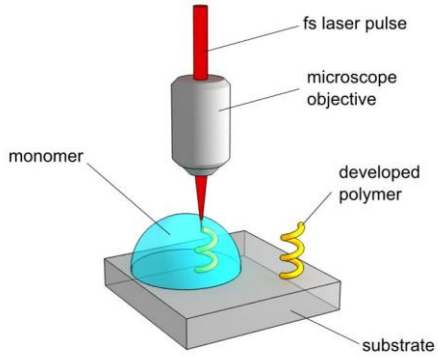

Figure 15 Scheme of the writing process.

Using a microscope objective to focalise the laser, the volumes activated by one-photon and two-photon absorption are very different in size (**Figure 16**) with a large improvement of the resolution: the volume of two-photon absorption requires a high intensity of light and it is confined to occur only in a small 3D volume around the close vicinity of the laser focus, less than the cubic wavelength. This is due to the very low probability of two-photon absorption, in which the cross section is about 31 orders of magnitude lower than the one-photon absorption cross section. Moreover, the two-photon absorption differs from linear absorption in that the strength of absorption depends on the square of the light intensity, as usual for nonlinear optical process.

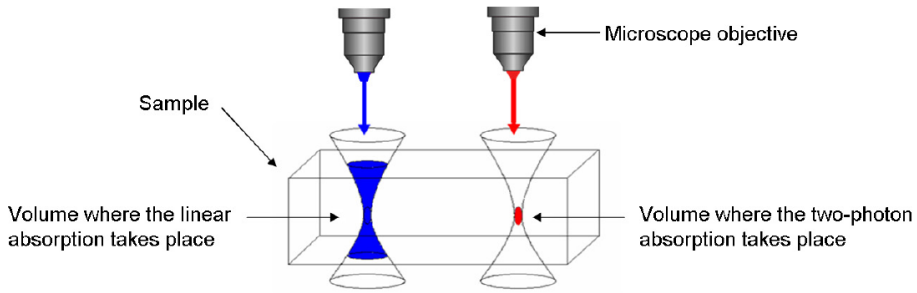

Figure 16 Comparison between one-photon and two-photon absorption.

For a given objective, its numerical aperture (NA) and the laser wavelength are crucial to determine the resolution of the fabrication process. NA is an

expression related to the maximum angle that light rays are collected from the object plane (for imaging) or the maximum angle that a laser is converged onto the focal spot (for excitation). Choosing large NA optics is essential to obtain a high fabrication resolution due to the fact that the voxel depends on 1/(NA).[40] The use of laser with shorter wavelength increases the resolution with both a proportionally reduction of the diffraction-limit focal spot size and a more efficient two-photon absorption. Nowadays, laser technology provides light sources with pulse duration of less than 5 fs, the wavelengths cover a region from a few nm in the XUV to the far IR and pulse energies reach up to 10^4 J.

Regarding the materials used for direct laser writing, initially commercially available photoresists based on urethane acrylates and epoxy groups were employed.[43] Afterwards, the increasing interest for different applications moved the research to new materials. For photonic applications, smooth 3D microstructures, like waveguides and photonic crystals, have been prepared using inorganic-organic hybrid polymers[44] and others hybrid materials containing metal ions.[45] By using two-photon initiated hydrosilylation and radical-initiated cross-linking, polydimethylsiloxane has been used to produce flexible microparts useful for microfluidic circuits and microcontact printing. Also different type of biological materials, as proteins and collagens, have been explored: protein structures, containing bovine serum albumin, thanks to their porosity are promising drug delivery devices,[46] while collagen based materials might be used for tissue engineering.[47]

[43] S. Kawata, H.-B. Sun, T. Tianaka, K. Tianaka, *Nature* **2001**, *412*, 697.
[44] J. Serbin, A. Egbert, A. Ostendorf, B. N. Chichkov, R. Houbertz, G. Domann, J. Schultz, C. Cronauer, L. Frohlich, M. Popall, *Opt. Lett.* **2003**, *28*, 301.
[45] F. Stellacci, C. A. Bauer, T. Meyer-Friedrichsen, W. Wenseleers, V. Alain, S. M. Kuebler, S. J. K. Pond, Y. Zhang, S. R. Marder, J. W. Perry, *Adv. Mater.* **2002**, *14*, 194.
[46] J. D. Pitts, P. J. Campagnola, G. A. Epling, S. L. Goodman, *Macromolecules* **2000**, *33*, 1514.
[47] S. Basu, L. P. Cunningham, G. D. Pind, K. A. Bush, R. Taboada, A. R. Howell, J. Wang, P. J. Campagnola, *Biomacromol.* **2005**, *6*, 1465.

Chapter 2

Synthesis and characterization of monomers for LCE development

2.1 Introduction

Free radical polymerization of mesogenic monomers and crosslinkers leads the formation of a liquid crystalline network (**Scheme 6**) with the simultaneous growth of different chains and their crosslinking.
Free radicals can be produced through application of heating, irradiation with light, redox agent or electricity with the relative initiation of the polymerization process. Light in the ultraviolet or visible range can break selected bonds, thereby forming free radicals and allowing the polymerization process at a choice temperature.[48] This aspect is fundamental in the LCE preparation where the monomer mixture must be aligned in nematic phase before the polymerization. The temperature is maintained in a selected range in which the LC phase is present and stable and, only at this moment, the polymerization can occur leading the formation of a LCE.

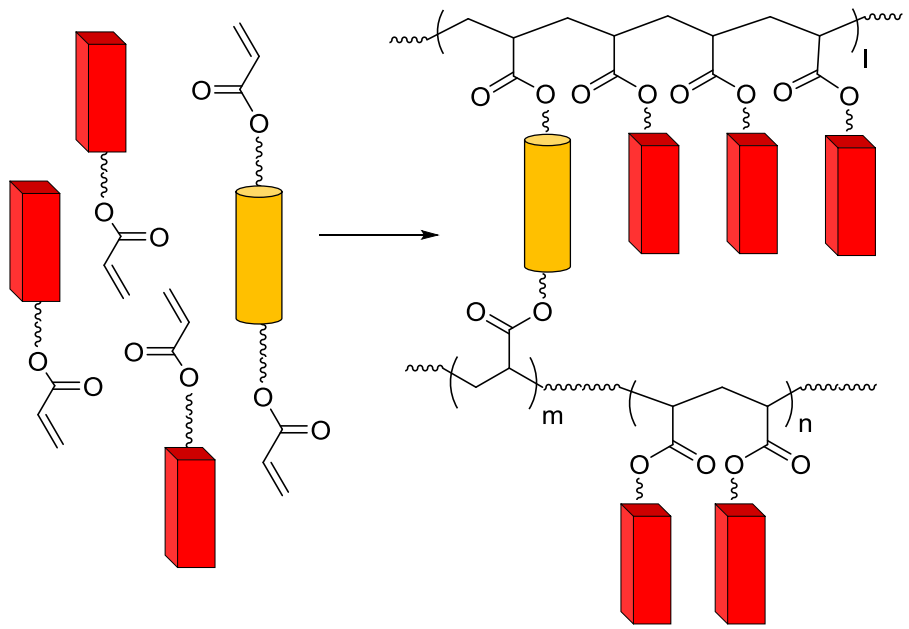

Scheme 6 Synthesis of a LCE using free radical polymerization of acrylate based monomers.

[48] C. E. Carraher, *Introduction to polymer chemistry*, CRC Press, Taylor & Francis Group **2010**.

Using photopolymerization to prepare LCEs, the monomer mixtures must contain at least the following molecules (**Scheme 7**):

- **mesogenic monomers** functionalized with a polymerizable group and responsible for the aligned structure of the material;
- **crosslinkers** functionalized with two or more polymerizable groups and responsible for the mechanical properties of the material. They can also contain a LC core;
- **photoiniators** that determine the wavelength used for the polymerization.

The polymerizable unit mainly used in this thesis is the **acrylate moiety** and all the molecules described in the chapter contain this group.
Moreover, to obtain a photoactive material, we chose to include **azobenzenes** in the mixture as monomer or crosslinker. In this case, it is essential to choose a light for polymerization that does not induce the *trans* to *cis* isomerization with the consequent N to I phase transition of the mixture: the absence of the LC alignment in the whole material or in part of it modifies the mechanical properties of the final structure.

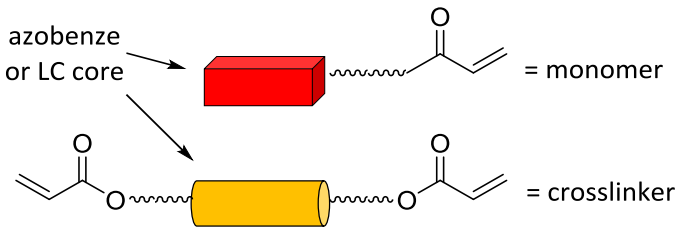

Scheme 7 General structure of monomers.

Photopolymerization occurs through different steps (**Scheme 8**): in the initiation step (**a**) light cleaves a bond of the initiator (**I**) homolytically producing radicals. Then, in the chain propagation step (**b**), they react with monomers producing new radicals able to react with other monomers. In this way, the chain propagates until there is no more monomer or other quenching of radical terminations happens. The termination step (**c**) occurs for combination of two radicals or for disproportionation, where a hydrogen atom is abstracted from one chain end to another.[48]

a) $I \longrightarrow R^{\bullet}$

b) $R^{\bullet} + M \longrightarrow RM^{\bullet} \longrightarrow RMM^{\bullet}.... \longrightarrow RM_n^{\bullet}$

c) $RM_n^{\bullet} + RM_m^{\bullet} \longrightarrow RM_{n+m}R$

$RM_n^{\bullet} + RM_m^{\bullet} \longrightarrow RM_n + RM_m$

Scheme 8 Steps of radical polymerization.

To design a new LC monomer or crosslinker, a general structural template for calamitic mesogens is shown in **Figure 17**, including those that exhibit nematic and smectic phases.[3]

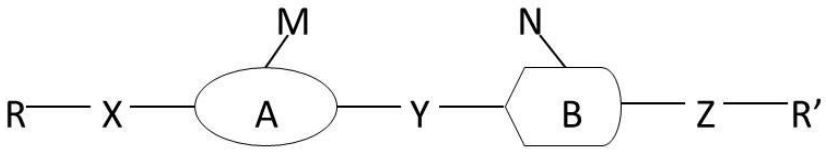

Figure 17 General structure of a calamitic LC.

The prototypical molecular design involves a central rigid core that is attached to flexible aliphatic chains, thereby generating a dichotomous structure with a semirigid polarizable section surrounded by flexible, apolar chains. The core unit can be composed by linearly cross linked ring systems (A and B) that are most often aromatic (for example 1,4-phenyl, 2,5-pyrimidinyl, 2,6-naphthyl) but can be also alicyclic (for example, 1,4-cyclohexyl). The rings can be directly linked or can be divided by a group (Y) which maintains the linearity of the core (for example, $-CO_2-$, $-C\equiv C-$). Moreover, different lateral substitutions, M and N, (for example F, Cl, CN, CH_3) are often used to modify the physical properties of the molecule. R and R' are usually alkyl or alkoxy chain; however, one terminal unit is often a small polar substituent (for example CN, F, NCS, NO_2). [3]

Some important generalizations on the structure-LC properties relationship of mesogens are:

- the nematic phase is favored by the use of a relatively short terminal chains. Longer chains tend to stabilize the lamellar arrangement of molecules;

- the increase of length of the chains reduces the melting temperatures due to an increased flexibility. However, when chains are very long, the excessive van del Waals intermolecular forces increase melting points.;
- the smectic phases are favored by a symmetrical molecular structure. Lateral substituents are often used to break symmetry of the molecule;
- the addition of an aromatic ring extends the linear which results in a large increase in the T_{LC-I}. This increase is generally bigger than the increase of the melting point, producing a material with a larger nematic range.[3]

Moreover, to design a new azobenzene-containing monomer or crosslinker we have to consider that photoisomerization occurs at different wavelengths and depend on the particular structure of each molecule. Azobenzenes are typically grouped into three classes (**Figure 18**): the azobenzene-type molecules, the aminoazobenzene ones, and the pseudo-stilbenes.[25]
Azobenzene-type molecules have characteristics similar to the unsubstituted azobenzene with a high absorption in the UV region. Dyes *ortho*- or *para*-substituted with EDG (such as a NH_2), results in a red-shifted π-π* absorption band which is very close or collapse to the n-π* band in the visible region. In the end, substitution of the azobenzene at the 4 and 4' positions with an EDG and an EWG (such as a NH_2 and a NO_2), also referred as ''push/pull'' substitution, induces a significantly red-shifted the π-π* band changing sometimes the appearance order with respect to the n-π* band. If the absorption spectra of the *trans* and the *cis* isomer overlap, a single wavelength of light activates both the forward and reverse isomerization, leading to a mixed stationary state and continuous interconversion of molecules. For some application, this rapid and efficient cycling of cromophore is advantageous, whereas in case where the azocromophore has to use as a switch, it is clearly undesiderable.[25,49]
Also the lifetimes of the *cis* state change for azobenzenes, aminoazobenzenes and pseudo-stilbenes and they are usually in the order of hours, minutes, and seconds respectively.[49]

[49] Z. Mahimwalla, K. G. Yage, J. Mamiya, A. Shishido, A. Priimagi, C. J. Barrett, *Polym. Bull.* **2012**, *69*, 967.

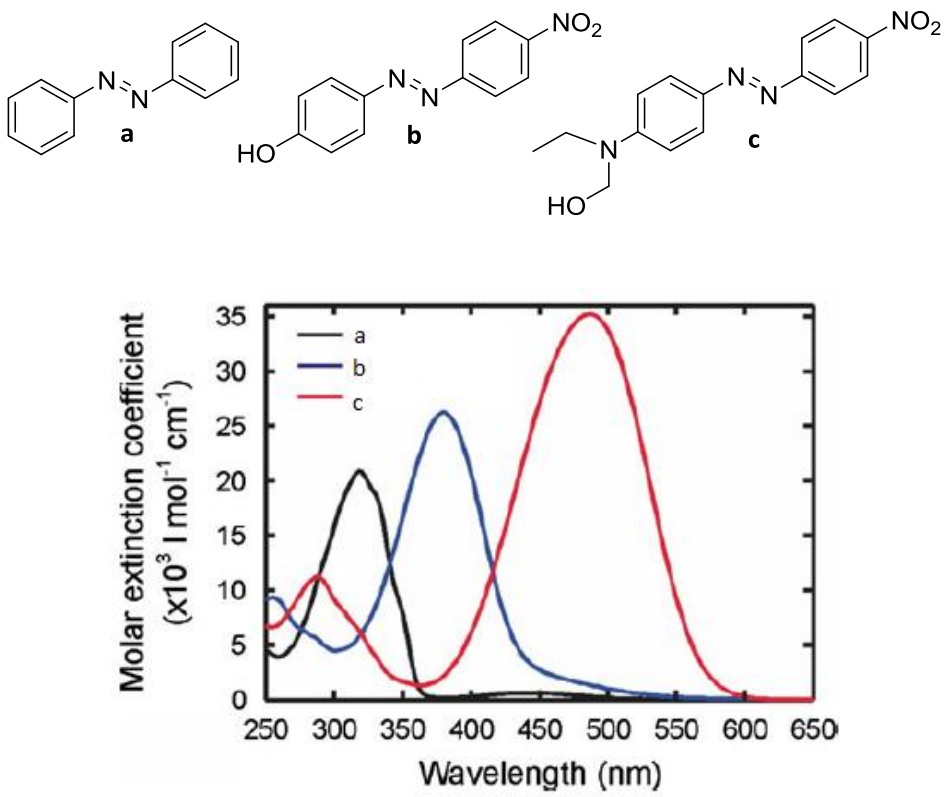

Figure 18 Different type of azo-dyes and their absorption spectra: azobenzene (a), aminoazobenzene (b) and pseudo-stilbene (c) type-molecules.

In the next sections, we describe the synthesis of different acrylate containing molecules and the study of their LC properties. At the end, the absorption properties of the prepared azobenzenes are discussed.

2.2 Results and discussion

2.2.1 Design of the synthesized molecules

The choice of molecules to prepare was the first important step in this project: we designed and synthesized monomers and crosslinkers shown in **Scheme 9** in order to study the effect of different molecular changes on the properties of both molecules and final materials. We prepared only structures with aromatic rigid core composed principally by 1,4-phenyl units with -CO_2- as linking group. **M_1** introduced by Keller and co-workers is a "side-on" monomer used by several groups.[12] In particular, it has been already employed for a DLW experiment and represents for us the starting point for the mixture preparations and the microfabrications. Other monomers were prepared changing the molecular architecture from "side-on" to "end-on". The number of aromatic rings was changed (2 for **M_{2-4}** and 3 for **M_5**) and, for monomers with two aromatic rings, also the length of the flexible spacer was changed. Regarding the crosslinker, we started our LCE preparation with the commercial **CL_1** and **CL_2** and then we tried to modulate the LC properties of **CL_2** by changing the length of the alkyl chains (**CL_{3-4}**) or using a different rigid core (**CL_5**). At the end, we prepared a trifunctional crosslinker **CL_6** useful to obtain more rigid structures.

The azobenzenes designed and prepared are shown in **Scheme 10**. **D_{1-4}** are functionalized with an acrylate to be incorporate in the polymer as side-chains, while **D_5**, bearing two acrylate groups, was prepare to use the azobenzene as a crosslinker. Indeed **D_{1-3}** are "end-on" molecules in which we changed the substituents in order to tune the absorption spectra. **D_4** is a "side-on" molecule already used from others research groups (with the methacrylate group instead of the acrylate one).[28]

Monomers

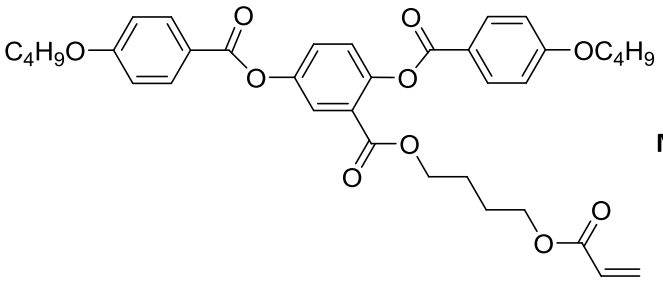

M_1

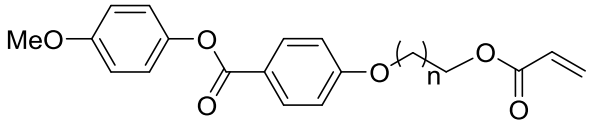

n=2 **M_2**
n=5 **M_3**
n=7 **M_4**

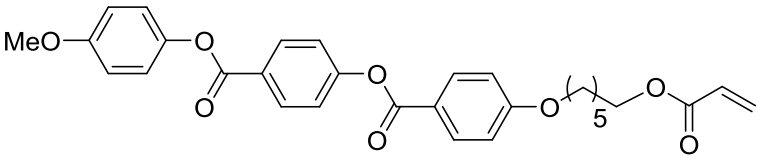

M_5

Crosslinkers

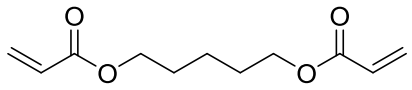

CL_1

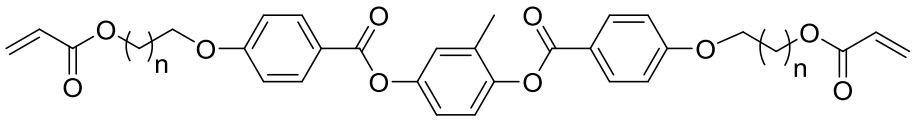

n=2 **CL_2**, n=5 **CL_3**, n=7 **CL_4**

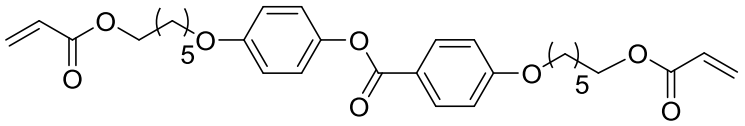

CL_5

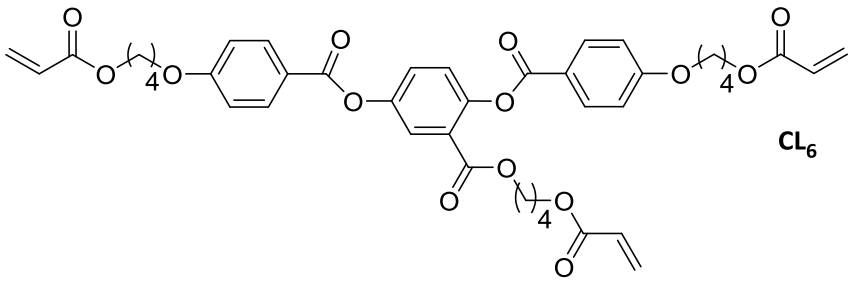

CL_6

Scheme 9 Molecules for LCE preparation.

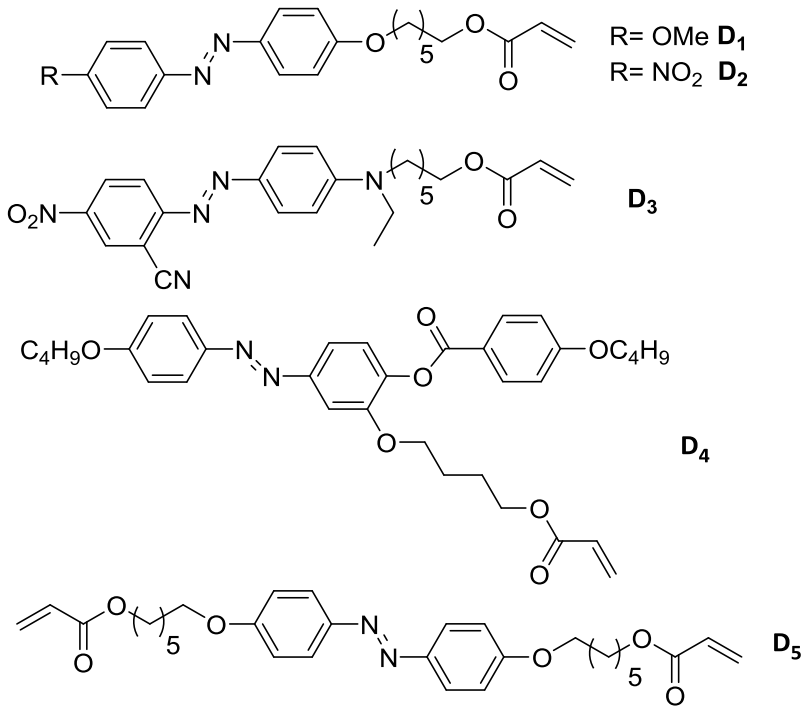

Scheme 10 Dyes for photoactive LCE preparation.

The mechanical properties of a photoactive LCE depend on the electronic properties of the dye and on its location in the polymeric structure, besides on its quantity in the monomer mixtures. We synthesized these structures in order to study the effect of the different molecular parameters of the dye on the mechanical behavior of LCE films.

2.2.2 Synthesis of monomers and crosslinkers

A crucial aspect of the project is the availability of monomers in gram scale. This allows to prepare many different mixtures and to test them in order to implement and optimize the materials. We needed to use simple synthetic strategies reducing if possible the number of steps and using procedures with high yields. Moreover, a difficult task was the purification of the final monomers, obtained trying first the recrystallization from different solvent and then the Flash Column Chromatography. A high purity of monomers is required in order not to modify first the LC properties of the mixtures and then

the mechanical properties of the LCEs, studied without any purification after their preparation.

Different hydroxybenzoic acids were employed as starting building blocks to construct the rigid core of the final molecules and three features were common to all the synthesis performed:

1. The connection between the aromatic rings was realized with an ester group, the most used linking group in LC field for its relative stability and its easy synthesis. The esters were prepared by Steglich procedure with the dicyclohexylcarbodiimide (DCC) as coupling reagent: this compound is able to form with a carboxylic acid an *O*-acylisourea intermediate, which offers reactivity similar to the corresponding carboxylic acid anhydride (**Scheme 11**).[50]

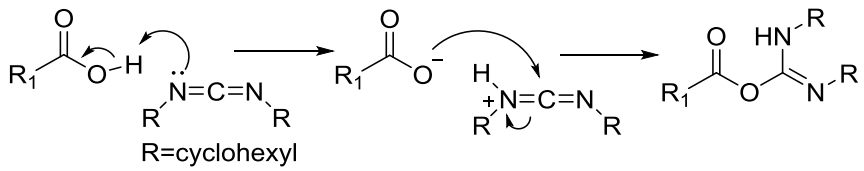

Scheme 11 Mechanism of formation of *O*-the acylisourea.

The alcohol attacks this intermediate, forming the dicyclohexylurea and the ester. This step is very slow and the use of additives is crucial to obtain an efficient formation of the ester: for example, 4-*N*,*N*-dimethylaminopyridine (DMAP), more nucleophile than alcohols, reacts with the *O*-acylisourea affording an amide able to reacts rapidly with alcohols. The formation of the *N*-acylurea derivative, a side product formed by the acyl migration on the *O*-acylisourea, is generally slow but it could be a problem in specific case.

2. The insertion of the flexible chain was made by Williamson synthesis on a phenol group of the aromatic core. This step involves the reaction of an alkoxide ion, often generated in situ by a carbonate base or potassium hydroxide, with an alkyl halide via an S_N2 substitution. A wide range of solvents can be used, but protic and apolar solvents tend to slow the reaction rate strongly while acetonitrile and DMF are commonly used. If less reactive alkyl chlorides are used, the reaction rate can be improved by

[50] B. Neises, W. Steglich, *Angew. Chem. Int. Ed.* **1978**, *17*, 522.

the addition of a catalytic amount of an iodide salt, which undergoes halide exchange with the chloride to yield a more reactive iodide derivative.

3. The acrylate moiety was introduced by functionalization of a hydroxyl group with acryloyl chloride. The procedure usually requires the use of a stoichiometric quantity of a base in CH_2Cl_2 or THF and leads to very high or quantitative yields in 1-2 h reaction.

Depending on the particular synthesis, a protecting group (generally the benzyl group) has been used to address the chemoselectivity of some reaction.

The first molecule prepared was **M_1** and its synthesis, shown in **Scheme 12**, follows a procedure already described in literature.[12]

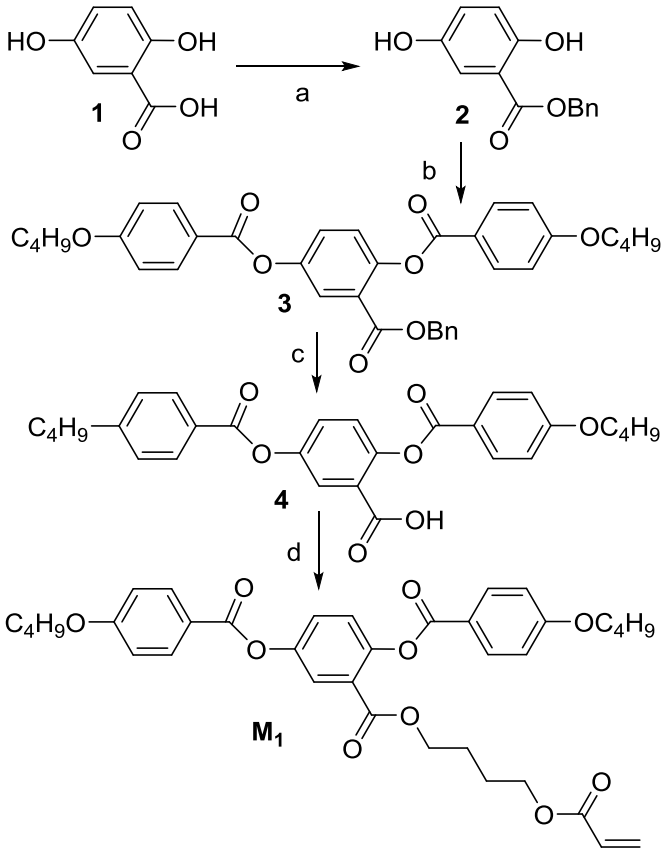

Scheme 12 Synthesis of M_1. Reagents and conditions: a) $NaHCO_3$, DMF, 70 °C, 1 h, then BnBr, 70 °C, 4 h, 90%; b) 4-butyloxybenzoic acid, DCC, DMAP, CH_2Cl_2, rt, 12 h, 81%; c) Pd/C, H_2, CH_2Cl_2, 48 h, 89%; d) 4-hydroxybutyl acrylate, DCC, 4-pyrrolidinopyridine, CH_2Cl_2, rt, 12 h, 71%.

The carboxylic group of the 2,5-dihydroxybenzoic acid (**1**) was protected as benzylic ester with $NaHCO_3$ in DMF at 70 °C**:** using the benzyl bromide in stoichiometric amount, only the carboxylate group reacts leading the formation of the desired product. Then the phenol groups of **2** were esterified with 4-butyloxybenzoic acid affording **3**: the use of the benzyl group was required to avoid the intramolecular coupling of the 2,5-dihydroxybenzoic acid and other side products difficult to separate. The benzyl group was then removed with a hydrogenolysis to give **4** in 85% yield over three steps. At the end, **4** was esterified with 4-hydroxybutyl acrylate leading to the final monomer in 46% yield from the starting benzoic acid.

Monomers $\mathbf{M_{2\text{-}4}}$ and crosslinkers $\mathbf{CL_{3\text{-}4}}$ were prepared by esterification between methoxyphenol (for monomers) or methylhydroquinone (for crosslinkers) and a 4-[6-(acryloyloxy)alkyloxy]benzoic acid, which represents an important building block also for other synthesis. Different conditions were studied during the preparation of the 4-[6-(acryloyloxy)hexyloxy]benzoic acid (**9**, **Scheme 13**). Starting from the 4-hydroxybenzoic acid (**5**), a Williamson reaction with 6-chloro-1-hexanol was tried by using K_2CO_3 as base and DMF or NMP as solvent. Unfortunately, in both cases the desired product was formed together with the monosubstituted product on the carboxylic acid and the disubstituted product. To avoid the problem, the starting material was first protected as methyl ester: reaction of **5** in methanol at reflux using H_2SO_4 as catalyst afforded **6**. This intermediate was subjected to the Williamson reaction in the condition previously described obtaining **7** in quantitative yield. Hydrolysis of the ester with potassium hydroxide in methanol allowed to obtain **8** in 83% yield over three steps and without intermediate purifications.
Following another procedure reported in literature,[51] the direct alkylation of **5** was tried changing both base and solvent: using potassium hydroxide and a mixture of ethanol and water at reflux, we obtained successfully **8** in one step and very high yield (79%). This one-step procedure obviously results advantageous in respect to the first one described.
Also the functionalization of **8** with acryloyl chloride presented chemoselectivity problems in standard conditions (CH_2Cl_2 as solvent and NEt_3 as base) affording also the anhydride containing product. Using NMP as solvent in absence of base, acryloyl chloride reacted selectively with the

[51] J.-H. Liu, C.-D. Hsieh, *J. Appl. Polym. Sci.* **2006**, *99*, 2443.

hydroxyl group on **8** affording **9** in very high yield and purity. No by-products were formed.

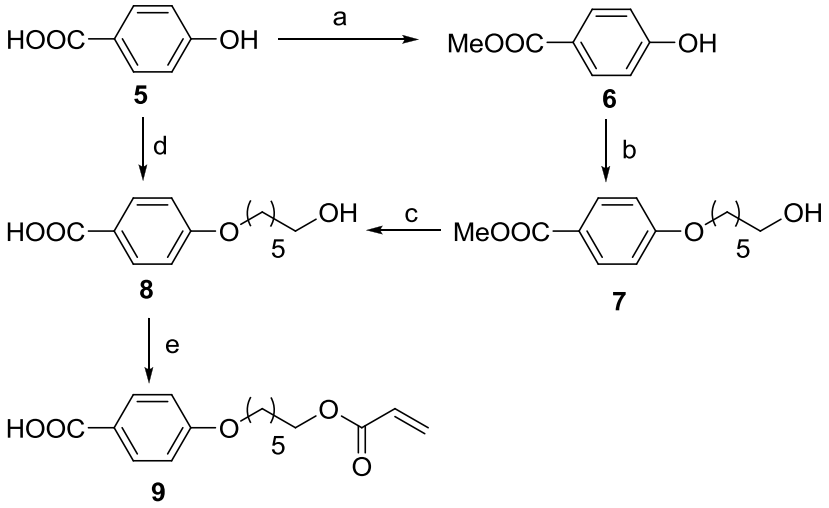

Scheme 13 Synthesis of 4-[6-(acryloyloxy)hexyloxy]benzoic acid. Reagents and conditions: a) H_2SO_4, MeOH, reflux, 12 h, 98%; b) 6-chloro-1-hexanol, K_2CO_3, NaI, NMP, 85 °C, 18 h, 100%; c) KOH, MeOH, 50 °C, 18 h, 85%; d) 6-chloro-1-hexanol, KOH, KI, EtOH:H_2O 5:1, reflux, 18 h, 79%; e) acryloyl chloride, NMP, rt, 3 h, 100%.

9 was then employed in the esterification with methoxyphenol to give **M_3** in 79% yield and with methylhydroquinone to give **CL_3** in 33% yield (**Scheme 14**).

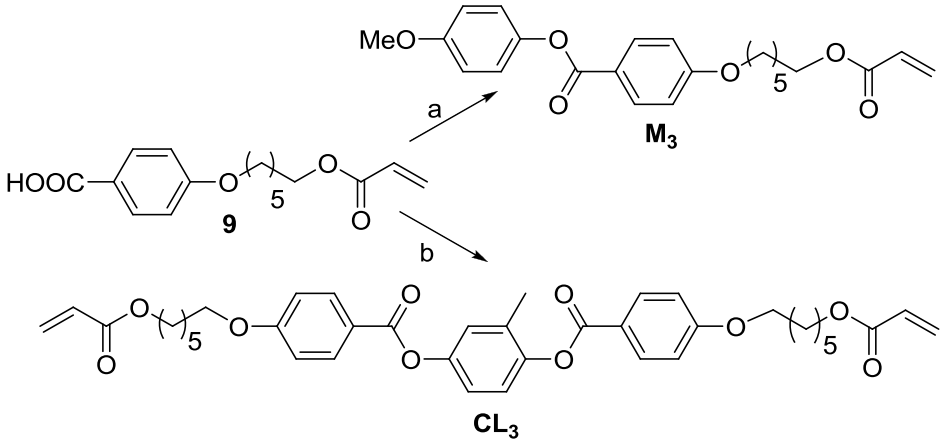

Scheme 14 Synthesis of M_3 and CL_3. Reagents and conditions: a) methoxyphenol, DCC, 4-pyrrolidinopyridine, CH_2Cl_2, rt, 18 h, 79%; b) methylhydroquinone, DCC, 4-pyrrolidinopyridine, CH_2Cl_2, rt, 18 h, 33%.

The synthetic route described above was employed also starting from different chloro-alcohols (**Scheme 15**). Using 1-chloro-3-propanol, **12** was obtained in 2 steps with 51% yield and it was subjected to esterification with methoxyphenol

affording **M_2**. 1-Chloro-8-octanol was used to prepare **13** (74% yield over 2 steps) then employed in different esterification to obtain **M_4** and **CL_4**. Yields of the mentioned esterification were not high (less than 50%) and other studies of the conditions for these couplings were under evaluation. The use of a different coupling reagent, as the 1-ethyl-3(3-dimethylaminopropyl) carbodiimide (EDC), or the formation of the acyl chloride followed by coupling with the phenol moiety are possible solutions for the synthesis improvement.

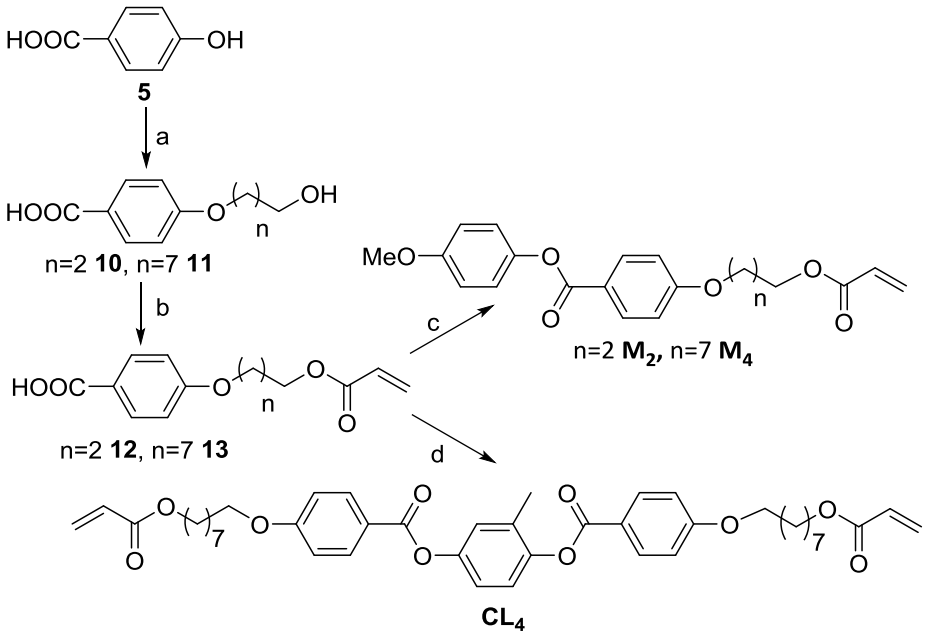

Scheme 15 Synthesis of M_2, M_4 and CL_4. Reagents and conditions: a) chloro-alcohol, KOH, KI, EtOH:H_2O 5:1, reflux, 18 h, 55% for **10**, 74% for **11**; b) acryloyl chloride, NMP, rt, 3 h, 93% for **12**, 100% for **13**; c) methoxyphenol, DCC, 4-pyrrolidinopyridine, CH_2Cl_2, rt, 18 h, 47% for **M_2**, 38% for **M_4**; d) methylhydroquinone, DCC, 4-pyrrolidinopyridine, CH_2Cl_2, rt, 18 h, 33%.

In order to extend the length of the rigid part in respect of the monomers previously reported, we designed the synthesis of **M_5**. It requires the coupling between 4-[6-(acryloyloxy)hexyloxy]benzoic acid (**9**) and a molecule containing two subsequent aromatic rings like **17**. The synthesis of **17** was performed in 4 steps starting from **5** and the protection of the phenol moiety was needed in order to avoid its competition with methoxyphenol in the first esterification of the strategy (**Scheme 16**).

In the first step we intent to introduce the above mentioned protection leading free the carboxylic acid on the starting material. The synthetic problem is opposite to that encountered in the synthesis of **M_1** in which we had

introduced the benzyl group selectively on the carboxylic acid of the 2,5-dihydroxybenzoic acid, and then we designed a complementary synthetic strategy. Starting from **5**, we first tried a single-step procedure using a small excess of benzyl bromide (1.1 equivalents) and NaOH as base in a mixture of ethanol and water. The target compound **15** was obtained in 40% yield after a chromatographic column of the crude containing also the starting material, the benzyl ester and the dibenzilated derivative. We changed strategy and we found out that in this case, a two-step procedure results advantageous[52]: the starting material was benzilated on both functional groups using an excess of benzyl bromide and K_2CO_3 as base in DMF affording **14**. Then, only the benzyl ester was hydrolyzed using potassium hydroxide in a mixture of ethanol and water at reflux. **15** was obtained in 88% yield in two steps and used without further purification in the next step that consists in the coupling with methoxyphenol to afford **16.** Hydrogenation of **16**, in order to deprotect the phenol group, and subsequent esterification of the resulting molecule, **17**, with **9** gave monomer $\mathbf{M_5}$ in 53% yield from 4-hydroxybenzoic acid (**5**).

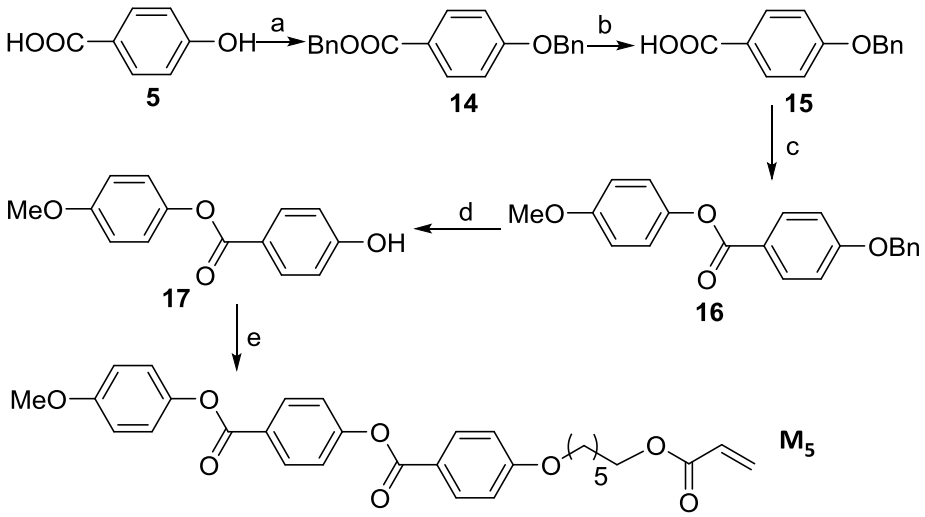

Scheme 16 Synthesis of $\mathbf{M_5}$. Reagents and conditions: a) BnBr, K_2CO_3, DMF, rt, 18 h, 100%; b) KOH, EtOH:H_2O 4:1, reflux, 1 h, 88%; c) 4-methoxyphenol, DCC, 4-pyrrolidinopyridine, CH_2Cl_2, rt, 18 h, 81%; d) Pd/C, H_2, CH_2Cl_2, rt, 48 h, 94%; 3) **9**, DCC, 4-pyrrolidinopyridine, CH_2Cl_2, rt, 18h, 79%.

[52] S. Tranchimand, T. Tron, C. Gaudin, G. Iacazio, *Synt. Comm.* **2006**, *36*, 587.

Molecule **9** can be used also to synthesize **CL_5** by coupling with **23**. This compound was prepared starting from the hydroquinone (**18**), a common and cheap reagent, by its functionalization with an alkyl chain only on one of the two phenol groups followed by the introduction of the acrylate moiety (**Scheme 17**). Obviously different protective strategies are required for both these steps.[53]

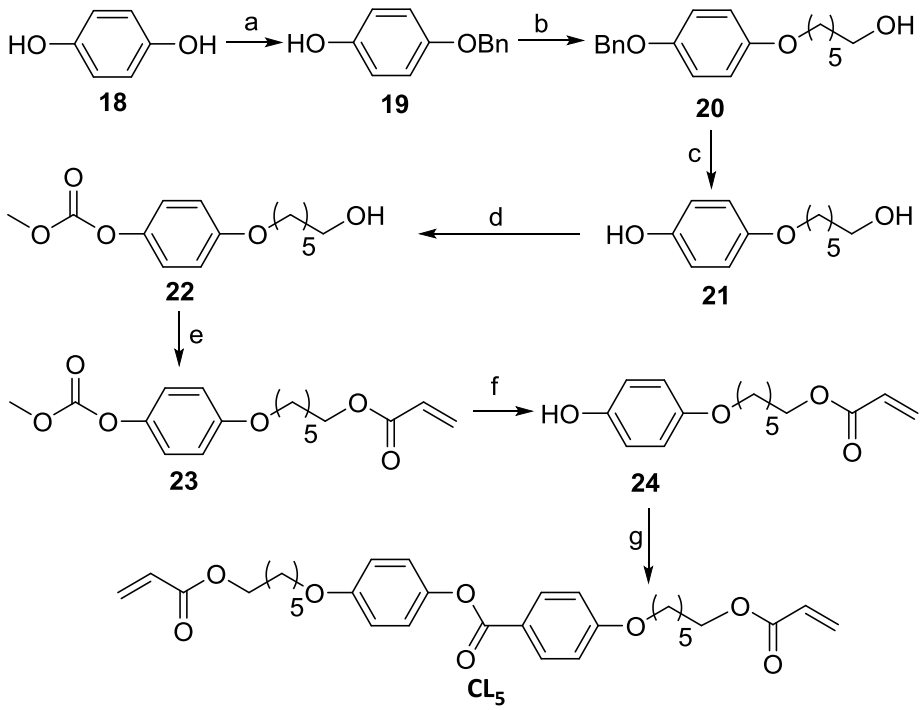

Scheme 17 Synthesis of CL_5. Reagents and conditions: a) BnBr, K_2CO_3, acetone, reflux, 18 h, 51%; b) 6-chloro-1-hexanol, K_2CO_3, DMF, 100°C, 18 h, 84%; c) Pd/C, H_2, CH_2Cl_2, rt, 48 h, 100%; d) methyl chloroformate, NaOH, H_2O, rt, 4 h, 64%; e) acryloyl chloride, TEA, CH_2Cl_2, rt, 18 h, 100%; f) NH_3 33%, EtOH, rt, 6 h, 62%; g) **9**, DCC, 4-pyrrolidinopyridine, CH_2Cl_2, rt, 18 h, 61%.

The monobenzilated derivative **18** was prepared using an excess of hydroquinone (2.5 equivalents), benzyl bromide and K_2CO_3 as base in acetone; nevertheless, a minor quantity of dibenzilated product was also formed and separation on FCC was required. **18** was subjected to Williamson reaction with 6-chloro-1-hexanol affording **19** (43% yield over two steps), which could not be directly used in the reaction with acryloyl chloride: the standard condition for the deprotection of benzyl group are not compatible with the acrylate moiety. For this reason, we removed the benzyl group by hydrogenolysis affording **20**

[53] D. Lacey, H. N. Beattie, G. R. Mitchell, J. A. Pople, *J. Mater. Chem.* **1998**, *8*, 53.

in quantitative yield and then we introduced the methoxycarbonyloxy group to protect the phenol using methyl chloroformate and NaOH in water. Intermediate **21** was treated with acryloyl chloride to introduce the polymerizable group affording **22.** Selective hydrolysis of the more labile ester with NH_3 33% in ethanol afforded **23** in 17% yield over 6 steps. At the end, its esterification with **9** gave **CL_5** in 61% yield.

The trifunctional crosslinker **CL_6** was prepared following the synthetic route shown in **Scheme 18**.

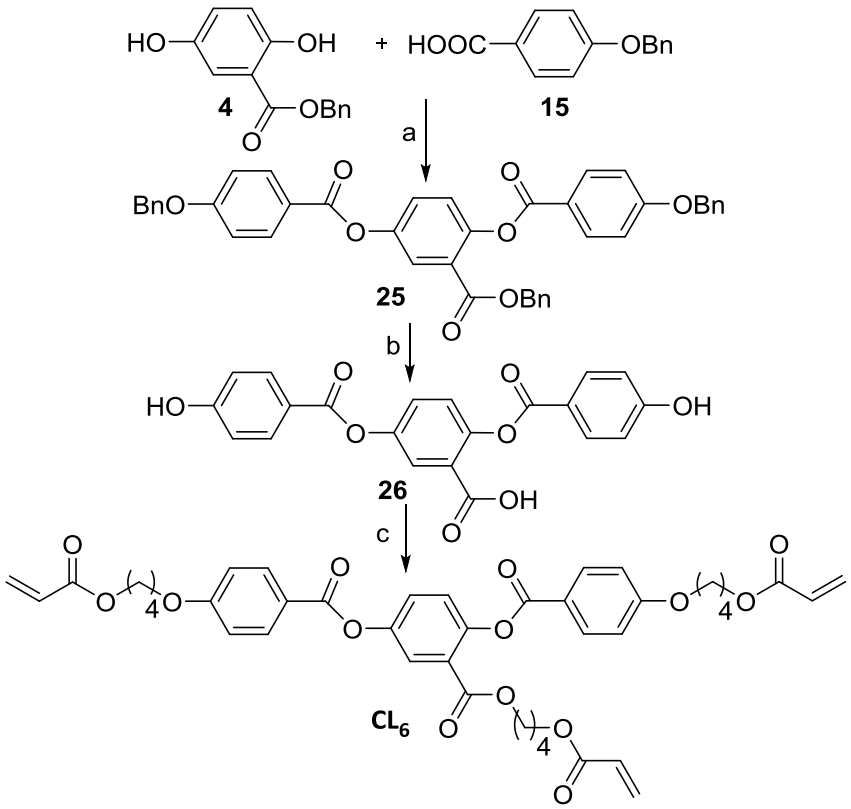

Scheme 18 Synthesis of CL_6. Reagents and conditions: a) DCC, 4-pyrrolidinopyridine, CH_2Cl_2, rt, 18 h, 83%; c) Pd/C, H_2, MeOH, rt, 48 h, 79%; c) 4-hydroxybutyl acrylate, PPh_3, DMEAD, CH_2Cl_2:DMF 5:1,rt, 18 h, 28%.

The synthetic strategy starts with the esterification between **4** and **15** affording the intermediate **25** in 83% yield**.** It was then deprotected by hydrogenolysis, in order to remove to benzyl groups, giving **26** in 79% yield. Functionalization of the three free functional groups of **26** with 4-hydroxybutyl acrylate through

a Mitsunobu reaction afforded **CL_6**. This reaction is based on cooperation of the oxidative nature of a dialkylazodicarboxylate ester (as DIAD or DMEAD, **Scheme 19**) and the reducing nature of PPh_3 to promote dehydratation between an alcohol and a carboxylic acid (or another acid nucleophile as a phenol group) affording an ester.

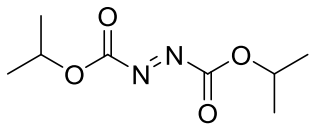

Diisopropyl azodicarboxylate
(**DIAD**)

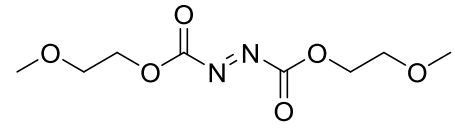

Di-2-methoxyethyl azodicarboxylate
(**DMEAD**)

Scheme 19 Example of dialkylazodicarboxylate esters used in Mitsunobu reaction.

We first used DIAD and dry CH_2Cl_2 as solvent but the reagents resulted insoluble, then we added a quote of DMF to dissolve the starting material (**26**). This condition allowed the formation of the desired product but unfortunately, its purification was unsuccessfully with both chromatographic methods and recrystallization from different solvents. We decided to perform the reaction using DMEAD instead of DIAD: with this reagent, the hydrazine formed during the reaction could be removed by a simple extraction with water allowing a simpler purification of the final product.[54] The use of DMEAD in a mixture of CH_2Cl_2:DMF (5:1) as solvent finally allowed to obtain pure **CL_6** in 28% yield from **26**. Further studies to improve the yield of reaction are undergoing following the synthetic strategy presented in **Scheme 20**.

This new approach employs the esterification of compound **27a**[55] with benzoic acid **27b** instead of the Mitsunobu reaction that resulted the critical step in the previous strategy.

[54] K. Hagiya, N. Muramoto, T. Misaki, T. Sugimura, *Tetrahedron* **2009**, *65*, 6109.
[55] R.Wei, L. Zhou, Y. He, X. Wang, P. Keller, *Polymer* **2013**, *54*, 5321.

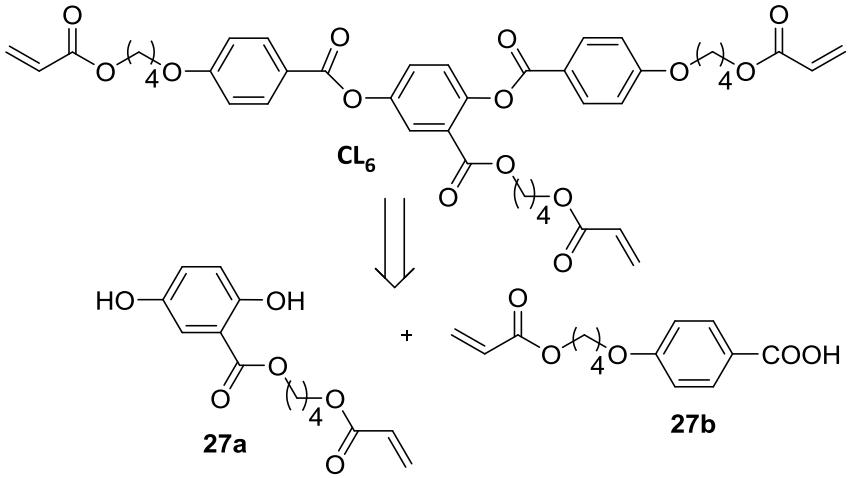

Scheme 20 Alternative synthetic approach to prepare CL_6.

2.2.3 Synthesis of dyes

Azobenezenes can be synthesized through different methods but each synthetic route is suitable only in specific cases, depending on the substitution pattern on the aromatic rings. Some examples to summarize the most used synthesis are shown in **Scheme 21**. The preparation of symmetrical azobenzenes has been reported by oxidation of primary aromatic amine with MnO_2, $KMnO_4$, H_3BO_2, Ag_2O or many other reagents, also in solvent-free conditions (as an example see **Scheme 21**.**1**). Another strategy to obtain the same molecules goes through the reduction of nitro compounds. The synthesis in this case can be performed in different way: a) by using Zn in a basic medium; b) via catalytic transfer hydrogenation using HCO_2H, NEt_3/Pb; c) by reduction with glucose in basic medium (example **Scheme 21**.**2**). Asymmetrical azobenzenes can be prepared by treatment of aromatic nitroso compounds and primary arylamines in acetic acid via Mills reaction (example **Scheme 21**.**3**) or by coupling of diazo compounds or diazonium salts with suitable nucleophiles (example **Scheme 21**.**4**).[56]

[56] F. Hamon, F. Djedaini-Pilard, F. Barbot, C. Len, *Tetrahedron* **2009**, *65*, 10105.

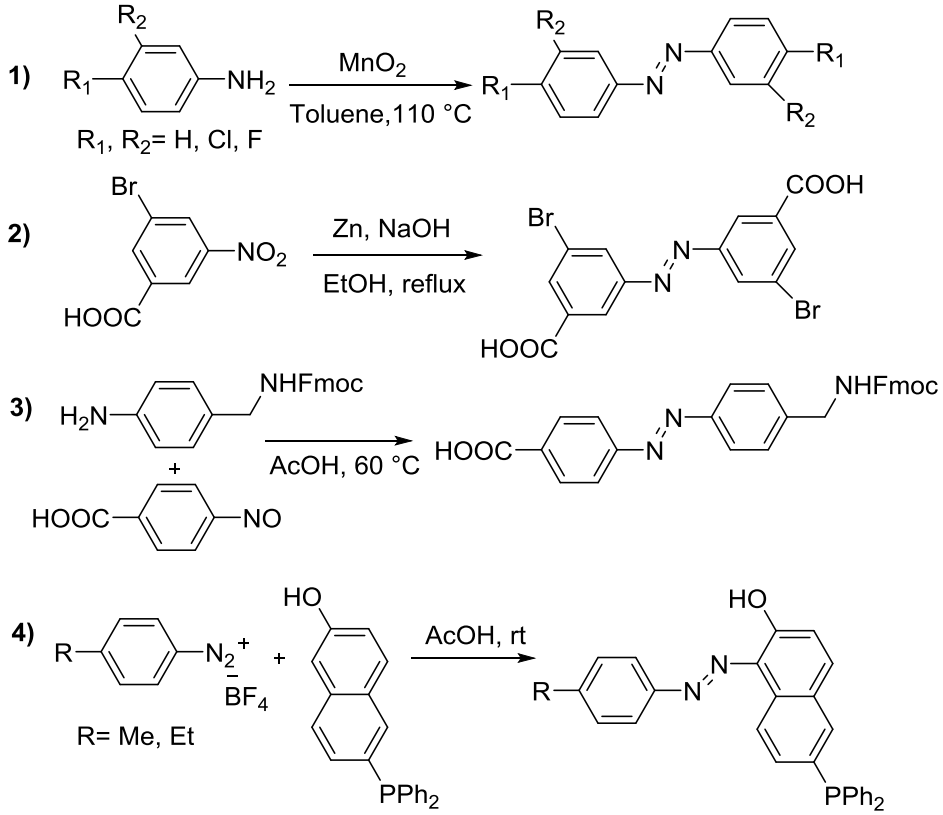

Scheme 21 Examples of azobenzene synthesis.

We chose to prepare the azodyes using the coupling of diazonium salt with phenols or anilines. The diazonium salts can be prepared for treatment of a primary amine with nitrous acid usually generated in situ from sodium nitrite and a mineral acid; the reaction goes through the attack of the reactive species NO^+, formed by nitrous acid, to the lone pair of the ammine followed by a dehydration step (**Scheme 22**).

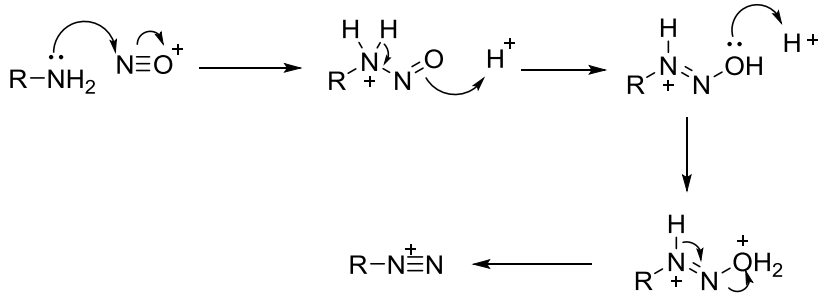

Scheme 22 Mechanism of formation of a diazonium salt.

If R is an alkyl group, the diazonium salt is very unstable and immediately loses nitrogen gas, while for aromatic groups, the salt results more stable and below the temperature of 5 °C the loss of nitrogen is slow. Diazonium compounds could be isolated as tetrafluoroborate salts even if generally they are prepared in situ and used immediately in further reactions with different nucleophiles.[57]

D_1[58] and **D_2**[59] were prepared as shown in **Scheme 23**: different *para*-substituted anilines (**28** and **29**) were dissolved in an acid aqueous solution and used to form the diazonium salt by addition of $NaNO_2$. These species were coupled with phenol to give the azobenzenes **30** and **31** in good yields (respectively 85% and 62%). The pH of the solution is an important factor: even if phenol is not active enough for the reaction, in alkaline solution, the more reactive phenoxide ion affords the target molecule. For this reason, phenol was first dissolved in a basic solution and then, diazonium salt solution was added dropwise to this solution: due to size of the attacking species, the substitution is *para* to the phenol group even if the *ortho* substitution could take place when the *para* position is occupied.

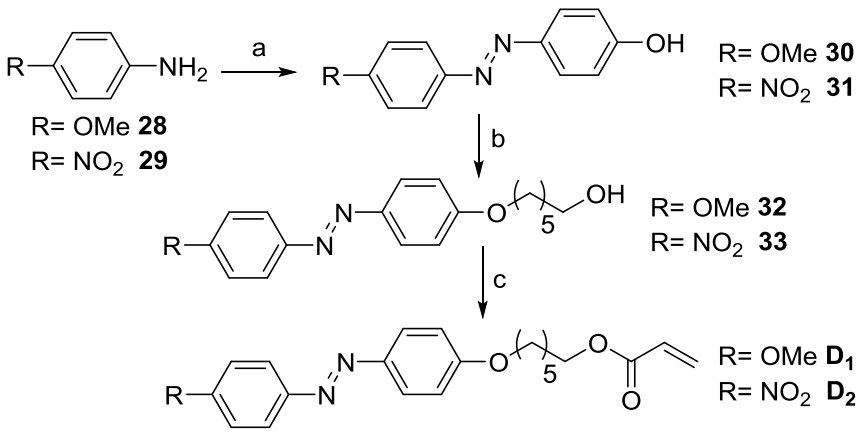

Scheme 23 Synthesis of D_1 and D_2. Reagents and conditions: a) $NaNO_2$, H_2O, HCl 37%, 0 °C, 15', then addition to phenol in NaOH aqueous solution, 0 °C, 30', 85% for **30**; 62% for **31**; b) 6-chloro-1-hexanol, K_2CO_3, NaI, NMP, 85 °C, 4 h, 89% for **32**, 82% for **33**; c) acryloyl chloride, TEA, CH_2Cl_2, rt, 2 h, 90% for **D_1**, 84% for **D_2**.

[57] J. Clayden, N. Grevees, S. Warren, P. Wothers, *Organic Chemistry*, Oxford University Press, **2001.**

[58] M. Moritsugu, S. Kim, S. Kubo, T. Ogata, T. Nonaka, O.Sato, S. Kurihara, *React. Funct. Polym.* **2011**, *71*, 30.

[59] J.-H. Liu, P.-C. Yang, *J. Appl. Polymer. Sci.* **2004**, *91*, 3693.

30 and **31** had to be subjected to Williamson reaction with 6-chloro-1-hexanol: a first attempt was done with NaOH as base in ethanol or methyl ethyl ketone at reflux but we did not obtain the desired substitution. Finally the use of K_2CO_3 in NMP allowed the preparation of **32** and **33** and both products were functionalized with acryloyl chloride to obtain $\mathbf{D_1}$ and $\mathbf{D_2}$, respectively in 68% and 43% yield from the starting aniline.

$\mathbf{D_3}$ was prepared starting from two anilines: 2-amino-5-nitrobenzonitrile (**34**) was used to prepare the diazonium salt and then coupled with aniline **36** (**Scheme 24**).

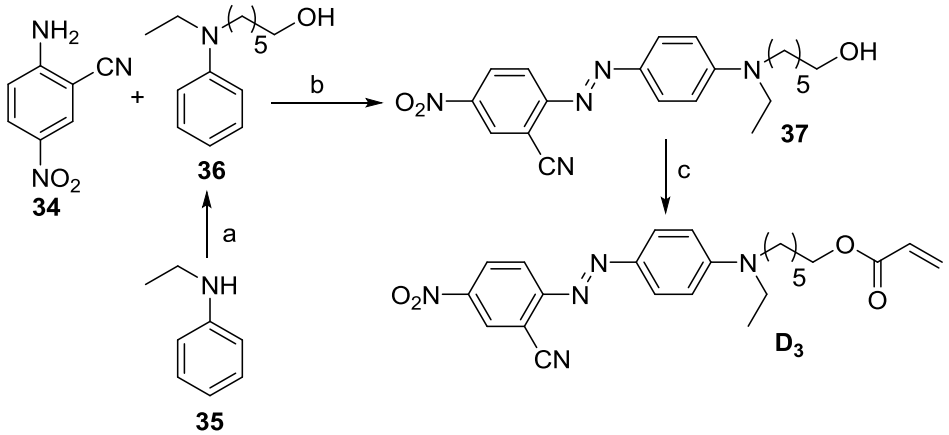

Scheme 24 Synthesis of $\mathbf{D_3}$. Reagents and conditions: a) 6-chloro-1-hexanol, K_2CO_3, NaI, DMF, 80 °C, 18 h, 70%; b) acetic and propionic acid, nitrosyl sulfuric acid, 0-5 °C, then addition to 36 in MeOH, 5°C, 30', 75%; c) acryloyl chloride, CH_2Cl_2, TEA, rt, 2 h, 79%.

To be coupled with a diazonium salt, the nucleophilic aniline has to be a tertiary one, otherwise the reaction undergoes on the NH site with the formation of the triazine derivative. For this reason, N-ethyl aniline (**35**) was subjected to a Williamson reaction with 6-chloro-1-hexanol to obtain **36** allowing both, the protection of the nucleophilic site on the N and the introduction of the desired spacer. Moreover, the use of **34** brings some problems in the formation of the diazonium salt due to the deactivation of the substrate by EWGs. Low yield was obtained dissolving the stating material in water and HCl and using $NaNO_2$, while the use of a mixture of acetic and propionic acids as solvent and nitrosyl sulfuric acid allowed to obtain **37** in 75%yield from the diazonium salt. This product was functionalized with acryloyl chloride affording $\mathbf{D_3}$ in only 3 steps and 41% overall yield.

The "side-on" type azobenzene **D_4** was prepared starting from 4-butoxyaniline (**38**) and resorcinol (**39**) (**Scheme 25**). In this case, the two phenol groups of **39** activate two different positions on the nucleophile and the attack of the diazonium salt could occur on both positions. For this reason, it was necessary to change the synthetic procedure in respect to the standard one. The problem was solved by the use of 3 equivalents of resorcinol and 1.1 equivalents of base in respect to the aniline, obtaining **40** and avoiding the attack of two electrophile molecules on the same molecule of resorcinol.[60]

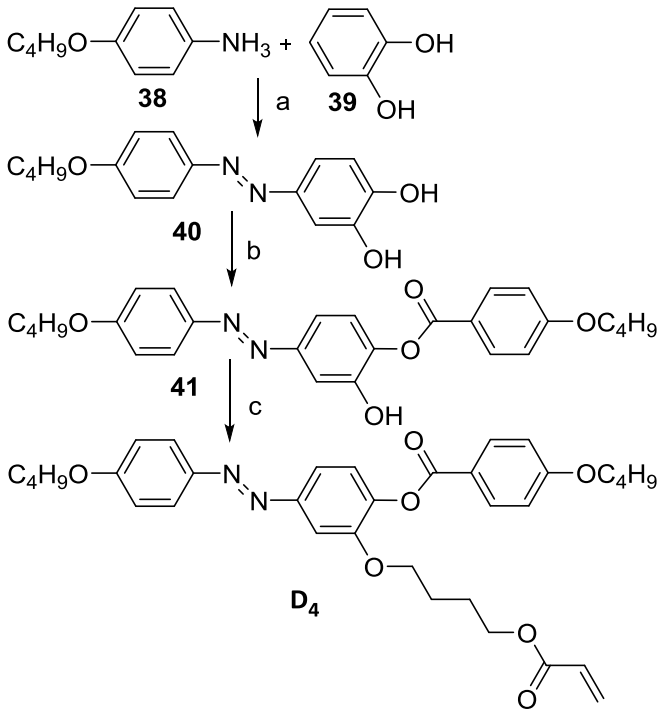

Scheme 25 Synthesis of D_4. Reagents and conditions: a) $NaNO_2$, H_20, HCl 37%, 0 °C, 15', then addition to the **39** in NaOH aqueous solution, 0 °C, 1 h, 20%; b) 4-butyloxybenzoic acid, DCC, 4-pyrrolidinopyridine, CH_2Cl_2, rt, 18 h, 72%. c) 4-hydroxybutyl acrylate, PPh_3, DIAD, CH_2Cl_2, rt, 18 h, 53%.

Esterification of **40** with 1 equivalent of 4-butoxybenzoic acid gave selectively product **41** in 72% yield and side reactions on the other free phenol moieties of **40** or **41** were not observed. At the end, the OH group of **41** was functionalised with 4-hydroxybutyl acrylate through a Mitsunobu reaction: the

[60] M.-H. Li, P. Auroy, P. Keller, *Liquid Crystal* **2000**, *27*, 1497.

use of DIAD in CH_2Cl_2 as solvent allowed to obtain **D_4** in 53% yield (8% yield over the three steps).

To synthesize **D_5** we first prepared the azobenzene core starting from 4-aminophenol. Unfortunately, the coupling with phenol resulted very difficult and allowed the formation of only a very small quantity of the product. Then, we decided to change the starting material and we prepared aniline **44** (**Scheme 26**). The 4-nitrophenol (**42**) was subjected to a Williamson reaction with 6-chloro-1-hexanol affording **43**, then the nitro group was reduced by hydrogenolysis to obtain the desired aniline **44** in 80% yield over 2 steps.[31] We did not choose the direct use of the 4-aminophenol instead of the 4-nitrophenol (**42**) because of the predictable problems during the Williamson coupling due to the nucleophility of the NH_2 group. **44** was employed to prepare the diazonium salt and coupled with phenol to successfully obtain **45** in 85% yield.

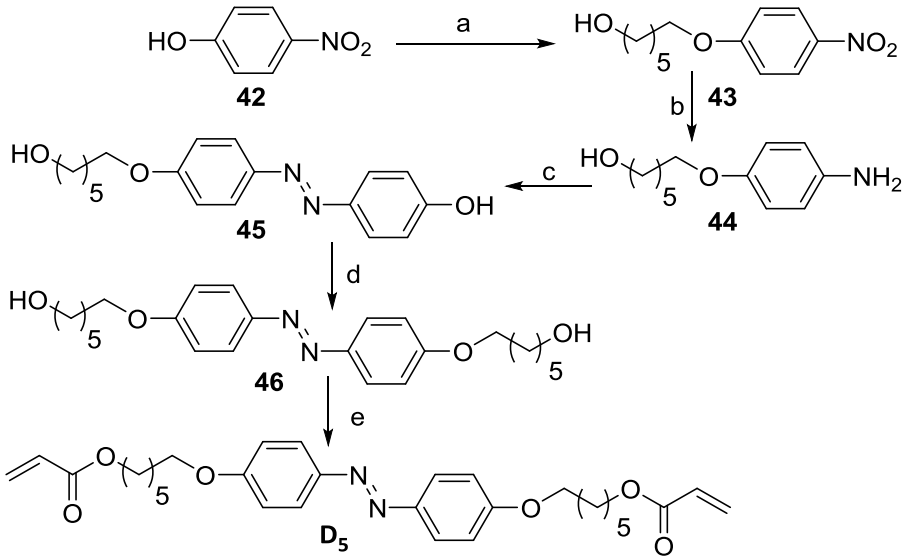

Scheme 26 Synthesis of D_5. Reagents and conditions: a) 6-chloro-1-hexanol, K_2CO_3, DMF, 100 °C, 18 h, 82%; b) MeOH, H_2, Pd/C, rt, 48 h, 98%; c) $NaNO_2$, H_20, HCl 37%, 0 °C, 15', then addition to the phenol in NaOH aqueous solution, 0 °C, 1 h', 85%; d) 6-chloro-1-hexanol, K_2CO_3, DMF, 100 °C, 18 h, 91%; e) acryloyl chloride, CH_2Cl_2, TEA, rt, 4 h, 67%.

Azoderivative **45** was subjected to a second Williamson reaction with 6-chloro-1-hexanol in order to introduce the second spacer, affording **46** in 91% yield. Functionalization with acryloyl chloride on both the OH groups give **D_5** in 52% yield from the starting aniline **44**.

2.2.4 Mesomorphic properties of molecules

Mesomorphic behavior of molecules was characterized by DSC and POM: DSC traces of all compounds and POM images of the LC phases are reported in Appendix.
Monomer transition temperatures are summarized in **Table 1**.

Monomer	Phase transition temperatures [°C][a]	
$\mathbf{M_1}$[b]	h: Cr 60.5 N 86.2 (0.93) I	c: I 83.3 (1.22) N
$\mathbf{M_2}$	h: Cr 67.2 I	c: I -13.5 Cr
$\mathbf{M_3}$[b]	h: Cr 55.2 I	c: I 44.9 (0.61) N
$\mathbf{M_4}$	h: Cr 51.7 I	c: I 51.5 (0.63) N 34.8 LC 26.6 Cr
$\mathbf{M_5}$	h: Cr 79.4 I	c: I 26.9 Cr

Table 1 Thermal properties of monomers obtained during the second heating (h)–cooling (c) cycle of DSC experiments. [a]Determined from the onset of the transition peak. In bracket is reported the enthalpy of the transition (kJ/mol) determined from the integration of peak. [b]Temperatures obtained from the first cycle (crystallization was not observed on cooling down to -50 °C and a second heating until I).

$\mathbf{M_1}$ presents an enantiotropic nematic phase in a range of temperature approximately of 25 °C. The formation of the crystalline phase is a very slow process and it is not observed in the DSC trace. These phase transition temperatures differ of some degrees from those reported in literature for the compound[12] probably due to the different instrument calibration. $\mathbf{M_2}$ does not present liquid crystalline properties: DSC trace shows only a melting peak to the isotropic phase on heating at 67.2 °C and a crystallization peak on cooling at -13.5 °C. Instead, analogous monomers with longer alkyl chains ($\mathbf{M_3}$ and $\mathbf{M_4}$) present monotropic nematic phases. $\mathbf{M_3}$ and $\mathbf{M_4}$ have a very close melting temperature showing that changing the length of the flexible chain from 6 to 8 carbon atoms bears only small modification in the mesomorphic properties of the structure. On cooling, samples present the nematic phase starting from 44.9 °C for $\mathbf{M_3}$ and 51.5 °C for $\mathbf{M_4}$. Crystallization of $\mathbf{M_3}$ is not observed under the DSC experimental condition. Moreover, DSC trace of $\mathbf{M_4}$ shows another exothermic peak (1.6 kJ/mol) on cooling at 34.8 °C which could be associated to the transition from N to another LC phase. Instead, POM observation of $\mathbf{M_4}$ shows only the transition from N to the crystalline phase without other intermediate LC phases. $\mathbf{M_5}$ does not present liquid crystalline properties: DSC trace shows only a melting process on heating above 79.4 °C and LC phases are not observed neither on cooling.

Table 2 summarizes the LC properties of crosslinkers. The three analogous **CL_{2-4}** present enantiotropic nematic phases. These phases are present in a broad range of temperature also on heating (at least 25 °C) and crystallization of **CL_2** and **CL_3** is not observed in the cooling cycle of the measurement. Cold crystallization is observed for **CL_3** in the second heating. The effect of the length of the flexible spacer on these molecules is different for T_m and T_{NI}. We observe a gradually increase of T_m using longer alkyl chain (56.8 °C, 72.6 °C and 79.7 °C respectively for **CL_2**, **Cl_3** and **CL_4**) while the changes of T_{NI} are smaller for the three compounds without a general trend. In particular, we observe an increase of 12 ° C of the T_{NI} from **CL_2** to **CL_3**, while **CL_4** presents a T_{NI} close that of **CL_2**. **Cl_5** does not present liquid crystalline properties and the DSC trace shows a melting peak on heating (55.7 °C) and two exothermic peak on cooling (45.6 °C and 25.1 °C). We verified with POM that the first smaller peak on cooling does not represent a transition to a monotropic LC phase and only crystallization from the isotropic liquid is observed. The peak could be associated to a crystal-crystal transition. The last crosslinker, **CL_6**, shows a monotropic nematic phase with the lower transition temperatures in respect to the other ones. On heating two very closed peaks are observed (49.6 °C and 57.6 °C), related to transitions within different two crystalline phases, followed by melting in the isotropic phase.

Crosslinker	Phase transition temperatures [°C][a]	
CL_2[b]	h: Cr 56.8 N 102.0 (0.80) I	c: I 107.1 (1.36) N
CL_3	h: Cr 72.6 N 113.9 (0.95) I	c: I 114.3 (1.16) N[c]
CL_4	h: Cr 79.7 N 104.1 (0.94) I	c: I 105.1 (1.08) N 35.2 Cr
CL_5	h: Cr 55.7 I	c: I 45.6 Cr_1 25.1 Cr_2
CL_6[b]	h: Cr_1 49.6 Cr_2 57.6 I	c: I 48.5 (0.69) N

Table 2 Thermal properties of crosslinkers obtained during the second heating (h)–cooling (c) cycle of DSC experiments. [a]Determined from the onset of the transition peak. In bracket is reported the enthalpy of the transition (kJ/mol) determined from the integration of peak. [b]Temperatures obtained from the first cycle (crystallization was not observed on cooling down to – 50 °C and a second heating until I). [c]Crystallization was not observed on cooling down to -50 °C. A peak related to cold crystallization is observed on the second heating cycle.

Transition temperature of dyes are summarized in **Table 3** and only **D_4** shows LC behavior with an enantiotropic nematic phase. DCS trace of the compound presents three very close peaks on heating: the first (85.6 °C) is related to the transition between two crystalline phases while the second (89.8 °C) shows the melting in the nematic phase that is present in only 3 °C of temperature range. On cooling a broad LC temperature range is observed (around 40 °C). **D_1**, **D_2**

and **D_3** show the endothermic peaks of melting in the isotropic phase on heating above 83°C and crystallization is observed on cooling only for **D_1** and **D_2**. DSC trace of **D_5** is more complex and various peaks are present on heating and cooling. POM observation clarifies that the molecule melts directly in the isotropic phase without any intermediate LC phase. Also on cooling, only the crystallization from the isotropic phase is observed. The different peaks could be related to transition between different crystalline phases.

Dye	Phase transition temperatures [°C][a]	
D_1	h: Cr 83.7 I	c: I 83.2 Cr
D_2	h: Cr 96.2 I	c: I 89.6 Cr
D_3[b]	h: Cr 94.4 I	
D_4	h: Cr_1 85.6 Cr_2 89.8 N 93.2 I	c: I 93.3 (0.94) N 50.9 Cr
D_5	h: Cr_1 77.6 Cr_2 83.9 Cr_3 95.7 I	c: : I 86.8 $Cr_1$78.8 Cr_2

Table 3 Thermal properties of dyes obtained during the second heating (h)–cooling (c) cycle of DSC experiments. [a]Determined from the onset of the transition peak. In bracket is reported the enthalpy of the transition (kJ/mol) determined from the integration of peak. [b]Temperatures obtained from the first cycle (crystallization was not observed on cooling down to -50 °C and a second heating until I)

2.2.5 Absorption properties of dyes

Absorption spectra of the synthesized dyes (**Scheme 27**), recorded in methanol, are shown in **Figure 19** and wavelengths of maximum absorption of the π-π* bands are summarized in **Table 4**.

D_1 and **D_5**, both with two alkyloxy groups (OR) in position 4 and 4' of the azobenzene system, present a strong absorption in the UV region. The addition of another OR group on the rings does not affect the absorption properties: the maximum of the π-π* band in **D_4** is red shifted only of 10 nm in respect to the absorption of **D_1** and **D_5** and its spectrum overlaps with the ones of the same dyes cited above. In the structure of **D_2**, one of the OR groups is replaced with a nitro group: the effect of this EWG is to red shift the absorption peak of 20 nm in respect to **D_1** but, on the other hand, the spectrum does not present big change respect to the others mentioned.

As explained in the Introduction, this kind of molecules have been extensively used to prepare films able to bend trough UV irradiation and return in the initial position with visible light. The control of movements with two different wavelength is possible only for azobenzenes with a stable *cis* state. Kinetic

studies of the thermal *cis* to *trans* isomerization are required to understand the mechanical behavior of polymers and several groups measured the relaxation time of the *cis* state for many azobenzenes.

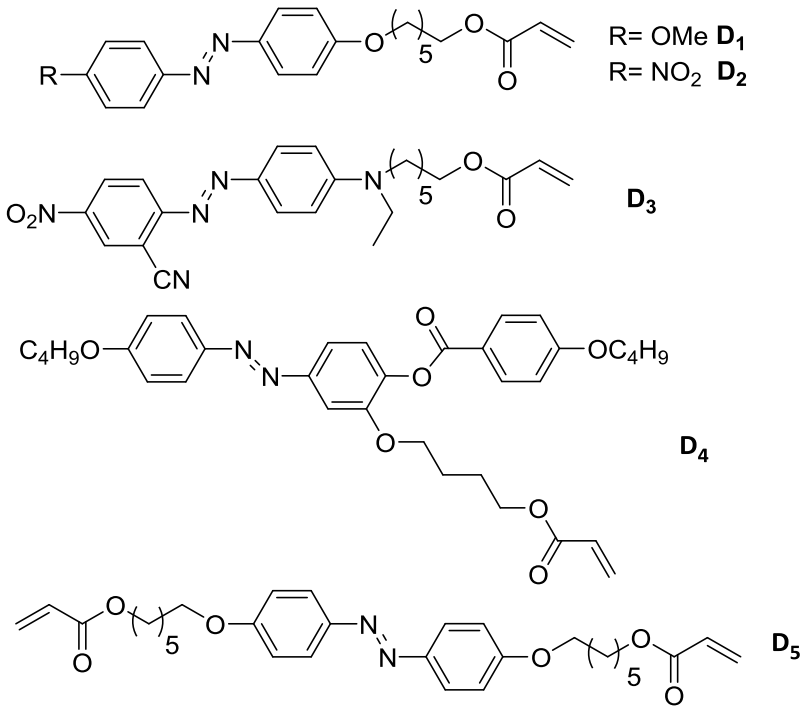

Scheme 27 Synthesized dyes.

Dye	λ_{max} (nm)	ε_{max} ($10^4 M^{-1}cm^{-1}$)
D_1	356	2,86
D_2	375	2,67
D_3	535	4,22
D_4	366	2,99
D_5	357	2,97

Table 4 λ_{max} and ε_{max} of the synthesized dyes.

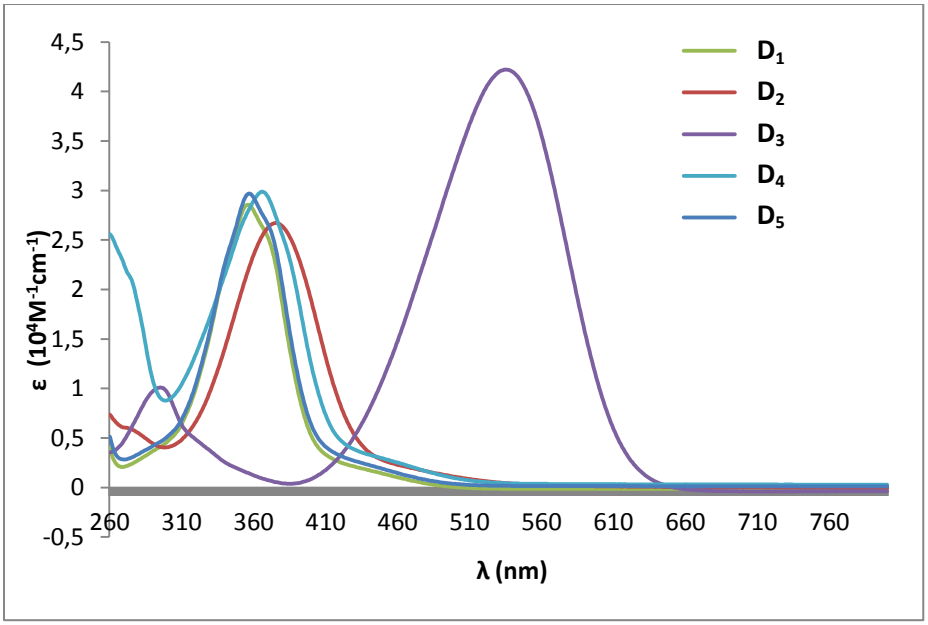

Figure 19 Absorption spectra of the synthesized dyes.

Molecules with the substitution pattern of $\mathbf{D_1}$ present a stable *cis* state in solution (around 10 hours) while the addition of EWG group decrease this time. A nitro group, for example, gives a relaxation time in the scale of minutes and the use of more EWG groups follows to destabilize the *cis* state (**Table 5**).[61]

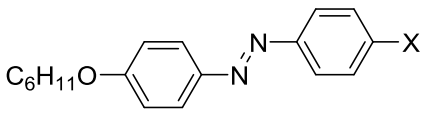

X	τ
H	70 h
OMe	13 h
OC_6H_{11}	12 h
CN	6 h
NO_2	24 min

Table 5 Thermal relaxation time (τ) in ethanol at 25 °C for some azobenzenes.

The thermal relaxation time was found 10^2 time faster when the dye was used as a guest dopant in a low molar mass nematic liquid crystal due to the cooperative interaction with the mesogens that tend to recover their alignment. Moreover, the covalent bond of dyes with the backbone of a liquid

[61] J. Garcia-Amorós, D. Velasco, *Beilstein J. Org. Chem.* **2012**, *8*, 1003.

crystalline polymer enhances furthermore the isomerization time that results 10^3 times faster that in an isotropic solvents.[62]

In **D_3** the strong push-pull configuration results in a large change of the absorption spectrum with a very low absorption in the UV range and a strong visible band: green light can be used to bend films containing this dye. Based on existing reference, **D_3** relaxation time is reasonably in the scale of millisecond.[61] For this reason, materials prepared with this dye work with a single wavelength: bending and unbending can be induced by shine on and off the light source. The full mechanism that induced the LCE contraction in this case is not predictable nowadays: both thermal effect, due to the transformation of light energy in heat, and optical effect, due to the isomerization, contribute to the process and we are not able to estimate the single contribute.

D_3 is then an example of photoswitches, which due to their capability of work at wavelength different from UV light, attracted a lot of attention for biological application. Azobenzenes have been employed to trigger change in structure or function of many biomolecular target, including protein, peptoides and nucleic acid in vitro but usually their use is limited by needed of UV light for photoisomerization. UV light is strongly scattered in vivo, making penetration of cells and tissues difficult and it can induce apoptotic event and other response, making studies on cell cultures and on model organism more complicated.[63]

The use of photoswitches with biological compatibility represent a big challenge to the design microrobots for biomedical application: we have recently focused our attention on this topic starting, as preliminary work, the synthesis of **D_6**. Hecht and co. workers reported that this molecule has a very stable *cis* state and the isomerization processes can be controlled with green light (for *trans* to *cis* state) and blue light (for the opposite isomerization) through the $n \rightarrow \pi^*$ absorption bands that are separated of 50 nm in the two isomers.[64] Therefore, we suppose that when this dye is used in photosensitive material, the resulting structure could be optically modified with green

[62] J. Garcia-Amorós, H. Finkelmann, D. Velasco, *Chem. Eur. J.* **2011**, *17*, 6518.
[63] A. A. Beharry, G. A. Woolley, *Chem. Soc. Rev.* **2011**, *40*, 4422.
[64] D. Bléger, J. Schwarz, A. M. Brouwer, S. Hecht, *J. Am. Chem. Soc.* **2012**, *134*, 20597.

irradiation and such modification could be conserved, differently than structures containing **D_3**, until the second exposure to a different wavelength.
D_6 was prepared as shown in **Scheme 28** using an oxidation procedure from aniline **50**.

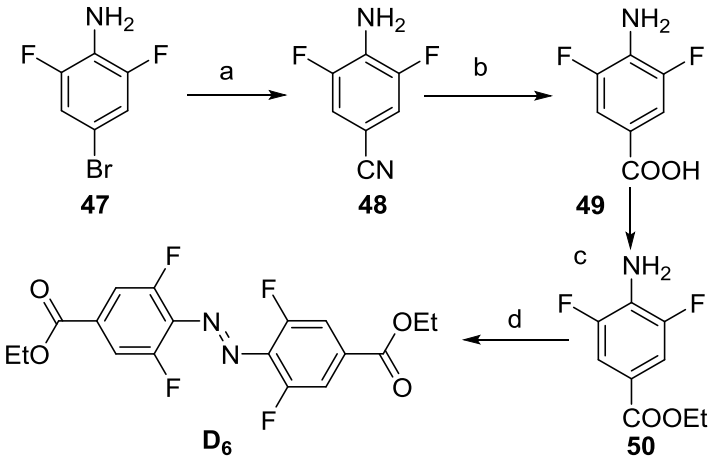

Scheme 28 Synthesis of D_6. Reagents and conditions: a) CuCN, NMP, 160 °C, 4 h, 80%; b) NaOH 4 M, reflux, 18 h, 95%; c) EtOH, H_2SO_4, reflux, 18 h, 90%; d) $KMnO_4$ on $CuSO_4 \cdot 5H_2O$, CH_2Cl_2, reflux, 24 h, 33%.

In the first step the 2,6-difluoro-4-bromoaniline (**47**) was subjected to a Rosenmund-Von Braun reaction to substitute the bromide with a nitrile group affording **48**. This reaction involves an excess of copper cyanide and the use of a polar, high-boiling point solvent generally making the purification of the products difficult. In addition, it requires elevated temperatures lowering the functional group tolerance of the procedure. We used 3 equivalent of CuCN and DMF or NMP as solvents: the reaction proceeds only above 150°C and NMP gave the best result decreasing the reaction time from the needed 18 h with DMF to 4 h. **48** was subjected to hydrolysis of nitrile group in NaOH 4M at reflux affording **49** and then the carboxylic acid was esterified in acid condition with EtOH at reflux. **50** was obtained in 68% yield over 3 steps. The oxidation of this compound resulted the crucial step of the synthesis and examples reported in literature for similar anilines show very low yields (10-25%).[64]
Oxidation with a heterogeneous permanganate mixture is commonly used for azobenzene preparation and often gives better results compared with other methods. The support play an essential role to determine the yield of reaction and different sulfates have been used showing that $CuSO_4 \cdot 5H_2O$ is the better

choice.[65] Using such $CuSO_4 \cdot 5H_2O$ support, we first tried the oxidation of the nitrile derivative **48** in CH_2Cl_2 or in toluene (both at room temperature or at reflux) for 24 h. In all cases, we did not isolate the desired product and we were not able to recover the starting material. Instead, the oxidation of **50** gave **D_6** in a relative better yield than previously reported (33% against the 24% reported).

Figure 20 shows the absorption spectrum of **D_6** in acetonitrile: we can suppose that the dye could be successfully used for DLW, due to very low absorption at the working wavelength of our system (390 nm). In order to confirm the isomerization properties, the sample was irradiated with a LOT-Oriel 1000 W medium pressure Xenon Lamp (without filter or with a filter for 360-370 nm) at different times and absorption spectra were recorded. Irradiation induced the isomerization with a corresponding decreasing of the π→π* band of the *trans* form but a total isomerization with this lamp was not possible. The spectrum did not change further for more than 30 minutes of irradiation. Indeed the spectrum recorded on the irradiated solution did not change after 2 weeks confirming that the thermal isomerization of *cis* to *trans* form is very slow.

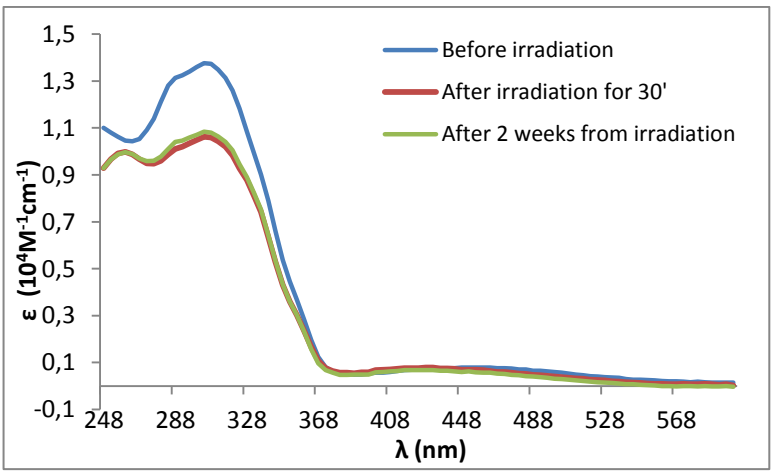

Figure 20 Absorption spectra of D_6 before and after UV irradiation.

Due to these interesting properties, **D_6** could be used in the next future for the preparation on a new class of crosslinker to be insert in LCEs with different mechanical behavior to that actually used. To prepare the new molecules we could employ a hydrolysis of the ethyl esters followed by a coupling with a suitable chain.

[65] N. A. Noureldin, J. W. Bellgarde, *Synthesis* **1999**, *6*, 939.

2.3 Experimental part

General methods. Commercial reagents were used as received. All reactions were magnetically stirred and monitored by TLC on 0.25 mm silica gel plates (Merck F_{254}) and column chromatography was carried out on Silica Gel 60 (32-63 μm). NMR spectra were recorded on a Varian INOVA-400, Varian Gemini-200 or Varian Gemini-200. Infrared spectra were recorded with a Shimadzu FTIR-8400S spectrophotometer. UV-vis spectra were recorded with a Perkin-Elmer Lamba 950 spectrophotometer. ESI full MS were recorded on a Thermo LTQ instrument by direct inlet; relative percentages are shown in brackets. Elemental analyses were performed with a Perkin-Elmer 2400 analyzer. Thermal transitions were measured using a DSC TA Instruments Q-2000 calorimeter under a nitrogen atmosphere (heating and cooling rate: 10 °C/min). An inverted microscope (Zeiss, Axio Observer A1) with cross polarisers was used to observe the LC phases.

Benzyl 2,5-dihydroxybenzoate (**2**). A mixture of 2,5-dihydroxybenzoic acid (2.15 g, 13.95 mmol) $NaHCO_3$ (3.39 g, 84.01 mmol) in DMF (20 mL) was stirred at 70 °C for 1 h. Then benzyl bromide (1.66 mL, 13.95 mmol) was added and the mixture was heated for 4 h. The mixture was cooled, diluted with water (100 mL), and extracted twice with 100 mL of AcOEt. The organic phases were washed twice with water (200 mL), dried over $MgSO_4$, filtered and evaporated under reduced pressure affording the desired product in 90% yield (3.05 g, 12.49 mmol) as a white solid. ^{1}H-NMR (400 MHz, $CDCl_3$) δ 7.45-7.37 (m, 5H, Ar), 7.32 (d, *J* = 3.0 Hz, 1H, Ar), 7.01 (dd, *J* = 8.9, 3.0 Hz, 1H Ar), 6.89 (d, *J* = 8.9 Hz, 1H, Ar), 5.37 (s, 2H, Bn), 4.46 (s, 2H, OH) ppm.

Benzyl 2,5-di(4'-butyloxybenzoyloxy)benzoate (**3**). A mixture of **2** (3.05 g, 12.49 mmol), 4-butyloxybenzoic acid (5.33 g, 27.38 mmol), DCC (5.67 g, 27.48 mmol) and DMAP (335 mg, 2.75 mmol) in dry CH_2Cl_2 (100 mL) was stirred at room temperature under Ar atmosphere for 12 h. The *N,N*-dicyclohexylurea was filtered and the filtrate was washed with water (100 mL), 5% acetic acid solution (100 mL) and water (100 mL). The organic layers were dried over Na_2SO_4, filtered and evaporated under reduced pressure. The crude material was recrystallized from ethanol affording the desired product in 81% yield (6.07 g, 10.17 mmol) as a white solid. ^{1}H-NMR (400 MHz, $CDCl_3$) δ 8.15-8.12 (m,2H, Ar), 8.08-8.06 (m, 2H, Ar), 7.91 (d, *J* = 2.9 Hz, 1H, Ar), 7.53 (d, *J* = 8.9 Hz,

1H, Ar), 7.46 (dd, *J* = 8.9, 2.9 Hz, 1H, Ar), 7.26-7.24 (m, 5H, Ar), 6.99-6.96 (m, 2H, Ar), 6.93-6.90 (m, 2H,Ar), 5.19 (s, 2H, Bn), 4.06 (t, *J* = 6.5 Hz, 4H, ArO-*CH_2*-A), 1.86-1.75 (m, 4H, aliphatic –CH_2-), 1.57-1.48 (m, 4H, aliphatic –CH_2-), 1.00 (t, *J* = 7.1 Hz, 6H, Me) ppm.

2,5-Di(4'-butyloxybenzoyloxy)benzoic acid (**4**). A solution of **3** (6.07 g, 10.17 mmol) in CH_2Cl_2 (150 mL) was hydrogenated in the presence of 10% Pd/C (600 g) for 48 h. The mixture was filtered through a Celite pad, washed with CH_2Cl_2 and evaporated to give the product in 89% yield (4.61 g, 9.10 mmol) as a white solid. ^{1}H-NMR (400 MHz, $CDCl_3$) δ 8.15-8.12 (m,4H, Ar), 7.94 (d, *J* = 2.7 Hz, 1H, Ar), 7.51 (dd, *J* = 8.6, 2.7 Hz, 1H, Ar), 7.30 (d, *J* = 8.6 Hz, 1H, Ar), 6.99-6.95 (m, 4H, Ar),4.08-4.03 (m, 4H, ArO-*CH_2*-A), 1.84-1.76 (m, 4H, aliphatic –CH_2-), 1.56-1.48 (m, 4H, aliphatic –CH_2-), 1.00 (t, *J* = 7.4 Hz, 6H, Me) ppm.

4-(Acryloyloxy)butyl 2,5-di(4'-butyloxybenzoyloxy)benzoate (**M_1**). A mixture of **4** (23.75 g, 46.88 mmol), 4-hydroxybutyl acrylate (7.44 g, 51.57 mmol), DCC (10.64 g, 51.57 mmol), and 4-pyrrolidinopyridine (764 mg, 5.16 mmol) in CH_2Cl_2 (250 mL) was stirred at room temperature under N_2 atmosphere for 12 h. The *N,N*-dicyclohexylurea was filtered and the filtrate was washed with water (200 mL), 5% acetic acid solution (200 mL) and water (200 mL). The organic layers were dried over Na_2SO_4, filtered and evaporated under reduced pressure. The crude was recrystallized from ethanol affording the desired product in 71% yield (19.99 g, 33.27 mmol) as a white solid. If the product still contains impurities, it can be purified by FCC (petroleum ether:AcOEt 6:1, R_f=0.6) and then recrystallized from ethanol. ^{1}H-NMR (300 MHz, $CDCl_3$) δ 8.18-8.14 (m, 4H, Ar), 7.86 (d, *J* = 2.7 Hz, 1H, Ar), 7.46 (dd, *J* = 8.8, 2.7 Hz, 1H, Ar), 7.30 (d, *J* = 8.8 Hz, 1H, Ar), 7.00-6.97 (m, 4H,Ar), 6.37 (dd, *J* = 17.3, 1.7 Hz, 1H, CH=C*H_2*), 6.08 (dd, *J* = 17.3, 10.4 Hz, 1H, C*H*=CH_2), 5.80 (dd, *J* = 10.4, 1.7 Hz, 1H, CH=C*H_2*), 4.21 (t, *J* = 6.2 Hz, 2H, ArCOOC*H_2A*-), 4.09-4.01 (m, 6H, -AOC*H_2A*-), 1.86-1.75 (m, 4H, aliphatic –C*H_2*-), 1.64-1.48 (m, 8H, aliphatic –C*H_2*-), 1.00 (t, *J* = 7.4 Hz, 6H, Me) ppm.

Methyl4-hydroxybenzoate (**6**). 4-Hydroxybenzoic acid (6 g, 43.4 mmol) in MeOH (60 mL) were taken in a 250 mL round bottom flask. Concentrated sulphuric acid (3 mL) was added and the mixture was refluxed for 12 h. A TLC control (petroleum ether:AcOEt 1:1) showed the disappearance of the starting material (R_f=0.35) and the appearance of a new product (R_f=0.47). The reaction mixture was cooled and methanol was removed under reduced pressure. The

residue was dissolved in CH_2Cl_2 and washed with a saturated aqueous solution of $NaHCO_3$. The organic layer was dried over anhydrous Na_2SO_4 and concentrated to give the product in 98% yield as a white solid (6.5 g, 42.7 mmol). ^{1}H-NMR (300 MHz, $CDCl_3$) δ 7.97-7.94 (m, 2H, Ar), 6.90-6.87 (m, 2H, Ar), 4.95 (br s, 1H, OH), 3.90 (s, 3H, Me) ppm.

Methyl4-[(6-hydroxyhexyl)oxy]benzoate (**7**). **6** (6.5 g, 42.7mmol) and 6-chloro-1-hexanol (7.0 g, 51.4 mmol) were dissolved into a mixture of K_2CO_3 (7.11 g, 51.4 mmol) and NaI (6.42 g, 42.7 mmol) in NMP (70 mL). After reaction at 85°C for 18 h, the mixture was poured into an excess of water and extracted with CH_2Cl_2 (3x50 mL). The combined organic layer was dried over anhydrous Na_2SO_4 and concentrated to obtain a white solid in 100% yield (10.77 g, 42.7 mmol). ^{1}H-NMR (300 MHz, $CDCl_3$) δ 7.98-7.96 (m, 2H,Ar), 6.91-6.88 (m, 2H, Ar), 4.03 (t, *J* = 6.5 Hz, 2H, ArOC*H*$_2$A), 3.88 (s, 3H, Me), 3.66 (t, *J* = 6.5 Hz, 2H, AC*H*$_2$OH), 1.86-1.77 (m, 2H, aliphatic –C*H*$_2$-) 1.66-1.44 (m, 6H, aliphatic –C*H*$_2$-) ppm.

4-[(6-Hydroxyhexyl)oxy]benzoic acid (**8**). **7** (2.0 g, 7.9 mmol) was dissolved in MeOH (25 mL) and stirred with KOH (1.5 g, 27.7mmol) at 50 °C for 18 h. Subsequently, MeOH was removed under reduced pressure, the residue was dissolved in water and acidified with diluted HCl to give a white precipitate. It was filtrated and washed with water to afford the product in 85% yield (1.6 g, 6.7 mmol) as white solid. ^{1}H-NMR (300 MHz, CD_3OD) δ 7.98-7.93 (m, 2H, Ar), 6.98-6.94 (m 2H, Ar), 4.05 (t, *J* = 6.4 Hz, 2H, ArOC*H*$_2$A), 3.56 (t, *J* = 6.5 Hz, 2H, AC*H*$_2$OH), 1.88–1.75(m, 2H, aliphatic –C*H*$_2$-), 1.61-1.43 (m, 6H, aliphatic–C*H*$_2$-) ppm.

4-[(6-Hydroxyhexyl)oxy]benzoic acid (**8**)**.** 4-Hydroxybenzoic acid (5 g, 36.1 mmol) was dissolved in a mixture of EtOH (36 mL) and water (7 mL). KOH (5.3 g, 94.1 mmol), KI (catalytic amount) and 6-chloro-1-hexanol (6.9 g, 50.6 mmol) were added and the solution was heated at reflux for 18 h. Then EtOH was removed under reduced pressure and the resulting mixture was poured into water and extracted with Et_2O. The water-phase solution was acidified with diluted HCl to give a white precipitate, which was filtrated and washed with water to afford the product in 79% yield (6.8 g, 28.5 mmol).

4-(3-Hydroxypropoxy)benzoic acid (**10**). It was synthesized in a single step by the same procedure described for **8** but using the 1-chloro-3-propanol. Yield: 55%; ^{1}H-NMR (300 MHz, CD_3OD) δ 7.96-7.94 (m, 2H, Ar), 6.99-6.97 (m 2H, Ar), 4.14 (t, *J* = 6.2 Hz, 2H, ArOC*H*$_2$A), 3.74 (t, *J* = 6.2 Hz, 2H, AC*H*$_2$OH), 2.00 (quint, *J* = 6.2 Hz, 2H, aliphatic –C*H*$_2$-)ppm.

4-[(8-Hydroxyoctyl)oxy]benzoic acid (**11**). It was synthesized in a single step by the same procedure described for **8** but using the 1-chloro-8-octanol. Yield: 74%; ^{1}H-NMR (300 MHz, CD_3OD) δ 7.96-7.94 (m, 2H, Ar), 6.97-6.94 (m 2H, Ar), 4.04 (t, *J* = 6.4 Hz, 2H, ArOC*H*$_2$A), 3.54 (t, *J* = 6.6 Hz, 2H, AC*H*$_2$OH), 1.83-1.76 (m, 2H, aliphatic –C*H*$_2$-), 1.53-1.37 (m, 10H, aliphatic –C*H*$_2$-) ppm.

*4-[6-(Acryloyloxy)hexyloxy]benzoic acid (***9**). To a solution of **8** (7.1 g, 29.8 mmol) in NMP (60 mL), acryloyl chloride (3 g, 32.8 mmol) was added dropwise and the mixture was stirred at room temperature for 3 h. Then water was added to give a white precipitate which was filtrated and washed thoroughly with water to afford the pure product in quantitative yield (8.7 g, 29.8mmol). ^{1}H-NMR (300 MHz, $CDCl_3$) δ 8.07-8.04 (m, 2H, Ar), 6.94-6.91 (m, 2H, Ar),6.40 (dd, *J* = 17.5, 1.5 Hz, 1H, CH=C*H*$_2$), 6.12 (dd, *J* = 17.5, 10.4 Hz, 1H, C*H*=CH$_2$), 5.82 (dd, *J* = 10.4, 1.5 Hz, 1H, CH=C*H*$_2$), 4.18 (t, *J* = 6.7 Hz, 2H, ArOC*H*$_2$A), 4.04 (t, *J* = 6.4 Hz, 2H, AC*H*$_2$OCO), 1.86-1.79 (m, 2H, aliphatic –C*H*$_2$-), 1.75-1.67 (m, 2H, aliphatic –C*H*$_2$-), 1.53-1.43 (m, 4H, aliphatic–C*H*$_2$-) ppm.

4-[3-(Acryloyloxy)propoxy]benzoic acid (**12**). It was synthesized by the same procedure described for **9** but starting from **10**. Yield: 93%; ^{1}H-NMR (400 MHz, $CDCl_3$) δ 8.07-8.05 (m, 2H, Ar), 6.95-6.93 (m, 2H, Ar), 6.42 (dd, *J* = 17.4, 1.4 Hz, 1H, CH=C*H*$_2$), 6.14 (dd, *J* = 17.4, 10.4 Hz, 1H, C*H*=CH$_2$), 5.84 (dd, *J* = 10.4, 1.4 Hz, 1H, CH=C*H*$_2$), 4.37 (t, *J* = 6.1 Hz, 2H, ArOC*H*$_2$A), 4.14 (t, *J* = 6.1 Hz, 2H, AC*H*$_2$OCO), 2.20 (quint, *J* = 6.1 Hz, 2H, aliphatic –C*H*$_2$-) ppm.

4-{[8-(Acryloyloxy)octyl]oxy}benzoic acid (**13**). It was synthesized by the same procedure described for **9** but starting from **11**. Yield: 100%; ^{1}H-NMR (400 MHz, $CDCl_3$) δ 8.06-8.04 (m, 2H, Ar), 6.94-6.92 (m, 2H, Ar),6.39 (dd, *J* = 17.4, 1.5 Hz, 1H, CH=C*H*$_2$), 6.12 (dd, *J* = 17.4, 10.4 Hz, 1H, C*H*=CH$_2$), 5.82 (dd, *J* = 10.4, 1.5 Hz, 1H, CH=C*H*$_2$), 4.16 (t, *J* = 6.5 Hz, 2H, ArOC*H*$_2$A), 4.02 (t, *J* = 6.4 Hz, 2H, AC*H*$_2$OCO), 1.84-1.77 (m, 2H, aliphatic –C*H*$_2$-), 1.69-1.64 (m, 2H, aliphatic –C*H*$_2$-), 1.49-1.37 (m, 8H, aliphatic–C*H*$_2$-) ppm.

4-Methoxyphenyl 4-{[6-(acryloyloxy)hexyl]oxy}benzoate (**M_3**). A mixture **9** (8.7 g, 29.8 mmol), 4-methoxyphenol (4.07 g, 32.8 mmol), DCC (6.77 g, 32.8 mmol), and 4-pyrrolidinopyridine (486 mg, 3.28 mmol) in dry CH_2Cl_2 (200 mL) was stirred at room temperature under N_2 atmosphere for 18 h. The *N*,*N*-dicyclohexylurea was filtered and the filtrate was washed with water (150 mL), 5% acetic acid solution (150 mL) and water (150 mL).The combined organic layers dried over Na_2SO_4, filtered and evaporated under reduced pressure to afford a crude that was purified by FCC (petroleum ether:AcOEt 8:1, then 4:1, then 2:1) to give the desired product in 79% yield (9.4 g, 23.6 mmol) as a white solid. ^{1}H-NMR (300 MHz, $CDCl_3$) δ 8.04-8.01 (m, 2H, Ar), 7.04-7.02 (m, 2H, Ar), 6.86-6.80 (m, 4H, Ar), 6.32 (dd, *J* = 17.0, 1.6 Hz, 1H, CH=CH_2), 6.04 (dd, *J*= 17.0, 10.5 Hz, 1H, C*H*=CH_2), 5.71 (dd, *J* = 10.5, 1.6 Hz, 1H, CH=CH_2), 4.08 (t, *J* = 6.6 Hz, 2H, ArOCH_2A), 3.88 (t, *J* = 6.5 Hz, 2H, ACH_2OCO), 3.66 (s, 3H, Me), 1.75-1.65 (m, 2H, aliphatic –CH_2-), 1.63-1.56 (m, 2H, aliphatic –CH_2-), 1.46-1.31 (m, 4H, aliphatic–CH_2-) ppm.

4-Methoxyphenyl 4-[3-(acryloyloxy)propoxy]benzoate (**M_2**). It was synthesized by the same procedure described for **M_3** but starting from **12**. The crude was recrystallized from EtOH affording the pure product in 47% yield. ^{1}H-NMR (400 MHz, $CDCl_3$) δ 8.15-8.13 (m, 2H, Ar), 7.13-7.10 (m, 2H, Ar), 6.98-6.92 (m, 4H, Ar), 6.42 (dd, *J* = 17.3, 1.4 Hz, 1H, CH=CH_2), 6.14 (dd, *J* = 17.3, 10.4 Hz, 1H, C*H*=CH_2), 5.85 (dd, *J* = 10.4, 1.4 Hz, 1H, CH=CH_2), 4.39 (t, *J* = 6.3 Hz, 2H, ArOCH_2A), 4.16 (t, *J* = 6.2 Hz, 2H, ACH_2OCO), 3.82 (s, 3H, Me), 2.21 (quint, *J* = 6.3 Hz, 2H,aliphatic –CH_2-) ppm.

4-Methoxyphenyl4-{[8-(acryloyloxy)octyl]oxy}benzoate (**M_4**). It was synthesized by the same procedure described for **M_3** but starting from **13**. The crude was recrystallized from EtOH affording the pure product in 38% yield. ^{1}H-NMR (400 MHz, $CDCl_3$) δ 8.15-8.12 (m, 2H, Ar), 7.12-7.10 (m, 2H, Ar), 6.97-6.92 (m, 4H, Ar), 6.40 (dd, *J* = 17.3, 1.5 Hz, 1H, CH=CH_2), 6.12 (dd, *J* = 17.3, 10.4 Hz, 1H, C*H*=CH_2), 5.82 (dd, *J* = 10.4, 1.5 Hz, 1H, CH=CH_2), 4.16 (t, *J* = 6.7 Hz, 2H, ArOCH_2A), 4.04 (t, *J* = 6.5 Hz, 2H, ACH_2OCO), 3.82 (s, 3H, Me), 1.86-1.78 (m, 2H, aliphatic –CH_2-), 1.70-1.65 (m, 2H, aliphatic –CH_2-), 1.50-1.38 (m, 8H, aliphatic –CH_2-) ppm.

2-Methyl-1,4-phenylenebis(4-{[6-(acryloyloxy)hexyl]oxy}benzoate) (**CL_3**). A mixture **9** (1.58 g, 5.4 mmol), methylhydroquinone (337 mg, 2.7 mmol), DCC

(1.23 g, 5.8 mmol), and 4-pyrrolidinopyridine (88 mg, 0.6 mmol) in dry CH_2Cl_2 (60 mL) was stirred at room temperature under N_2 atmosphere for 18 h. The *N,N*-dicyclohexylurea was filtered and the filtrate was washed with water (100 mL), 5% acetic acid solution (100 mL) and water (100 mL). The combined organic layers dried over Na_2SO_4, filtered and evaporated under reduced pressure to give a crude that was recrystallized from EtOH affording the pure product in 33% yield (611 mg, 0.9 mmol) as white solid. ^{1}H-NMR (400 MHz, $CDCl_3$) δ 8.17-8.12(m, 4H, Ar), 7.17 (d, *J* = 8.6 Hz, 1H, Ar), 7.13 (d, *J* = 2.7 Hz, 1H, Ar), 7.08 (dd, *J* = 8.6, 2.7 Hz, 1H, Ar), 6.99-6.95 (m, 4H, Ar), 6.39 (dd, *J* = 17.5, 1.4 Hz, 1H, CH=C*H*$_2$), 6.13 (dd, *J* = 17.5, 10.5 Hz, 1H, C*H*=CH_2), 5.82 (dd, *J* = 10.5, 1.4 Hz, 1H, CH=C*H*$_2$), 4.18 (t, *J* = 6.6 Hz, 4H, ArOC*H*$_2$A), 4.06 (t, *J* = 6.6 Hz, 2H, AC*H*$_2$OCO), 4.05 (t, *J* = 6.5 Hz, 2H, AC*H*$_2$OCO), 2.24 (s, 3H, Me), 1.88-1.81 (m, 4H, aliphatic –CH_2-), 1.76-1.69 (m, 4H, aliphatic –CH_2-), 1.56-1.45 (m, 8H, aliphatic –CH_2-) ppm.

2-Methyl-1,4-phenylene bis(4-{[6-(acryloyloxy)octyl]oxy}benzoate) (**CL_4**). It was synthesized by the same procedure for **CL_3** but starting from **13**.The crude was recrystallized from EtOH affording the pure product in 33% yield. ^{1}H-NMR (400 MHz, $CDCl_3$) δ 8.17-8.12 (m, 4H, Ar), 7.17 (d, *J* = 8.7 Hz, 1H, Ar), 7.13 (d, *J* = 2.6 Hz, 1H, Ar), 7.08 (dd, *J* = 8.7, 2.6Hz, 1H, Ar), 6.99-6.96 (m, 4H, Ar), 6.40 (dd, *J* = 17.2, 1.5 Hz, 1H, CH=C*H*$_2$), 6.12 (dd, *J* = 17.2, 10.4 Hz, 1H, C*H*=CH_2), 5.82 (dd, *J* = 10.4, 1.5 Hz, 1H, CH=C*H*$_2$),4.16 (t, *J* = 6.7 Hz, 4H, ArOC*H*$_2$A), 4.05 (t, *J* = 6.5 Hz, 2H, AC*H*$_2$OCO), 4.04 (t, *J* = 6.5 Hz, 2H, AC*H*$_2$OCO), 2.24 (s, 3H, Me), 1.86-1.79 (m, 4H, aliphatic –CH_2-), 1.70-1.60 (m, 4H, aliphatic –CH_2-), 1.50-1.39 (m, 16H, aliphatic –CH_2-) ppm.

Benzyl 4-(benzyloxy)benzoate (**14**). A mixture of 4-hydroxybenzoic acid (4.4 g, 31.8 mmol), benzyl bromide (9.5 mL, 79.5) and K_2CO_3 (10.9 g, 79.6) in dry DMF was left stirring at room temperature under N_2 atmosphere for 18 h. The mixture was then poured into water (300 mL) and extracted with AcOEt (2x300 mL). The combined organic layer was washed with water, dried over $NaSO_4$, filtered and evaporated under reduced pressure affording the product in 100% yield (10.1 g, 31.8 mmol) as a white solid. ^{1}H-NMR (300 MHz, $CDCl_3$) δ 8.06-8.01 (m, 2H, Ar), 7.45-7.35 (m, 10H, Ar), 7.00-6.95 (m, 2H, Ar), 5.33 (s, 2H, Bn), 5.11 (s, 2H, Bn) ppm.

4-(Benzyloxy)benzoic acid (**15**). A mixture of **14** (10.1 g, 31.8 mmol), KOH (8.9 g, 159 mmol) in water (50 mL) and EtOH (200 mL) was refluxed for 1 h. Ethanol was evaporated and the residue was poured into water (400 mL). The solution was acidified with HCl diluted until pH=1. The resulting precipitate was filtered, washed several times with water and dried affording the product in 88% yield (6.4 g, 28.0) as a white solid. ^{1}H-NMR (300 MHz, $CDCl_3$) δ 8.08-8.05 (m,2H, Ar), 7.45-7.35 (m, 5H, Ar), 7.04-6.99 (m, 2H, Ar), 5.14 (s, 2H,Bn) ppm.

4-Methoxyphenyl 4-(benzyloxy)benzoate (**16**). A mixture of **15** (1.59 g, 6.97 mmol), 4-methoxyphenol (951 mg, 7.66 mmol), DCC (1.58 g, 7.66 mmol), and 4-pyrrolidinopyridine (113 mg, 0.77 mmol) in dry CH_2Cl_2(50 mL) was stirred at room temperature under N_2 atmosphere for 18 h. The *N,N*-dicyclohexylurea was filtered and the filtrate was washed with water (50 mL), 5% acetic acid solution (50 mL) and water (50 mL). The organic layers were dried over Na_2SO_4, filtered and evaporated under reduced pressure. The crude product was recrystallized from EtOH affording the desired product in 81% yield (1.90 g, 5.68 mmol) as a white solid. ^{1}H-NMR (300 MHz, $CDCl_3$) δ 8.16-8.13 (m, 2H, Ar), 7.46-7.35 (m, 5H, Ar), 7.13-7.04 (m, 4H, Ar), 6.95-6.92 (m, 2H, Ar), 5.16 (s, 2H, Bn), 3.82 (s, 3H, Me) ppm.

4-Methoxyphenyl 4-hydroxybenzoate (**17**). A solution of **16** (1.90 g, 5.68 mmol) in CH_2Cl_2 (50 mL) was hydrogenated in the presence of 10% Pd/C (200 mg) for 48 h. The catalyst was filtered off, washed with CH_2Cl_2 and evaporated to give the product in 94% yield (1.30 g, 5.32 mmol) as a white solid. ^{1}H-NMR (300 MHz, $CDCl_3$) δ 8.13-8.09 (m, 2H, Ar), 7.13-7.09 (m, 2H, Ar), 6.94-6.90 (m, 4H, Ar), 3.82 (s, 3H, Me) ppm.

4-[(4-Methoxyphenoxy)carbonyl]phenyl 4-{[6-(acryloyloxy)hexyl]oxy}benzoate (**M_5**). A mixture of **9** (1.69 g, 5.80 mmol), **17** (1.30 g, 5.80 mmol), DCC (1.32 g, 6.38 mmol), and 4-pyrrolidinopyridine (94 mg, 0.64 mmol) in dry CH_2Cl_2 (100 mL) was stirred at room temperature under N_2 atmosphere for 18 h. The *N*,*N*-dicyclohexylurea was filtered and the filtrate was washed with water (100 mL), 5% acetic acid solution (100 mL) and water (100 mL). The organic layers were dried over Na_2SO_4, filtered and evaporated under reduced pressure. The crude product was recrystallized from EtOH affording the desired product in 79% yield (2.39 g, 4.61 mmol) as a white solid.^{1}H-NMR (400 MHz, $CDCl_3$) δ 8.27-8.25 (m, 2H, Ar), 8.16-8.13 (m, 2H, Ar), 7.36-7.34 (m, 2H, Ar), 7.14-7.12 (m, 2H, Ar),

6.98-6.93 (m, 4H, Ar), 6.40 (dd, *J* = 17.5, 1.5 Hz, 1H, CH=C*H*$_2$), 6.12 (dd, *J* = 17.5, 10.5 Hz, 1H, C*H*=CH$_2$), 5.82 (dd, *J* = 10.5, 1.5 Hz, 1H, CH=C*H*$_2$), 4.18 (t, *J* = 6.8 Hz, 2H, ArOC*H*$_2$A), 4.05 (t, *J* = 6.3 Hz, 2H, AC*H*$_2$OCO), 3.82 (s, 3H, Me), 1.85 (quint, *J* = 6.8 Hz, 2H, aliphatic –C*H*$_2$-), 1.73 (quint, *J* = 7.1 Hz, 2H, aliphatic –C*H*$_2$-), 1.56-1.45 (m, 4H, aliphatic–C*H*$_2$-) ppm; ^{13}C-NMR (50 MHz, $CDCl_3$) δ 164.8, 164.3, 163.7 (s, C=O), 157.8, 155.3, 144.4 (s, Ar), 132.4 (d, 2C, Ar), 131.7 (d, 2C, Ar), 130.5 (t, *C*H$_2$=CH), 128.5, 127.0 (s, Ar), 122.43- 122.0 (d, 5C, CH$_2$=*C*H, Ar), 121.1 (s, Ar), 114.6 (d, 2C, Ar), 114.4 (d, 2C, Ar), 68.2 (t, AO*C*H$_2$A), 64.4 (t, ArO*C*H$_2$A), 55.6 (q, Me), 29.0, 28.5 (t, aliphatic –*C*H$_2$-) 25.7 (t, 2C, aliphatic –*C*H$_2$-) ppm; IR ($CDCl_3$): 2921, 1733, 1603, 1507, 1256, 1194, 1160 1062 cm^{-1}; MS (ESI) *m/z*: 541.25 ([M+Na]+; 100); Anal. Calcd for $C_{30}H_{30}O_8$ (518.56): C 69.49, H 5.83; found C 69.14, H 5.80.

4-Benzyloxyphenol (**19**). Benzyl bromide (2.4 g, 14.0 mmol) was added dropwise to a stirred solution of hydroquinone (6 g, 35.1 mmol) and K_2CO_3 (1.9 g, 14.0 mmol) in acetone (60 mL). The mixture was heated at reflux for 18 h, filtered and washed with water (2x30 mL). The organic solution was dried over Na_2SO_4, filtered, evaporated under reduced pressure affording a crude that was purified by FCC (petroleum ether:AcOEt 2:1, R_f=0.39) to give the desired product in 51% yield (1.44 g, 7.2mmol) as a white solid. ^{1}H-NMR (300 MHz, $CDCl_3$) δ 7.41-7.36 (m, 5H, Ar), 6.89-6.73 (m, 4H, Ar), 5.01 (s, 2H, Bn) ppm.

1-Benzyloxy-4-(6-hydroxyhexyloxy)benzene (**20**). A stirred suspension of 6-chloro-1-hexanol (1.38 g, 10.1 mmol), K_2CO_3 (1.39 g, 10.1 mmol), and **19** (1.63 g, 8.14 mmol) in DMF (10 mL) was heated at 100 °C for 18 h. Water was added to give a white precipitate, which was filtrated and washed thoroughly with water. The crude was purified by FCC (petroleum ether:AcOEt 4:1, R_f=0.12) affording the pure product in 84% yield (1.95 g, 6.85 mmol) as a white solid. ^{1}H-NMR (300 MHz, $CDCl_3$) δ 7.40-7.33 (m, 5H, Ar), 6.92-6.78 (m, 4H, Ar), 5.00 (s, 2H, Bn), 3.90 (t, *J* = 6.5 Hz, 2H, ArOC*H*$_2$A), 3.65 (t, *J* = 6.5 Hz, 2H, AC*H*$_2$OH), 1.79-1.45 (m, 8H, aliphatic –C*H*$_2$-) ppm.

4-(6-Hydroxyhexyloxy) phenol (**21**). A solution of **20** (1.95 g, 6.85 mmol) in CH_2Cl_2 (50 mL) was hydrogenated in the presence of 10% Pd/C (150 mg) for 48 h. The catalyst was filtered off, washed with CH_2Cl_2 and evaporated to give the product in quantitative yield (1.33 g, 6.85 mmol). ^{1}H-NMR (300 MHz, $CDCl_3$) δ

6.76 (s, 4H, Ar), 3.89 (t, *J* = 6.4 Hz, 2H, ArOC*H*$_2$A), 3.66 (t, *J* = 6.4 Hz, 2H, AC*H*$_2$OH), 1.80-1.42 (m, 8H, aliphatic –C*H*$_2$-) ppm.

1-(Methoxycarbonyloxy)-4-(6-hydroxyhexyloxy)benzene (**22**). **21** (1.33 g, 6.85 mmol) was added, with vigorous stirring, to a solution of NaOH (685 mg, 17.12 mmol) in water (8 mL) maintained at 0 °C. Methyl chloroformate was added slowly to the resulting suspension keeping the temperature at 0 °C and then the reaction mixture was stirred at room temperature for 4 h. The reaction was adjusted to pH=1 by the addition of concentrated HCl. The product was extracted with CH_2Cl_2 and the organic solution was dried over Na_2SO_4 and evaporated to give the product in 64% (1.1 g, 4.36 mmol) as a white solid. ^{1}H-NMR (300 MHz, $CDCl_3$) δ 7.07-7.04 (m, 2H, Ar), 6.87-6.84 (m, 2H, Ar), 3.94 (t, *J*= 6.5 Hz, 2H, ArOC*H*$_2$A), 3.88 (s, 3H, Me), 3.66 (t, *J* = 6.4 Hz, 2H, AC*H*$_2$OH), 1.82-1.39 (m, 8H, aliphatic -C*H*$_2$-) ppm.

1-Methoxycarbonyloxy-4-(6-methacryloyloxyhexyloxy)benzene (**23**)**.** To a solution of **22** (1.1 g, 4.36 mmol) in dry CH_2Cl_2 (50 mL), TEA (1.8 mL, 13.8 mmol) and acryloyl chloride (0.53 mL, 6.53 mmol) were added, then the mixture was stirred at room temperature under N_2 atmosphere for 18 h. The solution was washed with water (3x20 mL) and the combined organic layers dried over Na_2SO_4, filtered and evaporated under reduced pressure affording the desired product in quantitative yield (1.41 g, 4.36 mmol) as a white solid. ^{1}H-NMR (300 MHz, $CDCl_3$) δ 7.07-7.04 (m,2H, Ar), 6.87-6.84 (m, 2H, Ar) 6.40 (dd, *J* = 17.4, 1.6 Hz, 1H, CH=C*H*$_2$), 6.11 (dd, *J* = 17.4, 10.3 Hz, 1H, C*H*=CH$_2$), 5.81 (dd, *J* = 10.3, 1.6 Hz, 1H, CH=C*H*$_2$), 4.17 (t, *J* = 6.6 Hz, 2H,AC*H*$_2$OCO), 3.94 (t, *J* = 6.4 Hz, 2H, ArOC*H*$_2$A), 3.88 (s, 3H, Me), 1.79-1.35 (m, 8H, aliphatic –C*H*$_2$-) ppm.

4-(6-Methacryloyloxyhexyloxy)phenol (**24**). **23** (1.41 g, 4.36 mmol) was stirred at room temperature for 6 h in a mixture of NH_3 33% and EtOH (1:6, 70 mL). The solvent was removed under reduced pressure and the crude was purified by FCC (petroleum ether:AcOEt 2:1, R_f=0.46) to give the desired product in 62% yield (713 mg, 2.70 mmol) as a colorless oil. ^{1}H-NMR (300 MHz, $CDCl_3$) δ 6.76 (s, 4H, Ar), 6.40 (dd, *J* = 17.4, 1.6 Hz, 1H, CH=C*H*$_2$), 6.11 (dd, *J* = 17.4, 10.3 Hz, 1H, C*H*=CH$_2$), 5.81 (dd, *J* = 10.3, 1.6 Hz, 1H, CH=C*H*$_2$), 4.16 (t, *J*= 6.4 Hz, 2H, AC*H*$_2$OCO), 3.88 (t, *J* = 6.4 Hz, 2H,ArOC*H*$_2$A), 1.79-1.35 (m, 8H, aliphatic –C*H*$_2$-) ppm.

4-{[6-(Acryloyloxy)hexyl]oxy}phenyl 4-{[6-(acryloyloxy)hexyl]oxy}benzoate (**CL_5**). A mixture of **9** (788 mg, 2.70 mmol), **24** (713 mg, 2.70 mmol), DCC (613 mg, 2.97 mmol), and 4-pyrrolidinopyridine (44 mg, 0.29 mmol) in of dry CH_2Cl_2 (50 mL) was stirred at room temperature under N_2 atmosphere for 18 h. The *N,N*-dicyclohexylurea was filtered and the filtrate was washed with water (100 mL), 5% acetic acid solution (100 mL) and water (100 mL). The combined organic layers dried over Na_2SO_4, filtered and evaporated under reduced pressure affording a crude that was purified by FCC (petroleum ether:AcOEt 4:1, R_f=0.33) to give the desired product in 61% yield (893 mg, 1.66 mmol) as a white solid. ^{1}H-NMR (300 MHz, $CDCl_3$) δ 8.14-8.11 (m, 2H, Ar), 7.11-7.08 (m, 2H, Ar), 6.97-6.89 (m, 4H, Ar), 6.40 (dd, *J* = 17.4, 1.6 Hz, 2H, CH=CH_2), 6.12 (dd, *J* = 17.4, 10.4 Hz, 2H, C*H*=CH_2), 5.82 (dd, *J* = 10.4, 1.6 Hz, 2H, CH=CH_2), 4.17 (t, *J* = 6.6 Hz, 4H, -CH_2O-), 4.04 (t, *J* = 6.4 Hz, 2H, -CH_2O-), 3.96 (t, *J* = 6.4 Hz, 2H, -CH_2O), 1.86-1.67 (m, 4H, aliphatic –CH_2-), 1.57-1.41 (m, 4H, aliphatic –CH_2-) ppm.

Benzyl 2,5-bis{[4-(benzyloxy)benzoyl]oxy}benzoate (**25**). A mixture of **4** (4.65 g, 19 mmol), **15** (10 g, 44 mmol), DCC (9.1 g, 44 mmol), and 4-pyrrolidinopyridine (565 mg, 3.8 mmol) in CH_2Cl_2 (300 mL) was stirred at room temperature under N_2 atmosphere for 18 h. The *N,N*-dicyclohexylurea was filtered and the filtrate was washed with water (200 mL), 5% acetic acid solution (200 mL) and water (200 mL). The organic layers were dried over Na_2SO_4, filtered and evaporated under reduced pressure. The crude material was recrystallized from toluene affording the desired product in 83% yield (10.5 g, 15.8 mmol) as a white solid. Mp 162 °C; ^{1}H-NMR (400 MHz, $CDCl_3$) δ 8.20-8.18 (m, 2H, Ar) 8.12-8.10 (m, 2H, Ar), 7.91 (d, *J* = 2.9 Hz, 1H, Ar), 7.48-7.36 (m, 12H, Ar), 7.27-7.25 (m, 5H, Ar), 7.11-7.09 (m, 2H, Ar), 7.05-7.03 (m, 2H, Ar), 5.19 (s, 2H, Bn), 5.17 (s, 4H, Bn) ppm; ^{13}C-NMR (50 MHz, $CDCl_3$) δ 164.8 (s, C=O), 164.5 (s, C=O), 163.8 (s, C=O), 163.3, 162.9 (s, 2C, Ar), 148.3 (s, 2C), 136.2, 136.1, 135.2 (s, 3C, Ar), 132.4 (d, 4C, Ar), 128.7-127.3 (17C, Ar), 125.0 (d, Ar), 124.6 (d, Ar), 121.8 (s, Ar), 121.5 (s, Ar), 114.8 (d, 2C, Ar), 114.7 (d, 2C, Ar), 70.2 (t, 2C, Bn), 67.2 (t, Bn) ppm; IR (KBr): *v* = 3683, 3620, 3022, 3016, 2975, 2894, 2434, 2399, 1521, 1475, cm^{-1}; ESI-MS *m/z* (%): 687.17 (100) [M+Na+]; Anal. calcd for $C_{42}H_{32}O_8$: C 75.89, H 4.85; found: C 75.53, H 4.48.

2,5-bis[(4-hydroxybenzoyl)oxy]benzoic acid (**26**). A solution of **25** (10.3 g, 15.5 mmol) in MeOH (350 mL) was hydrogenated in the presence of 10% Pd/C (1.2

g) for 48 h. The mixture was filtered through a Celite pad, washed with MeOH and evaporated. The crude material was recrystallized from a mixture acetone:toluene (1:2) affording the desired product in 79% yield (4.8 g, 12.2 mmol) as a white solid. Mp 206-209 °C; ^{1}H-NMR (400 MHz, CD_3OD) δ 8.07-8.03 (m, 4H, Ar), 7.82 (d, *J* = 2.9 Hz, 1H, Ar), 7.48 (dd, *J* = 8.8, 2.9 Hz, 1H, Ar), 7.31 (d, *J* = 8.8 Hz, 1H, Ar), 6.92-6.87 (m, 4H, Ar) ppm; ^{13}C-NMR (50 MHz, CD_3OD) δ 165.9 (s, C=O), 165.5 (s, C=O), 164.9, 162.9, 162.6, 148.4, 148.1 (s, 5C, Ar), 132.3 (d, 2C, Ar), 132.2 (d, 2C, Ar), 126.7 (d, Ar), 125.6 (s, Ar), 124.7 (d, Ar), 124.4 (d, Ar), 120.3 (s, Ar), 119.6 (s, Ar), 115.1 (d, 2C, Ar), 114.9 (d, 2C, Ar) ppm; IR (KBr): *v* = 3415, 3371, 1712, 1699, 1608, 1591, 1512, 1278cm^{-1}; ESI-MS *m/z* (%): 417.17 (98) [M+Na+]; Anal. calcd for$C_{21}H_{14}O_8$: C 63.96, H 3.58; found: C 63.50, H 3.29.

4-(acryloyloxy)butyl2,5-bis({4-[4-(acryloyloxy)butoxy]benzoyl}oxy)benzoate (**CL_6**). To an ice cooled solution of **26** (514 mg, 1.30 mmol), 4-hydroxybyutyl acrylate (0.72 mL, 5.2 mmol), PPh_3 (1.36 g, 5.2 mmol) in dry CH_2Cl_2 (200 mL) and DMF (40 mL) under N_2 atmosphere, was added DMEAD (1.22 g, 5.2 mmol). The mixture was stirred at room temperature for 18 h and then washed with water (2x200 mL). The organic layers were dried over Na_2SO_4, filtered and evaporated under reduced pressure. The crude material was purified by FCC (petroleum ether:AcOEt 1:1) and recrystallized from EtOH to give the desired product in 28% yield (282 mg, 0.36 mmol) as a white solid. ^{1}H-NMR (400 MHz, $CDCl_3$) δ 8.17-8.14 (m, 4H, Ar), 7.88 (d, *J* = 2.9 Hz,1H, Ar), 7.46 (dd, *J* = 8.7, 2.9 Hz, 1H, Ar), 7.27 (d, J = 8.8 Hz, 1H, Ar), 6.99-6.97 (m, 4H, Ar), 6.44-6.33 (m, 3H, CH=CH_2), 6.16-6.04 (m, 3H, C*H*=CH_2), 5.85-5.78 (m, 3H, CH=CH_2), 4.26 (t, *J* = 6.1 Hz, 4H, -CH_2O-), 4.21 (t, *J* = 6.2 Hz, 2H, -CH_2O-), 4.12-4.08 (m, 4H, -CH_2O-), 4.02 (t, *J* = 6.2 Hz, 2H, -CH_2O-), 1.96-1.89 (m, 8H, aliphatic –CH_2-), 1.66-1.57 (m, 8H, aliphatic –CH_2-), ppm; ^{13}C-NMR (50 MHz, $CDCl_3$) δ 166.2, 166.1, 164.8, 164.5, 164.0, 163.5 (s, 6C, C=O), 163.4(s, 2C, Ar), 148.3, 148.1 (s, 2C, Ar), 132.4 (d, 4C, Ar), 130.7 (t, 3C, C*H*=CH_2),128.4 (d, 3C, *C*H=CH_2), 127.2 (d, Ar), 125.0 (d, Ar), 124.8 (d, Ar), 121.6 (s,2C, Ar), 121.3 (s, Ar), 114.4 (d, 4C, Ar), 67.6 (t, 2C, -*C*H_2O-), 64.9 (t, , -*C*H_2O-), 64.0 (t, 2C, , -*C*H_2O-), 63.9 (t,, -*C*H_2O-), 25.8 (t, 2C, aliphatic –*C*H_2-), 25.4 (t, 2C, aliphatic –*C*H_2-), 25.1 (t, 2C, aliphatic –*C*H_2-) ppm; ESI-MS *m/z*(%): 795.33 (100) [M+Na+]; Anal. calcd. for $C_{42}H_{44}O_{14}$: C 65.28, H 5.74; found: C 64.96, H 5.40.

4-[(E)-(4-methoxyphenyl)diazenyl]phenol (**30**). A solution of 4-methoxyaniline (1 g, 8 mmol) in 10 mL of water and 5 mL of 37% HCl solution was cooled at 0 °C and some crushed ice were added. $NaNO_2$ (616 mg, 9 mmol) in water (5 mL) was added dropwise at 0-5 °C and the mixture was stirred for 15 min. Phenol (764 mg, 8 mmol) and NaOH (2.7 g) were placed in another flask, 10 mL of water were added and this solution was kept below 5 °C. Afterwards, the first solution of the diazonium salt was dropped slowly and after 30 min the azobenzene derivative was precipitated using 2 M HCl solution. The precipitate was filtered, washed with water and dried. The crude was purified by FCC (CH_2Cl_2, R_f=0.16) affording the desired product in 85% yield (1.56 g, 6.83 mmol) as a red solid. ^{1}H-NMR (300 MHz, $CDCl_3$) δ 7.89-7.86 (m, 2H, Ar), 7.85-7.82 (m, 2H, Ar), 7.02-6.99 (m, 2H, Ar), 6.95-6.92 (m, 2H, Ar), 3.50 (br s, 1H, OH), 3.85 (s, 3H, Me) ppm.

4-[(E)-(4-nitrophenyl)diazenyl]phenol (**31**). It was synthesized by the same procedure described for **30** but starting from 4-nitroaniline.The crude was recrystallized from EtOH affording the desired product in 62% yield as an orange solid. ^{1}H-NMR (300 MHz, $CDCl_3$) δ 8.38-8.35 (m, 2H, Ar), 7.99-7.92 (m, 4H, Ar), 6.99-6.97 (m, 2H, Ar) ppm.

6-{4-[(E)-(4-methoxyphenyl)diazenyl]phenoxy}hexan-1-ol (**32**). **30** (313 mg, 1.37 mmol) and 6-chlorohexan-1-ol (225 mg, 1.64 mmol) were dissolved into a mixture of K_2CO_3 (227 mg, 1.64 mmol) and NaI (205 mg, 1.37 mmol) in NMP (6 mL). After reaction at 85 °C for 4 h, water (30 mL) was added to give a precipitate which was filtrated and washed thoroughly with water affording the product in 89% yield (399 mg, 1.22 mmol) as a red solid. ^{1}H-NMR (300 MHz, $CDCl_3$) δ 7.89-7.85 (m, 4H, Ar), 7.02-6.97 (m, 4H, Ar), 4.04 (t, *J* = 6.5 Hz, 2H, ArOCH_2A), 3.89 (s, 3H, Me), 3.68 (t, *J* = 6.5 Hz, 2H, ACH_2OH), 1.87-1.80 (m, 2H, aliphatic –CH_2-), 1.65-1.41 (m, 6H, aliphatic –CH_2-) ppm.

6-{4-[(E)-(4-nitrophenyl)diazenyl]phenoxy}hexan-1-ol (**33**). It was synthesized by the same procedure described for **32** but starting from **31**. The crude was recrystallized from EtOH affording the desired product in 82% yield as a yellow solid. ^{1}H-NMR (300 MHz, $CDCl_3$) δ 8.38-8.35 (m, 2H, Ar), 7.99-7.95 (m, 4H, Ar), 7.04-7.01 (m, 2H, Ar), 4.09 (t, *J* = 6.4 Hz, 2H, ArOCH_2A), 3.69 (t, *J* = 6.4 Hz, 2H, ACH_2OH), 1.88-1.82 (m, 2H, aliphatic –CH_2-), 1.68-1.60 (m, 2H, aliphatic –CH_2-) 1.56-1.47 (m, 4H, aliphatic –CH_2-) ppm.

6-{4-[(E)-(4-methoxyphenyl)diazenyl]phenoxy}hexylacrylate (**D_1**). To a solution of **32** (399 mg, 1.22 mmol) in dry CH_2Cl_2 (20 mL), TEA (369 mg, 3.65 mmol) and acryloyl chloride (132 mg, 1.46 mmol) were added, then the mixture was stirred at room temperature under N_2 atmosphere for 2 h. The solution was washed with water (3x20 mL) and the organic layers dried over Na_2SO_4, filtered and evaporated under reduced pressure. The crude product was purified by FCC (petroleum ether:AcOEt 6:1, R_f=0.4) affording the desired product in 90% yield (420 mg, 1.10 mmol) as a red solid. ^{1}H-NMR (300 MHz, $CDCl_3$) δ 7.89-7.84 (m, 4H, Ar), 7.02-6.96 (m, 4H, Ar), 6.41 (dd, *J* = 17.3, 1.5 Hz, 1H, CH=C*H*$_2$), 6.13 (dd, *J* = 17.3, 10.3 Hz, 1H, C*H*=CH_2), 5.82 (dd, *J* = 10.3, 1.5 Hz, 1H, CH=C*H*$_2$), 4.18 (t, *J* = 6.5 Hz, 2H, ArOC*H*$_2$A), 4.04 (t, *J* = 6.7 Hz, 2H AC*H*$_2$OCO), 3.89 (s, 3H, Me), 1.88-1.79 (m, 2H, aliphatic –C*H*$_2$-), 1.75-1.68 (m, 2H, aliphatic –C*H*$_2$-), 1.60-1.47 (m, 4H, aliphatic –C*H*$_2$-) ppm.

6-{4-[(E)-(4-nitrophenyl)diazenyl]phenoxy}hexylacrylate (**D_2**). It was synthesized by the same procedure described for **D_1** but starting from **33**. The crude was washed several times with hot EtOH and hot water affording the pure product in 84% yield. ^{1}H-NMR (300 MHz, $CDCl_3$) δ 8.38-8.35 (m, 2H, Ar), 8.00-7.95 (m, 4H, Ar), 7.04-7.01 (m, 2H, Ar), 6.41 (dd, *J* = 17.2, 1.5 Hz, 1H, CH=C*H*$_2$), 6.13 (dd, *J* = 17.2, 10.3 Hz, 1H, C*H*=CH_2), 5.82 (dd, *J* = 10.3, 1.5 Hz, 1H, CH=C*H*$_2$), 4.19 (t, *J* = 6.6 Hz, 2H, ArC*H*$_2$A), 4.07 (t, *J* = 6.4 Hz, 2H, AC*H*$_2$OCO), 1.90-1.81 (m, 2H,aliphatic-C*H*$_2$-), 1.78-1.69 (m, 2H, aliphatic -C*H*$_2$-) 1.59-1.41 (m, 4H, aliphatic -C*H*$_2$-) ppm.

6-(N-Ethyl-N-phenylamino)hexan-1-ol (**36**). *N*-Ethylaniline (1 g, 8.25 mmol) and 6-chloro-1-hexanol (1.02 g, 7.43 mmol) were dissolved into a mixture of K_2CO_3 (1.14 g, 8.25 mmol) and NaI (1.24 g, 8.25 mmol) in DMF (10 mL). After reaction at 80 °C for 18 h the mixture was poured into an excess of water. The product was extracted from water with AcOEt (3x20 mL). Combined organic layers were dried over Na_2SO_4, filtered and evaporated under reduced pressure affording a crude that was purified by FCC (petroleum ether:AcOEt 4:1, R_f=0.22) to give the desired product in 72% yield (1.19 g, 5.38 mmol) as a yellow liquid. ^{1}H NMR (300 MHz, $CDCl_3$) δ 7.24-7.18 (m, 2H, Ar H), 6.68-6.60 (m, 3H, Ar H), 3.65 (t, *J* = 6.5 Hz, 2H, CH_2C*H*$_2$O), 3.36 (q, *J* = 7.0 Hz, 2H, CH_3C*H*$_2$N), 3.25 (pseudo t, *J* = 7.8 Hz, 2H, CH_2C*H*$_2$N), 1.64-1.54 (m, 4H, C*H*$_2$$CH_2$O, C*H*$_2$$CH_2$N), 1.44-1.36 (m, 4H, C*H*$_2$$CH_2$$CH_2$O, C*H*$_2$$CH_2$$CH_2$N), 1.15 (t, *J* = 7.0 Hz, 3H, C*H*$_3$$CH_2$N) ppm.

2-((E)-{4-[ethyl(6-hydroxyhexyl)amino]phenyl}diazenyl)-5-nitrobenzonitrile (**37**). 2-Amino-5-nitrobenzonitrile (387 mg, 2.37 mmol) was dissolved in a mixture of acetic:propionic acid (5:1, 6mL), cooled to 0 °C and nitrosylsulphuric acid (40 wt % solution in sulphuric acid, 753 mg, 2.37 mmol) added dropwise. The reaction mixture was stirred for 10 minutes then added dropwise to a mixture of **36** (525 mg, 2.37 mmol) in MeOH (12 mL) at 0 °C. After 30 minutes the resulting precipitate was filtered, washed with water and dried. The desired product was obtained pure in 75% yield (700 mg, 1.77 mmol) as a purple solid. ^{1}H NMR (400 MHz, $CDCl_3$) δ 8.59 (d, *J* = 2.5 Hz, 1H, Ar), 8.40 (dd, *J* = 9.1, 2.5 Hz, 1H, Ar), 7.98-7.96 (m, 3H, Ar), 6.73-6.71 (m, 2H, Ar), 3.67 (t, *J* = 6.3 Hz, 2H, CH_2CH_2O), 3.52 (q, *J* = 7.1 Hz, 2H, CH_3CH_2N), 3.42 (pt, *J* = 7.7 Hz, 2H, CH_2CH_2N), 1.72-1.57 (m, 4H, CH_2CH_2O, CH_2CH_2N), 1.48-1.38 (m, 4H, $CH_2CH_2CH_2O$, $CH_2CH_2CH_2N$), 1.26 (t, *J* = 7.1 Hz, 3H, CH_3CH_2N) ppm; ^{13}C NMR (50 MHz, $CDCl_3$) δ 157.89, 152.83, 145.97, 143.87 (s, 5C, Ar), 129.06, 128.12 (d, Ar), 117.68 (d, 3C, Ar), 115.76 (s, CN), 111.70, 111.55 (d, Ar), 62.75 (t, CH_2CH_2O), 50.82 (t, CH_2CH_2N), 45.71 (t, CH_3CH_2N), 32.61 (t, CH_2CH_2O), 27.62 (t, CH_2CH_2N), 26.86, 25.62 (t, $CH_2CH_2CH_2O$, $CH_2CH_2CH_2N$), 12.51 (q, CH_3CH_2N) ppm. IR (KBr): *ν* = 3409, 2929, 2856, 2356, 2320, 2229, 1598, 1519 cm^{-1}; ESI-MS *m*/*z* (%): 418.33 (66) [$M+Na^+$]; Anal. calcd for $C_{21}H_{25}N_5O_3$: C 63.78, H 6.37, N 17.71; found: C 63.56, H 6.21, N 17.42.

6-[{4-[(E)-(2-cyano-4-nitrophenyl)diazenyl]phenyl}(ethyl)amino]hexylacrylate (**D_3**). To a solution of **37** (435 mg, 1.10 mmol) in dry CH_2Cl_2 (38 mL), TEA (0.46 ml, 3.30 mmol) and acryloyl chloride (0.13 ml, 1.65 mmol) were added, then the mixture was stirred at room temperature under N_2 atmosphere for 2 h. The solution was washed with water (3x20 mL) and the combined organic layers dried over Na_2SO_4, filtered and evaporated under reduced pressure affording a crude that was purified by FCC (petroleum ether:AcOEt 4:1) to give the desired product in 85% yield (420 mg, 0.94 mmol) as a purple solid. ^{1}H NMR (400 MHz, $CDCl_3$) δ 8.54 (d, *J* = 2.5 Hz, 1H, Ar), 8.36 (dd, *J* = 9.1, 2.5 Hz, 1H, Ar), 7.95-7.91 (m, 3H, Ar), 6.71-6.68 (m, 2H, Ar), 6.40 (dd, *J* = 17.3, 1.4 Hz, 1H, $CH=CH_2$), 6.11 (dd, *J* = 17.3, 10.3 Hz, 1H, $CH=CH_2$), 5.82 (dd, *J* = 10.4, 1.4 Hz, 1H, $CH=CH_2$), 4.17 (t, *J* = 6.6 Hz, 2H, CH_2CH_2O), 3.51 (q, *J* = 7.1 Hz, 2H, NCH_2CH_3), 3.41 (pt, *J* = 7.7 Hz, 2H, CH_2CH_2N), 1.69 (dt, *J* = 13.7, 6.87 Hz, 4H, $CH_2CH_2CH_2O$, $CH_2CH_2CH_2N$) 1.50-1.42 (m, 4H, $CH_2CH_2CH_2O$, $CH_2CH_2CH_2N$), 1.26 (t, *J* = 7.1 Hz, 3H, NCH_2CH_3) ppm; ^{13}C NMR (50 MHz, $CDCl_3$) δ 166.29 (s, C=O), 157.81, 152.78, 145.92, 143.83 (s, 5C, Ar), 130.66 (t, CH_2=CH), 129.02-128.09

(d, 4C, CH_2=*C*H, Ar), 117.65 (d, 2C, Ar), 115.74 (s, CN), 111.70, 111.55 (d, Ar), 64.33 (t, CH_2*C*H_2O), 50.78 (t, CH_2*C*H_2N), 45.72 (t, CH_3*C*H_2N), 28.56, 27.54 (t, CH_2*C*H_2CH_2O, CH_2*C*H_2CH_2N), 26.68, 25.81 (t, *C*$H_2CH_2CH_2$O, *C*$H_2CH_2CH_2$N), 12.49 (q, *C*H_3CH_2N) ppm; IR (KBr): *v* = 3448, 2972, 2931, 2862, 2231, 1718, 1596, 1349 cm^{-1}; ESI-MS *m*/*z* (%): 472.17 (29) [M+Na^+]; Anal. calcd for $C_{24}H_{27}N_5O_4$: C 64.13, H 6.05, N 15.58; found: C 64.51, H 6.44, N 15.62.

(E)-4-[(4-butoxyphenyl)diazenyl]benzene-1,2-diol (**40**). A solution of 4-butoxyaniline (1.06 g, 6.41 mmol) in 10 mL of water and 5 mL of 37% HCl solution was cooled at 0 °C and some crushed ice were added. $NaNO_2$ (499 mg, 7.24 mmol) in water (5 mL) was added dropwise at 0-5 °C and the mixture stirred for 15 min. Resorcinol (1.94 g, 19.23 mmol) and NaOH (282 mg, 7.05 mmol) were placed in another flask, 10 mL of water were added and this solution was kept below 5 °C. Afterwards, the first solution of the diazonium salt was dropped slowly and after 1 h the azobenzene derivative was precipitated using 2 M HCl solution. The precipitate was filtered, washed with water and dried affording the desired product in 20% yield (361 mg, 1.26 mmol) as orange solid. ^{1}H-NMR (300 MHz, $CDCl_3$) δ 7.79-7.71 (m, 3H, Ar), 7.00-6.96 (m, 2H, Ar), 6.41 (dd, *J* = 8.8, 2.3 Hz, 1H, Ar), 6.52 (dd, *J* = 8.8, 2.3 Hz, Ar), 4.03 (t, *J* = 6.4 Hz, 2H, ArO-*CH_2*-A), 1.83-1.46 (m, 4H, aliphatic –CH_2-), 1.00 (t, *J* = 7.3 Hz, 3H, Me) ppm.

(E)-4-[(4-butoxyphenyl)diazenyl]-2-hydroxyphenyl4-butoxybenzoate (**41**). A solution of **40** (409 mg, 1.43 mmol), 4-butyloxybenzoic acid (277 mg, 1.43 mmol), DCC (354 mg, 1.71 mmol) and 4-pyrrolidinopyridine (25 mg, 0.17 mmol) in dry CH_2Cl_2(100 mL) was stirred at room temperature under N_2 atmosphere for 18 h. The *N,N*-dicyclohexylurea was filtered and the filtrate was washed with water (100 mL), 5% acetic acid solution (100 mL) and water (100 mL). The organic layers were dried over Na_2SO_4, filtered and evaporated under reduced pressure. The crude material was recrystallized from EtOH:toluene 4:1 affording the desired product in 72% yield (473 mg, 1.02 mmol) as an orange solid. ^{1}H-NMR (300 MHz, $CDCl_3$) δ 8.16-8.12 (m, 2H, Ar), 7.94-7.81 (m, 3H, Ar), 7.03-6.96 (m, 4H, Ar), 6.90-6.88 (m, 2H, Ar), 4.06 (t, *J* = 6.4 Hz, 4H, ArO-*CH_2*-A), 1.88-1.75 (m, 4H, aliphatic –CH_2-), 1.58-1.47 (m, 4H, aliphatic –CH_2-), 1.00 (t, *J* = 7.3 Hz, 6H, Me) ppm.

(E)-2-[4-(acryloyloxy)butoxy]-4-[(4-butoxyphenyl)diazenyl]phenyl 4-butoxy benzoate (**D_4**). To an ice cooled solution of **41** (387mg, 0.84 mmol), 4-hydroxybyutyl acrylate (241 mg, 1.67 mmol), PPh_3 (438 mg, 1.67 mmol) in dry CH_2Cl_2 (30 mL) under N_2 atmosphere, DIAD (338 mg, 1.67 mmol) was added dropwise. The mixture was stirred at room temperature for 18 h, then the solvent removed under reduced pressure and the residue was purified by FCC (petroleum ether:AcOEt 9:1, R_f=0.2) to give the desired product in 53% yield (263 mg, 0.45 mmol) as an orange solid. ^{1}H-NMR (300 MHz, $CDCl_3$) δ 8.17-8.13 (m, 2H, Ar), 7.92-7.88 (m, 2H, Ar), 7.74 (d, *J* = 8.8 Hz, 1H, Ar), 7.02-6.97 (m, 5H, Ar), 6.88 (dd, *J* = 8.8, 2.3 Hz, 1H,Ar), 6.41 (dd, *J* = 17.3, 1.7 Hz, 1H, CH=C*H*$_2$), 6.12 (dd, *J* = 17.3, 10.3 Hz, 1H, C*H*=CH$_2$), 5.81 (dd, *J* = 10.3, 1.7 Hz, 1H, CH=C*H*$_2$), 4.32-4.19 (m, 4H, -OC*H*$_2$-), 4.10-4.02 (m, 4H, -OC*H*$_2$-), 1.98-1.78 (m, 8H, aliphatic –CH$_2$-), 1.55-1.47 (m, 4H, aliphatic –CH$_2$-), 1.00 (t, *J* = 7.3 Hz, 6H, Me) ppm.

6-(4-nitrophenoxy)hexan-1-ol (**43**). 4-nitrophenol (1 g, 7.19 mmol) and 6-chloro-1-hexanol (1.12 g, 8.63 mmol) were dissolved into a mixture of K_2CO_3 (1.19 g, 8.63 mmol) in DMF (5 mL). After reaction at 100 °C for 18 h, water (30 mL) was added to give a precipitate which was filtrated and washed thoroughly with water affording the product in 82% yield (1.42 g, 5.93 mmol) as a yellow solid.^{1}H-NMR (300 MHz, $CDCl_3$) δ 8.21-8.26 (m, 2H, Ar), 6.96-6.90 (m, 2H, Ar), 4.04 (t, *J* = 6.4 Hz, 2H, ArOC*H*$_2$A), 3.65 (t, *J* = 6.5 Hz, 2H, AC*H*$_2$OH), 1.87-1.78 (m, 2H, aliphatic -C*H*$_2$-), 1.64-1.42 (m, 6H, aliphatic -C*H*$_2$-) ppm.

6-(4-aminophenoxy)hexan-1-ol (**44**). A solution of **43** (1.42 g, 5.93 mmol) in MeOH (30 mL) was hydrogenated in the presence of 10% Pd/C (150 mg) for 48 h. The catalyst was filtered off, washed with methanol and evaporated to give the product in 98% yield (1.22 g, 5.83 mmol) as a brown solid. ^{1}H-NMR (300 MHz, $CDCl_3$) δ 6.76-6.61 (m, 4H, Ar), 3.88 (t, *J* = 6.5 Hz, 2H, ArOC*H*$_2$A), 3.65 (t, *J* = 6.3 Hz, 2H, AC*H*$_2$OH), 1.79-1.72 (m, 2H, aliphatic -C*H*$_2$-), 1.63-1.38 (m, 6H, aliphatic -C*H*$_2$-) ppm.

4-((E)-{4-[(6-hydroxyhexyl)oxy]phenyl}diazenyl)phenol (**45**). A solution of **44** (793 mg, 3.79 mmol) in 7 mL of water and 3.5 mL of 37% HCl was stirred at room temperature for 18 h. Then the mixture was cooled at 0 °C, a solution of $NaNO_2$ (295 mg, 4.28 mmol) in water (3 mL) was added dropwise and the mixture stirred for 15 min. Phenol (357 mg, 3.79 mmol) and NaOH (1.2 g) were

placed in another flask, 7 mL of water were added and this solution was kept below 5 °C. Afterwards, the first solution of the diazonium salt was dropped slowly and after 1 h the azobenzene derivative was precipitated using 1 M HCl solution. The precipitate was filtered, washed with water and dried. The product was obtained in 85% yield (1.01 g, 3.21 mmol) and used in the next step without other purification. ^{1}H-NMR (300 MHz, $CDCl_3$) δ 7.88-7.80 (m, 4H, Ar), 7.00-6.91 (m, 4H, Ar), 4.04 (t, *J* = 6.5 Hz, 2H, ArOC*H*$_2$A), 3.68 (t, *J* = 6.5 Hz, 2H, AC*H*$_2$OH), 1.88-1.76 (m, 2H, aliphatic -C*H*$_2$-), 1.64-1.47 (m, 6H, aliphatic -C*H*$_2$-) ppm.

6,6'-[(E)-diazene-1,2-diylbis(4,1-phenyleneoxy)]dihexan-1-ol (**46**). **45** (1.29 g, 4.10 mmol) and 6-chloro-1-hexanol (672 mg, 4.92 mmol) were dissolved into a mixture of K_2CO_3 (679 mg, 4.92 mmol) in DMF (10 mL). After reaction at 100 °C for 18 h, water (60 mL) was added to give a precipitate which was filtrated and washed thoroughly with water affording the product in 91% yield (1.55 g, 3.74 mmol). ^{1}H-NMR (300 MHz, $CDCl_3$) δ 7.88-7.83 (m, 4H, Ar), 7.00-6.96 (m, 4H, Ar), 4.04 (t, *J* = 6.3 Hz, 4H, ArOC*H*$_2$A), 3.68 (t, *J* = 6.1 Hz, 4H, AC*H*$_2$OH,), 1.88-1.78 (m, 8H, aliphatic -C*H*$_2$-), 1.66-1.45 (m, 8H, aliphatic -C*H*$_2$-) ppm.

(E)-diazene-1,2-diylbis(4,1-phenyleneoxyhexane-6,1-diyl) bisacrylate (**D$_5$**). To a solution of **46** (1.55 g, 3.74 mmol) in dry CH_2Cl_2 (100 mL), TEA (2.26 g, 22.374 mmol) and acryloyl chloride (810 mg, 8.95 mmol) were added and then the mixture was stirred at room temperature under N_2 atmosphere for 4 h. The solution was washed with water (3x100 mL) and the organic layers dried over Na_2SO_4, filtered and evaporated under. The crude product was recrystallized from methanol affording the desired product in 67% yield (1.31 g, 2.51 mmol) as a yellow solid.^{1}H-NMR (300 MHz, $CDCl_3$) δ 7.90-7.85(m, 4H, Ar), 7.00-6.96 (m,4H, Ar), 6.41 (dd, *J* = 17.2, 1.6 Hz, 2H, CH=C*H*$_2$), 6.12 (dd, *J* = 17.2, 10.2 Hz, 2H, C*H*=CH$_2$), 5.80 (dd, *J* = 10.2, 1.6 Hz, 2H, CH=C*H*$_2$), 4.18 (t, *J*= 6.6 Hz, 4H, ArOC*H*$_2$A), 4.04 (t, *J* = 6.3 Hz, 4H,AC*H*$_2$OCO), 1.87-1.66 (m, 8H, aliphatic -C*H*$_2$-), 1.52-1.46 (m, 8H, aliphatic -C*H*$_2$-) ppm.

4-Amino-3,5-difluorobenzonitrile (**48**). A suspension of 2,6-difluoro-4-bromoaniline (1.59 g, 7.64 mmol) and CuCN (2.05 g, 22.93 mmol) in NMP (4 mL) was stirred at 160 °C under Ar atmosphere for 4 h. The mixture was poured into a NH_3 12% aqueous solution and then filtered through a Celite pad. After extraction with AcOEt (2x50 mL) the organic layers were washed

with water, dried over $MgSO_4$, filtered and concentrated under reduced pressure. The crude material was purified by FCC (hexane:AcOEt 4:1, R_f=0.32) to give **48** as a yellow solid in 80% yield (937 mg, 6.08 mmol). ^{1}H NMR (400 MHz, $CDCl_3$) δ 7.14 (dd, *J* = 6.1, 2.2 Hz, 2H, Ar), 4. 74 (brs, 2H, NH_2) ppm.

4-Amino-3,5-difluorobenzoic acid (**49**). A suspension of **48** (1 g, 6.48mmol) in NaOH 4M (40 mL) was stirred on reflux for 18 h. After cooling down to room temperature, HCl 1M was added until the precipitation of a product which was filtered, washed with water and dried. The product, obtained in 95% yield as a pale brown solid (1.07 g, 6.18 mmol) was used without any purification in the next step. ^{1}H NMR (400 MHz, DMSO) δ 7.39 (dd, *J* = 7.2, 2.4 Hz, 2H, Ar), 6.04 (br s, 2H, NH_2) ppm.

Ethyl 4-amino-3,5-difluorobenzoate (**50**). A solution of **49** (1.07 g, 6.18mmol) in EtOH (25 mL) and H_2SO_4 (0.5 mL) was stirred on refluxed 18 h. A saturated $NaHCO_3$ solution was added until pH=7 and the mixture was extracted with CH_2Cl_2. The organic phase was dried over $MgSO_4$, filtered and concentrated under reduced pressure. The product, obtained in 90% yield as a pale brown solid (1.12 g, 5.56 mmol) was used without any purification in the next step. ^{1}H NMR (400 MHz, $CDCl_3$) δ 7.53 (dd, *J* = 7.1, 2.1 Hz, 2H, Ar), 4.33 (q, *J* = 7.1 Hz, 2H, CH_2CH_3),4.13 (br s, 2H, NH_2), 1.37 (t, *J* = 7.1 Hz, 3H,CH_2CH_3) ppm.

Diethyl-4,4'-(2,2',6,6'-tetrafluoro)azobenzene dicarboxylate (**D_6**). A suspension of **50** (1.82 g, 9.05 mmol) and the oxidant mixture (30 g) in dry CH_2Cl_2(150 mL) was stirred on reflux for 24 h under Ar atmosphere. The oxidant was prepared by grinding equal amount in weight of $KMnO_4$ and $CuSO_4{\cdot}5H_2O$ in a mortar until to obtain a homogeneous powder. The solution was then filtered through a Celite pad, concentrated under reduced pressure and the residue was purified by recrystallization from ethanol to obtain **D_6** as a red solid in 33% yield (591 mg, 1.48 mmol). ^{1}H NMR (400 MHz, $CDCl_3$) δ 7.81-7.74 (m, 4H, Ar), 4.44 (q, *J* = 7.1 Hz, 4H, CH_2CH_3), 1.43 (t, *J* = 7.01 Hz, 6H, CH_2CH_3) ppm.

Chapter 3

Fabrication and optimization of the material: micro- and macro-scale experiments

3.1 Introduction

Researchers have long been fascinated by microscopic machines, obtained by different materials and fabrication processes, for their potential application as beams, cantilevers, gears, and membranes In present day technology, micromechanical systems have been deployed to perform mundane tasks, such as opening and closing valves, turning mirrors, regulating electric current or light flow.[66] The use of LCE microstructures would result a big improvement of microtechnologies thanks to the possibility to manage responses by different stimuli. Nowadays fabrication of LCE microstructures employs mainly soft-lithographic methods as the replica molding technique.[67] Free form microstructures are difficult to prepare limiting the potential use of LCEs in this scale.

Direct Laser Writing (DLW) is a versatile fabrication technique that can allow to overcome these drawbacks and to prepare LCE structures in different shapes, not obtained with other approaches. DWL has been already applied to create 2D LCE microstructures: Dorkenoo and co-workers demonstrated the possibility to prepare micro-patterns of such material and an increase of the resolution by two-photon initiation. The structures reported, with a resolution of 5 to 10 μm, showed a contraction of 20% of their length on heating above the nematic to isotropic transition temperature (T_{NI}).[68] These results were very promising even if the resolution of the process was limited, as well as was the control over the molecular alignment in the final structures. Moreover, only thermal responsive LCEs have been used with DLW, while more useful photoactive structures have never been fabricated with this technique.

Miniaturization of LCE structures is only the first step towards obtaining useful microactuators. Since the contraction occurs preferentially along the director, mesogen alignment in the LCE is another crucial aspect to control in order to improve the stimulated movement. Previous works on macroscopic samples

[66] K. L. Ekinci, M. L. Roukes, *Rev. Sci. Instrum.* **2005**, *76*, 061101.
[67] A. Buguin, M.-H. Li, P. Siolberzan, B. Ladoux, P. Keller, *J. Am. Chem. Soc.* **2006**, *128*, 1088.
[68] E. Sungur , M. Li , G. Taupier , A. Boeglin , M. Romeo , S. Méry , P. Keller , K. D. Dorkenoo , *Opt. Epress* **2007**, *15* , 6784.

use stretching of pre-polymerized film[69] or electric or magnetic fields to orientate LC monomers.[70]

Nematic LCs can be oriented by adequate treatment of the confining substrates: the use of sacrificial layers on polymerization cell surfaces can induce different alignment in the monomer mixture. In particular, molecules can take orientation either parallel to the glass plane (homogeneous orientation), perpendicular (homeotropic orientation) or tilted in respect to the plane of the cell (**Figure 21**).[4]

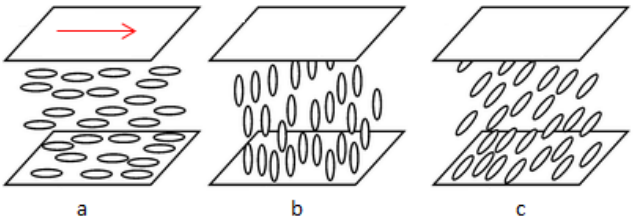

Figure 21 Homogeneous (a), homeotropic (b) or tilted (c) orientation of a nematic LC. The arrow shows the rubbing direction of the surface.

Homogeneous alignment is achieved by a thin, rubbed polymer layer on the glass substrate. First, polymers as polyimides, nylon-6,6 or polyvinyl alcohol (PVA), are spin coated on the glass. Then the surface is buffed unidirectionally with a cloth to deform the sacrificial layer and to form microgrooves along the rubbing direction (**Figure 22**): LCs tend to align along the direction of the microgrooves to give a planar alignment.[2]

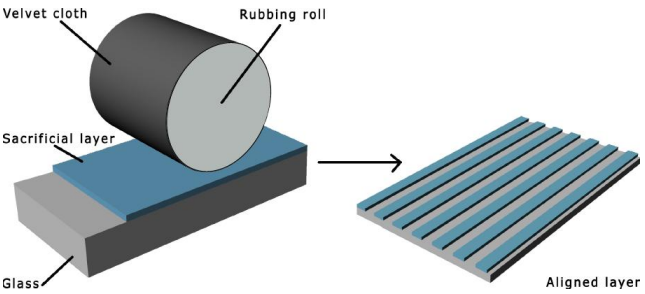

Figure 22 Rubbing process of a coated surface.

Homeotropic alignment is induced by agents able to create “a sea” of long alkyl chains that orient perpendicular to the plane of the glass. The surface is

[69] J. Kupfer, H. Finkelmann, *Macromol. Chem. Phys.* **1994**, *195*, 1353.
[70] O. Tetsuya, U. Kenji, T. Toshikazu, *Soft Matter* **2 011**, *7*, 10585.

generally coated with a surfactant, as lecithin or hexadecyltrimehylammonium bromide, or treated with other compounds able to form permanent bonds with the glass. Examples of these are the octylsilane or the octadecylsilane which are formed by reacting directly the corresponding alkyltrichlorosilane with the glass. Different tilted alignments can be obtained by coating with specific polyimides.[2]

Different bending behaviors are determined by different mesogen alignments in the film. For example, irradiation induces a bending toward the direction of the actinic light in homogeneous films, with a contraction on the film surface along the rubbing direction and an expansion on the perpendicular direction. In homeotropic films, the bent is away from the light source due to an expansion on the irradiated surfaces (**Figure 23**).[71]

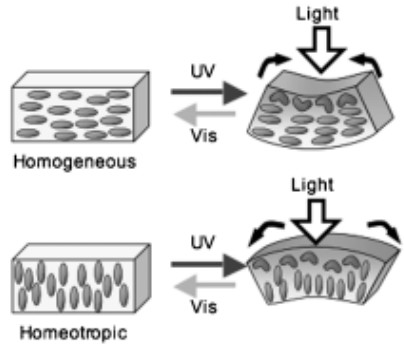

Figure 23 Bending in homogeneous and homeotropic films.

Scientists strived to engineer the molecular orientation also on the microscale and different approaches, such as photo-alignment,[72] ion beam irradiation,[73] and micro-rubbing[74] have been reported to generate surface micro patterns capable to align LCs. However, the micro pattern induced LC orientation techniques have never been integrated with DLW for fabrication of LCE structures. The possibility to control the alignment in the microscale allows to create structures containing different alignment regions, and then able to

[71] M. Kondo, Y. Yu, T. Ikeda, *Angew. Chem. Int. Ed*. **2006**, *45*, 1378.
[72] M. Schadt, H. Seiberle, A. Schuster, *Nature* **1996**, *381*, 212.
[73] Y. G. Kang, H. G. Park, H. J. Kim, Y. H. Kim, B. Y. Oh, B. Y. Kim, D. H. Kim, D. S. Seo, *Opt. Express* **2010**, *18*, 21594.
[74] S. Varghese, G. P. Crawford, C. W. M. Bastiaansen, D. K. G. de Boer, D. J. Broer, *Appl. Phys. Lett.* **2004**, *85*, 230.

asymmetric deformations, or to integrate on the same surface, actuators able to contract (or expand) in different directions under a single stimulus.

In this chapter, we discuss how to combine materials reported in Chapter 2 and DLW to obtain light driven microactuators. In particular, we report the fabrication of different 3D LCE structures with sub-micrometer resolution.
Moreover, different structures with local control of the molecular orientation were prepared by imprinting micro-grating patterns on the inside of a cell that also contains the components to create the elastomeric network.
Part of this chapter is instead dedicated to macroscopic film preparation. These studies on macroscale are interesting to better understand material properties and responses. We always conduced a parallel work on macroscopic sample useful for the optimization of the materials also for their use in the microscale.

3.2 Results and discussion

Preparation of LCE structures requires several steps. The first is the preparation of the monomer mixture that results very crucial to modulate polymer properties. The choice of the percentage and the structure of each molecule of the mixture is responsible for the transition temperatures of the final material which determine the range of use and hence the functionality of the LCE structure. These parameters are the glass transition temperature (T_g), the temperature in which the material transfer from glassy to LC state, and the LC to isotropic phase transition temperature (T_{LC-I}), above that the material lost the LC properties (order) resulting on a net contraction. T_g can be changed by the flexibility of the main chain and by the interaction between mesogens and the polymer backbone, as well as by interactions between mesogens. In addition, the crosslinker flexibility and its density play an important role on the glass transition temperature. T_{LC-I} depends mainly from the structure of mesogenic monomers and it can be modified by copolymerization of different LC or non-LC molecules.[11] Changing the mixture is possible also to modulate mechanical properties, as the contraction or the bending speed of the film.

The mixture is infiltrated in an appropriate cell and aligned in the nematic phase by cooling it from the isotropic liquid phase. The polymerization step requires different light sources depending on the initiator added to the mixture. To obtain microstructures, the laser of the DLW workstation is focused in the monomer mixtures allowing to create a voxel of polymer only near the focal volume. By scanning the position of the cell in respect to the focus of the laser, the desired 3D pattern is written point by point. After the writing process, the structure is developed by washing with an organic solvent: unpolymerized remainder of the mixture is removed, leaving on the cell surface only the fabricated structures.
Macroscopic film preparation proceeds by irradiation of the entire cell with an appropriate lamp to polymerize the mixture, then the obtained film is directly removed from the cell and cut in the desired form.
Every step of the LCE preparation is described in details below and relevant examples of materials are shown.

3.2.1. Cell preparation and alignment of the mixture

The cells used for LCE polymerization are generally composed by two glasses coated with a sacrificial layer and separated by apposite spacers (generally of 10, 20 or 50 µm) as shown in **Figure 24**.

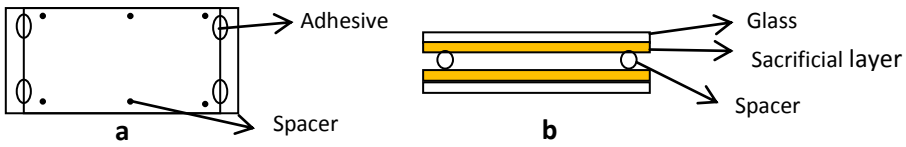

Figure 24 Cell for LCE preparation: top view (a) and lateral view (b).

To achieve the homogeneous alignment, we employed a coating made by a PVA aqueous solution or by polyimide PI130 (Nissan Chemical Industries) rubbed unidirectionally with a velvet cloth. The homeotropic alignment was reached by the use of the polyimide PI1211 (Nissan Chemical Industries), without any rubbing process.
Using different inner glass surfaces, we also prepared cells able to induce more complexes alignments of the LC mixture (**Figure 25**). For example, twisted alignments are generated using different rubbing directions for the two surfaces while the splayed alignment, in which molecules switch from homogeneous to homeotropic alignment trough the thickness of the sample, is reached by different coating materials for the two glasses.

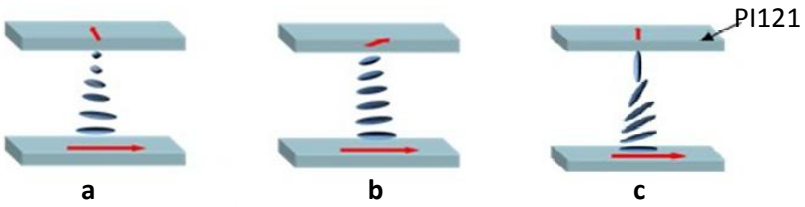

Figure 25 Different twisted alignments (a and b) and splayed alignment of a nematic LC. Arrows show the rubbing directions; surfaces are treated with PVA or PI1311 if not specified.

The monomer mixture was melted and infiltrated for capillarity in the cell. Cooling down slowly the cell from the isotropic to the nematic phase, the LC mixture organizes the desired alignment through epitaxial growth on the coating surface. Type and quality of the reached alignment are evaluated and checked by POM observation by measuring the trasmittance of the sample as function of the rotating angle in respect to the cross polarizer. In a

homogeneous LC, the trasmittance changes and regular maximum and minimum values are observed by rotation of 90° of the polarizer in respect to the rubbing direction, while a homeotropic LC shows a very low trasmittance without an angular dependence (**Figure 26**).[71]

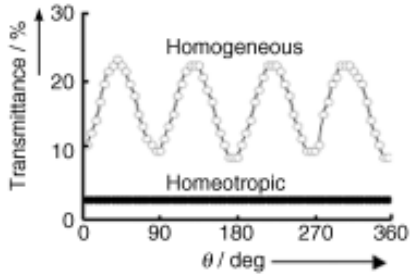

Figure 26 Optical properties of homogeneous and homeotropic LCs analyzed by POM.

As an example, **Figure 27** shows POM images of a cell infiltrated with a LC mixture (**E_3**, described in the next section) at different temperatures. The cell was prepared to obtain a homogeneous uniaxial alignment and a red filter was used during the observation in order to prevent the polymerization.

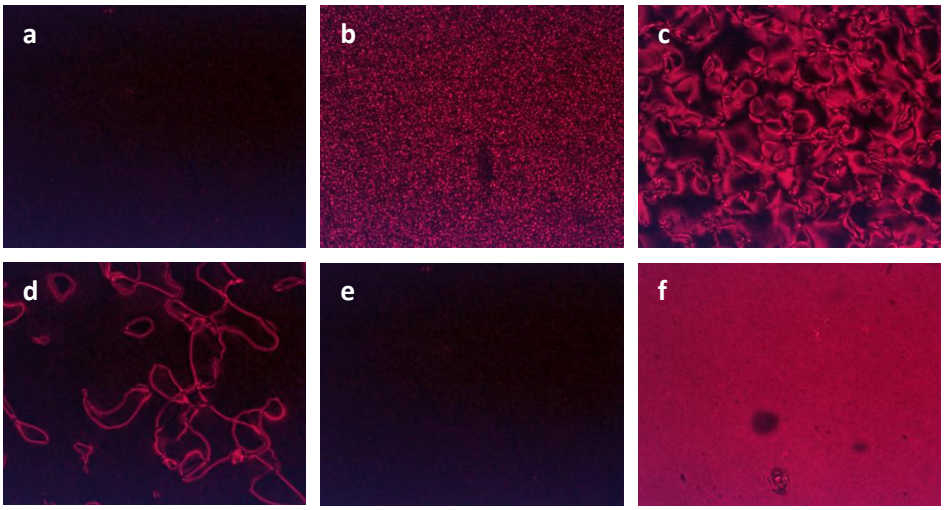

Figure 27 POM images collected on cooling from isotropic to nematic phase of the mixture E_3. a) isotropic phase; b) formation of the nematic phase; c) and d) growth of LC domains; e) monodomain homogeneous alignment; c) monodomain homogeneous alignment rotated 45° in respect to the polarizer.

Starting from the isotropic phase (**Figure 27a**), we cooled down slowly the sample observing first the formation of a LC phase (**Figure 27b**) and then the growth of different nematic domains (**Figure 27c-d**) until the final

monodomain was observed (**Figure 27e**). We verified that the alignment was homogeneous by observing a strong change in the trasmittance intensity when the sample was rotate of 45°in respect to the analyzer (**Figure 27f**). Temperature was maintained constant with the sample aligned for the polymerization step.

3.2.2. 3D printing of LCE microstructures

DLW experiments were carried out with the commercial workstation Photonic Professional of Nanoscribe GmbH. The instrument is equipped with a 780 nm femtosecond laser and the cell is installed onto a homemade heating stage fixed to the 3D piezo translation stage of the workstation.
To prepare photopolymerizable mixtures, we chose to use **Irgacure 369** (**IN_1**, 2-benzyl-2-(dimethylamine)-4'-morpholinobutyrophenone, **Scheme 29**) as UV photoinitiator as the two-photon absorption occurs at 390 nm with our working laser.

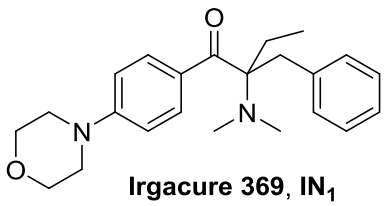

Irgacure 369, **IN_1**

Scheme 29 An UV photoinitiator.

In order to have a sort of reference, we performed the first DLW experiments with the mixture **E_1** (**Table 6**), already used by Dorkenoo et al.[68]

Mixture	Monomer	Crosslinker	Dye	Initiator
E_1	**M_1** (89%)	**CL_1**(10%)	-	**IN_1** (1%)

Table 6 First mixture for DLW. In bracket is reported the percentage in mol of each component.

Examples of the relative developed structures are shown in **Figure 28**. SEM images show patterns with lot of defects: the structures were very soft and they deformed greatly during the development with a consequent destruction of part of them and loss of resolution. Since the first fabrications, we noticed that main problems of this technique were the structure deformations during both writing and development with solvent. A high viscosity of the mixture is necessary to maintain the early produced volumes where they are created,

while a low viscosity facilitates the removal of unsolidified material during the development. Moreover, the use of harder LCE materials reduces the swelling of the structures allowing the fabrication of more complex 3D shapes.

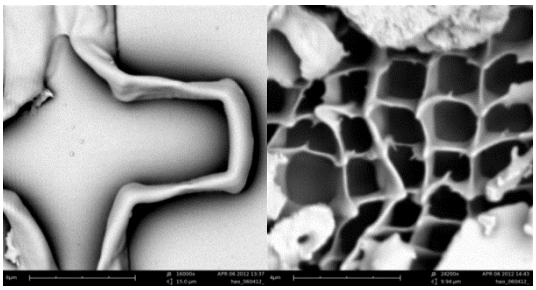

Figure 28 SEM images of DLW structures prepared with E_1.

We explored the DLW fabrication with different mixtures in order to find the best material for our fabrication technique. First, to investigate if a different LCE architecture could affect the resolution of the process, we prepared mixtures containing both the monomers $\mathbf{M_1}$ and $\mathbf{M_3}$ (**Scheme 30**): the resulting structures were more defined than the previous ones suggesting that "end-on" type polymers could give better results than "side-on" polymers. The result moved us to replace totally $\mathbf{M_1}$ with $\mathbf{M_3}$ in the mixture. $\mathbf{M_3}$ presents a metastable monotropic phase and the use of a LC crosslinker was required to improve the liquid crystalline properties of the mixture. For this reason we replaced also $\mathbf{CL_1}$ with $\mathbf{CL_2}$ (**Scheme 30**): the use of mixture $\mathbf{E_2}$ (**Table 7**) allowed finally to obtain the first good structures (**Figure 29**) encouraging us to develop further the writing process.

Mixture	Monomer	Crosslinker	Dye	Initiator
$\mathbf{E_2}$	$\mathbf{M_3}$ (78%)	$\mathbf{CL_2}$(20%)	-	$\mathbf{IN_1}$ (2%)

Table 7 A mixture based on an "end-on" monomer. In bracket is reported the percentage in mol of each component.

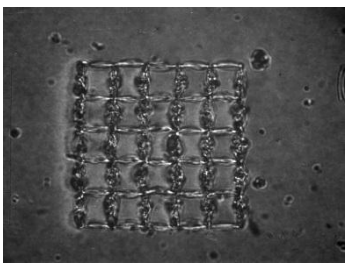

Figure 29 Optical image of a structure realized with E_2 before development.

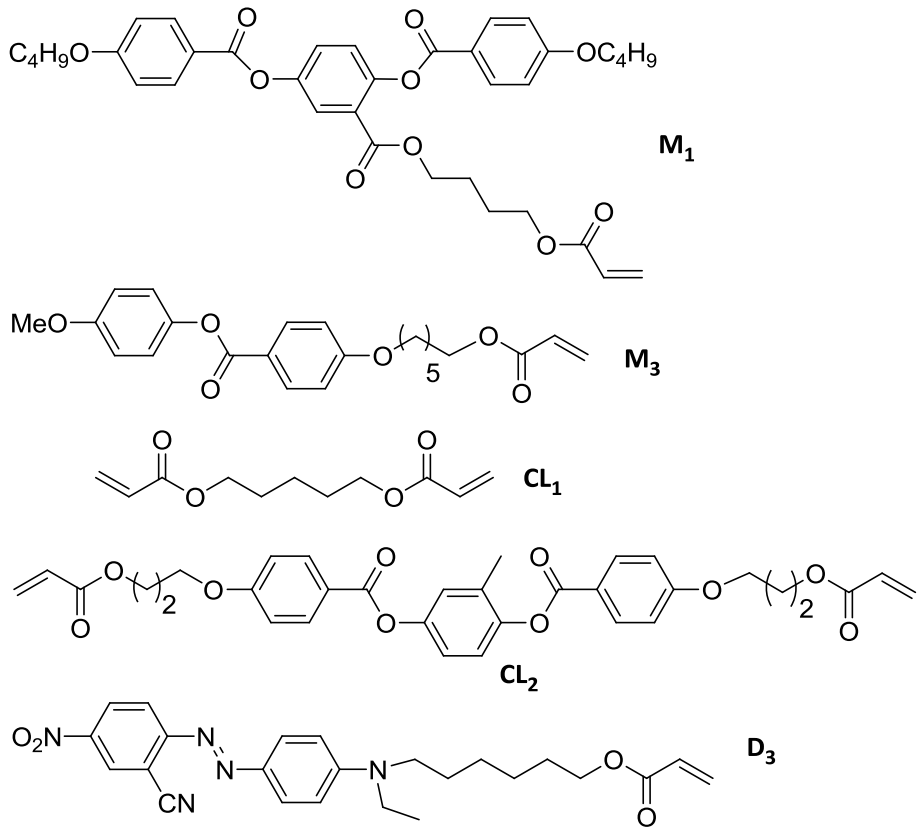

Scheme 30 Molecules used with DLW.

Mixture was further modified including an azobenzene dye in order to obtain a photoactive material. Since the dyes commonly used in LCE compositions[75] have the π-π* absorption band around 350 nm, they are not suitable for fabrication with our system, as this overlaps with the photoinitiator two-photon absorption peak. In **Figure 30** the absorption of $\mathbf{D_1}$ and $\mathbf{D_3}$ (**Scheme 31**) is compared: the first molecule is part of the just mentioned class of dye and actually, it cannot be used with our DLW equipment. To circumvent the problem, the azo-dye absorption has been tuned by changing the substituents on the aromatic rings: $\mathbf{D_3}$ satisfies all the requirement of the setup with a gap of minimum absorption around 390 nm and a transparency window above 700 nm. We included different percentage of this dye in the mixture $\mathbf{E_2}$ observing

[75] T. Ikeda, J.Mamiya, Y. Yu, *Angew. Chem. Int. Ed.* **2007**, *46,* 506.

that 1% of **D_3** was enough to obtain good deformation of structures under irradiation with a green wavelength.

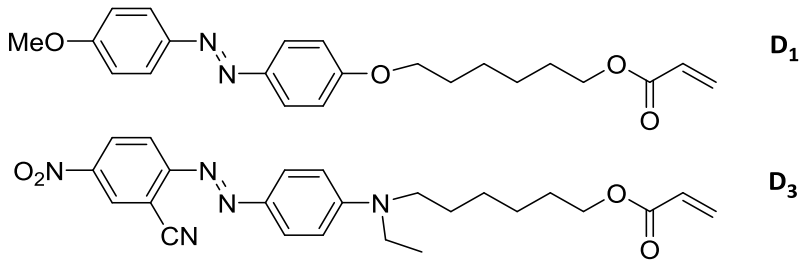

Scheme 31 Example of dyes.

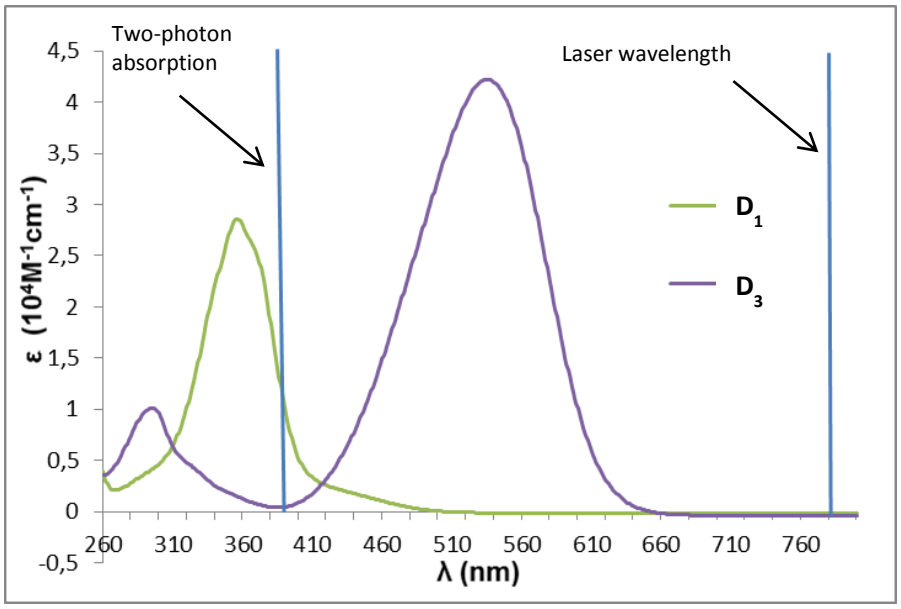

Figure 30 Absorption spectra of different dyes.

Finally, mixture **E_3** (**Table 8**) was successfully used to obtain many different microstructures: experiments described below were all realized with this mixture while the test of other ones is currently under evaluation.

Mixture	Monomer	Crosslinker	Dye	Initiator
E_3	**M_3** (78%)	**CL_2** (20%)	**D_3** (1%)	**IN_1** (1%)

Table 8 Mixture used in microfabrication. In bracket is reported the percentage in mol of each component.

To determine the best DLW process conditions, we performed a calibration experiment by writing a series of lines with different laser powers and writing speeds. The writing process was conducted on a cell treated to obtain homogeneous alignment of the mixture. A SEM photograph of the developed LCE lines (**Figure 31a**) shows the decrease in width with decreasing laser power and increasing writing speed. Polymerization thresholds appear at 1.8 mW at 15 μms^{-1}, 2.0 mW at 30 μms^{-1}, and 2.2 mW at 60 or 90 μms^{-1}, showing a minimum resolution for a free standing LCE structure of 300 nm near the threshold (**Figure 31b**). POM observation of the structures (**Figure 31c**) reveals a high ratio of the molecular alignment whit the relative change in the intensity of trasmittance by rotation of 45° of the sample in respect to the analyzer.[76]

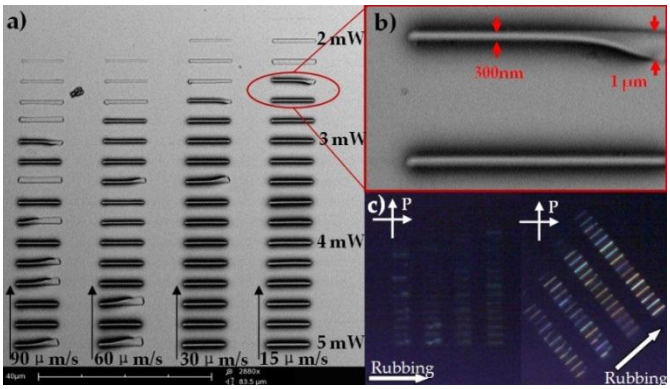

Figure 31 A calibration experiment. a) SEM image of LCE lines fabricated on the surface of a PI rubbed glass. Lines were written using powers ranging from 5.0 mW to 1.6 mW (bottom to top), and a speed of 15, 30, 60, 90 μms^{-1} (right to left); b) enlarged SEM image of two LCE linear structures fabricated around the threshold; c) POM image of LCE linear structures.

During the writing process, before the development, the structures always exhibit a certain degree of deformation probably due to the non-polymerized monomer penetrating into the laser written structures. After scanning the laser beam, the monomers are cross-linked within the laser scanning volume (voxel) and the surrounding non-polymerized monomers may penetrate into the LCE network, resulting in an anisotropic expansion perpendicular to the rubbing direction. Since the bottom sides of the LCE lines are fixed to the glass substrate, swelling only occurs on the top parts. For the LCE lines written perpendicular to the cell rubbing, swelling makes them curl (**Figure 32a**) while,

[76] H. Zeng, D. Martella, P. Wasylczyc, G. Cerretti, J.-C. Gomez Lavocat, C.-H. Ho, C. Parmeggiani, D. S. Wiersma, *Adv. Mater.* **2014**, *26*, 2319.

for those written along the rubbing, it makes them thicker, without any curl along the rubbing direction (**Figure 32b**).[76] Some curling was also observed after the laser scan (5 to 30 s) and may be related with the rate of the non-polymerized monomers diffusing into the LCE network. The swelling depends on the laser power: higher powers results in stronger LCE structures, exhibiting less swelling. Swelling brings a complication to 3D micro construction, as the swelled structure always moves out of the designed position during the writing process. Higher laser scanning speed and laser power become necessary to maintain the LCE structures in the designed position.

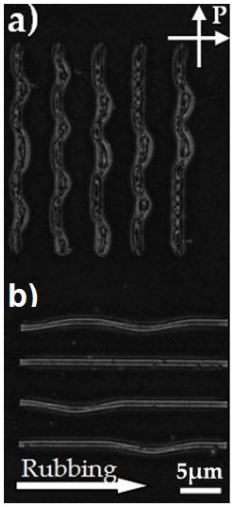

Figure 32 POM images of lines during DLW process (3 mW laser power, writing speed of 60 µms^{-1}): a) lines written perpendicular to the rubbing direction; b) lines written along the rubbing direction.

Based on preliminary studies, a power of 4 mW, and a writing speed of 60 µm s^{-1} have been chosen for the following fabrication processes and other 2D structures were prepared. A series of rings with the diameters ranging from 8 to 30 µm and the same height of 2 µm are shown in **Figure 33**.

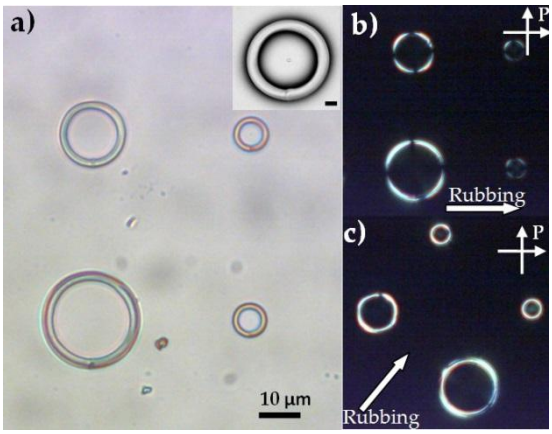

Figure 33 Optical image of LCE ring structures after developing. a) series of rings with diameter ranges from 30 to 8 µm. Inset: SEM image of the smallest ring structure. The scale bar in the SEM image is 1µm; b) POM image of LCE rings; the rubbing direction matches with the analyzer; c) POM image of LCE rings rotated by 45° respect to the analyzer.

The rings have the designed shape and flat surface (compare the SEM image in the inset of **Figure 33a**), and the molecular orientation along the cell rubbing direction (**Figure 33b-c**). In the micrometer length scale, light is strongly scattered by the surface topologies, which also changes the polarization of the transmitted light: as a result, birefringence does not only depend on LC molecular alignment, but also on the specific LCE structures. These kinds of LCE rings each contains tens of round circles, which act as a circular grating. Thus, we can observe a cross brightness pattern even when the rubbing direction is parallel to the analyzer (**Figure 33b**). The resolution of the structures exceed the previously reported for LCE microstructures but a true 3D fabrication capability was not yet demonstrated. [76]

For this purpose, a 40×40 μm^2, 4 layers woodpile structure was used as a testbed for the performance of the technique. The structure has been fabricated with a line pitch of 5 µm in the horizontal direction, and 1.3 µm separation between layers in the vertical direction, maintaining the molecular orientation within each single layer (**Figure 34**).[76]

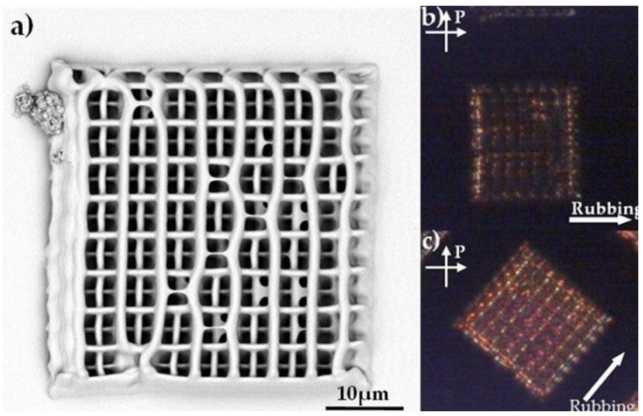

Figure 34 An example of 3D LCE structure. a) 4 layers woodpiles structure, with 5 µm lines distance in horizontal direction, and 1.3 µm distance between two consecutive layers; b) POM image of LCE woodpiles placed with the rubbing direction along the analyzer; c) POM image of LCE woodpiles rotated by 45° with respect to the analyzer.

An isotropic swelling was observed after development of the woodpile. Differently from the swelling during the laser writing, in this case, it depends on the solvent used and results in a broadening of each woodpile layer irrespective of the rubbing direction (see detail SEM image of the woodpile mentioned above in **Figure 35**). The first layer, which is in contact with the glass, has an average width of 0.7 µm. The second and third layers show an

average width of 1 µm, which can be understood from the fact that they are more distant from the substrate and hence have more freedom to move and expand. The maximum average woodpile width is 1.5 µm in the top layer, which is about 4 µm away from the substrate. The freedom on the top layer also results in missing rods and a few joined sections that we observe happens only during the development step. We believe that stickiness should be the main reason for irregular configuration after developing.

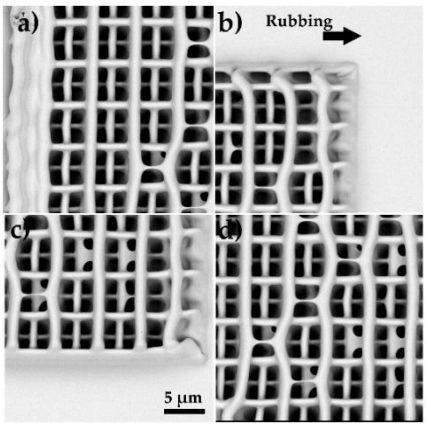

Figure 35 SEM images of the laser written 3D LCE structures. a) Left side; b) right upper corner; c) right bottom corner; d) center part of DLW LCE woodpile structure.

Another example of 3D structure is shown in **Figure 36a** while the capability of the system to undergo submicron resolution is shown in **Figure 36b**.[76]

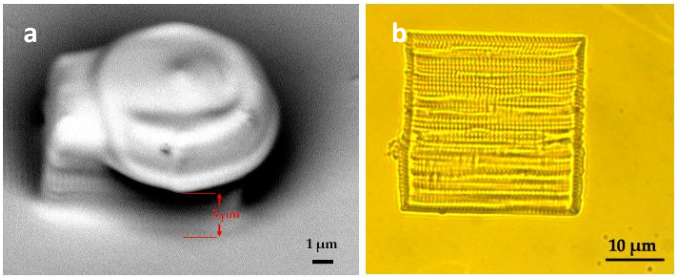

Figure 36 3D LCE structures. a) 45° oblique SEM image of a disk standing on an support, 3 µm above the ground; b) 30×30 μm^2 size forest structure written with a distance of 0.7 µm between two rows of columns in the horizontal direction.

In order to test the light induced deformation of the LCE microstructures, we used a cuboid structure of 100x100x40 μm^3 excited with a 532 nm solid state laser with controllable continuous ND filter (**Figure 37**). For power density above 1.6 Wmm^{-2} the structure shrinks along the rubbing direction and expands in the perpendicular one (**Figure 37b**) with a contraction of 8% in the

rubbing direction and an expansion of 5% in the perpendicular direction with a response time in the sub-second scale.

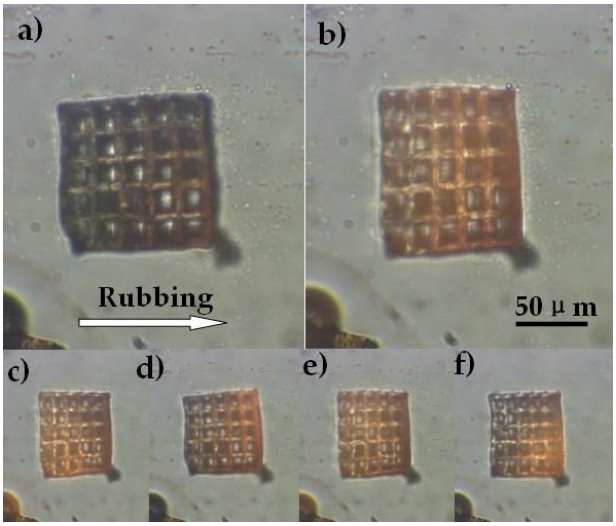

Figure 37 Light induced movement of 100x100x40 µm^3 size LCE actuator: a) no illumination; b) illuminated with a 532 nm laser incident on the center of the structure, with a 50 µm diameter focal spot and 1.6 Wmm^{-2} intensity. Different light induced deformations shining laser spot on left bottom corner (c), right up corner (d), left edge (e), and right bottom corner (f).

After switching off the laser, it returns to the original shape. When scanning the laser spot (about 50 µm in diameter) through different positions of the actuator, different deformations can be obtained (**Figure 37d-f**).

Another example of light actuation is shown in **Figure 38**: a cylinder structure, with 160 µm diameter and 40 µm height, is elongated vertically to the designed orientation under a laser excitation and deformed in an elliptic shape. After switching off the laser, it returns to its original shape. These results are the proof of principle that the dye has not been destroyed during the writing or development processes.[76]

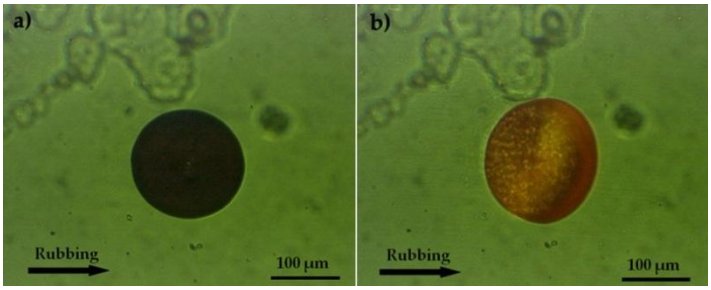

Figure 38 Light induced deformation of a LCE. a) No illumination; b) illuminated with a 532 nm laser incident on the center of the structure, with a 200 µm diameter focal spot and 6 Wmm^{-2} intensity.

DLW offers also the fascinating possibility to integrate different materials on the same surface: **Figure 39** shows a ring resonator coupled to a waveguide, both prepared with a commercial photoresist, and a block of LCE close to it. In this case, a two steps writing process was required. First, the coated glass cell was infiltrated with the commercial IP-G mixture and the relative structures were written. Then the non-polymerized material was washed away with solvents and the LCE mixture was infiltrated. At the end, the elastomeric block was written and developed with toluene. As an example, such LCE structures could be use to tune the properties of an optical circuit prepared with other polymeric materials.

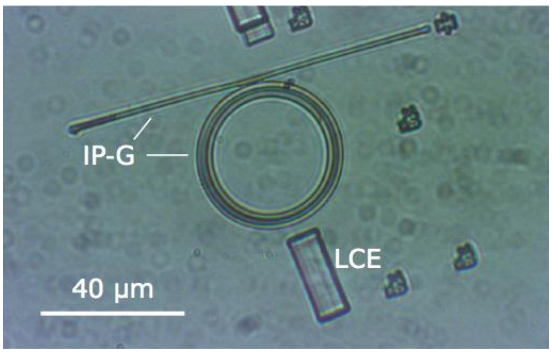

Figure 39 Optical image of a ring resonator coupled to a waveguide made by IP-G and a block of LCE close to them.

3.2.3. Local alignment control in LCE microstructures

The use of PI coated cells allows to create structures containing a determined alignment direction but local control of this in specific part of a structure is not possible. The problem can be exceeded with a different alignment technique, described below, which permits the control of the molecular orientation in selected domains of the sample.

We employed a commercial photopolymerizable material, IP-L, to create surface structures on both side of the cell able to generate different local alignment in the LC mixture. This method is another application of two-step writing processes that integrate different materials in the same glass cell.
First, a glass cell was filled with IP-L and micro-grating patterns were created by DLW on both internal surfaces the cell. The non-polymerized photoresist was removed with a solvent, leaving only the IP-L grating structures on the

glass substrates as shown in **Figure 40a**. The micro-gratings had a groove spacing of 600 nm (see the SEM image in **Figure 40b**) and the grooves are about 700 nm high (top-to-valley). Similar to the grooves created by rubbing of a PI coated surface, it has been demonstrated that this kind of grating structures can orient the LC molecules along the direction of such patterned surfaces.[77] Depending on the angle between the two gratings (written on the top and bottom cell surfaces) different LC alignments can be achieved.

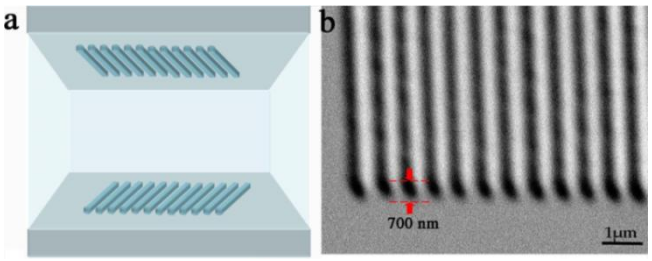

Figure 40 IP-L micro-grating used to induce liquid crystal orientation. a) Scheme of a glass cell with IP-L grating structures; b) SEM image of the micro-grating structure.

The use of different IP-L micrograting allows to prepare structures with different designed molecular orientation on the same glass surface. To test the potentiality of the method, we prepared four kinds of micro-grating pattern with 100×100 μm^2 size each on the opposite sides of a glass cell, as shown in **Figure 41a**. After fabrication of the grating patterns, the cell was infiltrated with the monomer mixture kept above the phase changing temperature and then cooled down to the nematic phase.

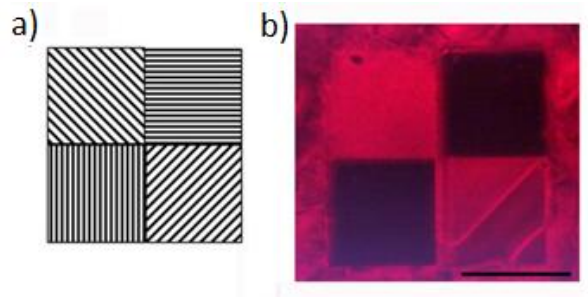

Figure 41 Example of 4 kind of micro-grating pattern. a) Scheme of the cell with different micro-grating patterns. b) POM image of the monomer mixture alignment induced by the micro-grating. A red filter is used to prevent the photopolymerization. The scale bar is 50 µm.

POM observation showed the different alignment in each regions, exhibiting a contrast in the trasmittance with 45° of inversion in respect to the alignment

[77] C. H. Lee, H. Yoshida, Y. Miura, A. Fujii, M. Ozaki, *Appl. Phys. Lett.* **2008**, *93*, 173509.

direction (**Figure 41b**): we observed a dark background in the 0° and 90° grating regions and a bright background in 45° and 135° regions.

POM images showed that the boundaries between two different alignments were always sharp, which indicates that the LC reorientation induced by IP-L micro-grating can reach high resolution, that which we estimate to be below 1 µm in a 50 µm thick cell (**Figure 42**).

Figure 42 POM image of the boundary between two alignment regions.

A series of LCE rings were fabricated by DLW with diameters ranging from 6 to 30 µm and the same height of 2 µm on each micro-grating region. **Figure 43** shows the optical images of the micro-rings before and after developing. During laser writing, the LCE structures exhibit swelling in the direction perpendicular to the molecular orientation which results in the elongation of the LCE rings, generating a discontinuity in the ring structures perpendicular to the grating (**Figure 43a**). After developing, the LCE structures stick onto the surface of the gratings and all the structures maintain the designed molecular orientation at room temperature, as shown by POM image (**Figure 43c**).

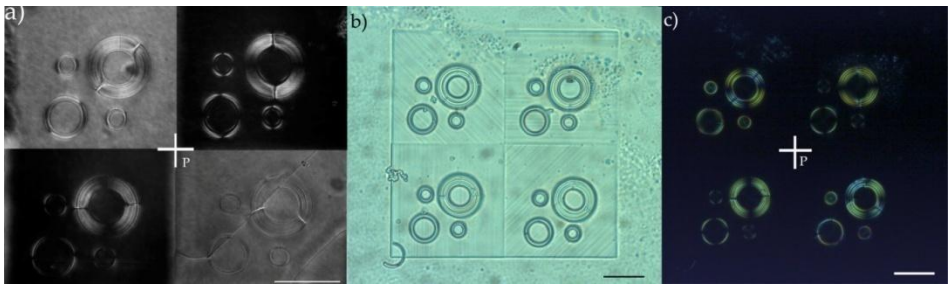

Figure 43 Optical images of the LCE micro rings with diameter from 6 to 30 µm fabricated in different grating orientation regions. a) POM image before the developing process; b) optical image after the development; c) POM image after development. The scale bars are 30 µm.

To demonstrate that such type of structures have a controlled deformation properties, we fabricated some LCE cylindrical structures of 60 µm diameter and 20 µm height within the four different micro-grating regions. After developing, all the LCE structures stand on the micro-gratings and maintain their circular shapes (**Figure 44a**). We observed some broken IP-L lines stuck on the top of the cylinders. A 532 nm laser was used to switch on the actuating

action of the structures: under irradiation, the deformation occurs along the chosen direction demonstrating the possibility to obtain different deformations in each region of the grating (**Figure 44b**). After switching off the laser, the cylinders return to their original shapes.

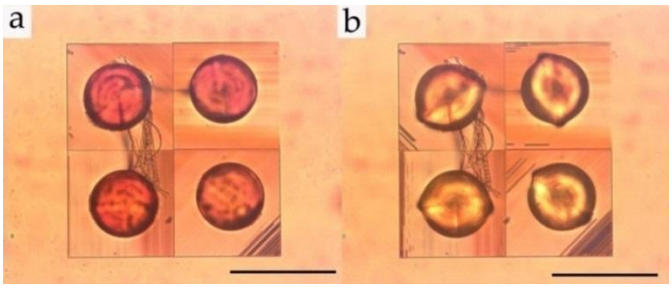

Figure 44 Light induced deformation of the structures with different alignment orientation. a) Four cylindrical structures with 60 µm diameter and 20 µm height, written on four differently orientated micro-grating regions. b) deformation of the structures when exposed to a 532 nm laser radiation, with a 200 µm diameter focal spot and 10 Wmm^{-2} intensity.

Similar cells can be used to prepare structures that contain within them different alignments. For example, we proposed to fabricate a stripe able to bend into opposite directions at the two ends under the same light excitation. We first created a cell with two pairs of crossed IP-L gratings, as shown in **Figure 45**, to generate two local region of different 90° twisted alignment.

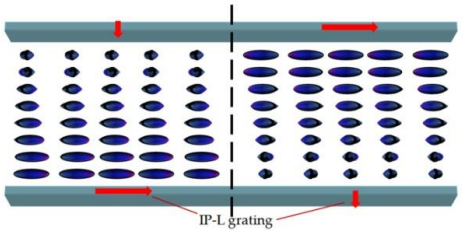

Figure 45 Double bending orientation pattern design.

The cell was used to write a LCE stripe (400 µm length, 40 µm width, 20 µm thickness) which contains the two desired orientations: the capability of the structure of a double bending is shown in **Figure 46** with the movement into opposite directions under excitation with 532 nm laser beam. This method allows free-form fabrication of elastomeric elements which can support multiple functionalities, and which cannot be fabricated with existing techniques.

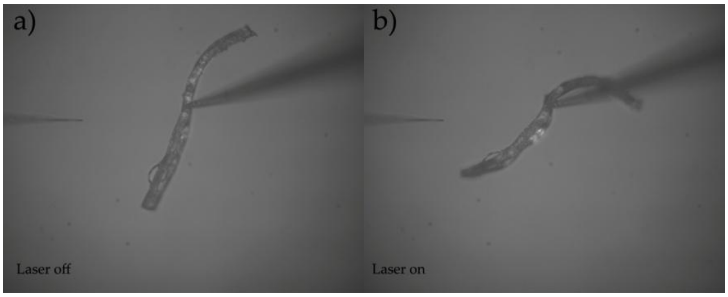

Figure 46 Deformation of a double bending LCE stripe. a) Stripe held on a glass tip in the air; b) stripe bends under excitation with 532 nm laser beam (intensity 3 Wmm^{-2}).

3.2.4. First examples of LCE nano-structures

With microtechnology now pushing deep into the submicron scale, versatile LCE properties received researchers' attention also in the nanoscale. However, structuring the material on this scale is a hard challenge and literature described only the preparation of liquid crystalline nanoparticles.[78]

We started exploring our fabrication technique also in the nanoscale. Actually the use of DLW to fabricate of LCE nano-structures results very difficult due to the limited mechanical stability of them and the capillary forces present during wet development process that often destroy structures also on the microscale, as described in the previous sections. Further, the swelling during the laser writing as well as in the solvent, becomes bigger decreasing the scale of the structures making difficult to maintain the designed configuration. Despite this, we recently found that within the IP-L micro-grating network the LCE structures become more confined, with much higher resistance to the development. As shown in **Figure 47**, four different gratings were first made and then LCE dots and lines with sub-micron size were fabricated, embedded inside the grating network. These gratings were 700 nm high and held the LCE structures in the designed position. The resolution of the nanostructures depends from the grating: the same LCE structures appeared to be of low quality while fabricated within a ~200 nm high grating.

Taking the advantage of such grating network, further studies could permit the real use of DLW to obtain different 3D nano-objects and the fabrication on large scale of LCE photonic structures becomes feasible.

[78] S. Tsoi, J. Zhou, C. Spillmann, J. Naciri, T. Ikeda, B. Ratna, *Macroml. Chem. Phys.* ***2*013**, *214*, 734.

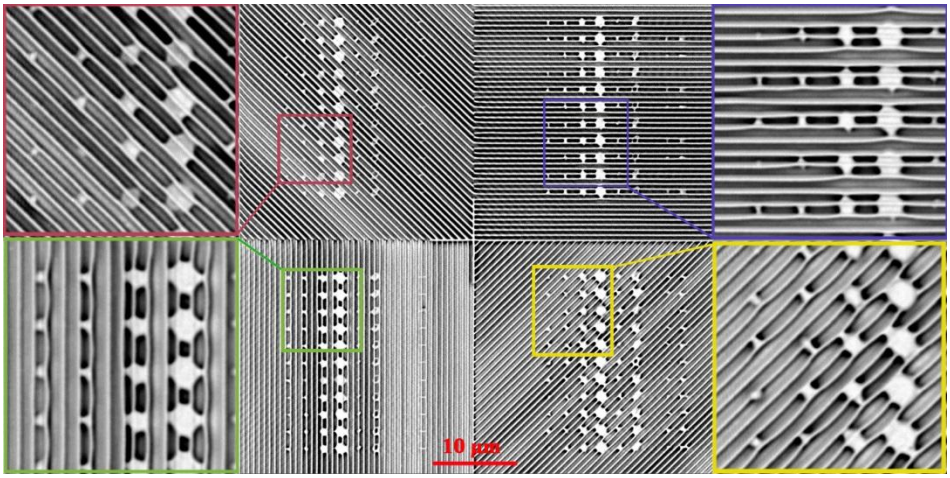

Figure 47 SEM images of LCE nano-structures. Four micro-grating patterns were fabricated along different directions with the same period of 600 nm and 700 nm height. LCE structures were made embedded inside the grating network.

3.2.5. Toward material optimization: macroscopic films evaluation

Characterization of LCE microstructures is very difficult and macroscopic samples can be prepared in order to study thoroughly material properties. Preparation of different LCE films and comparison between their properties can clarify the relationship between the composition of the monomer mixture and polymer properties. Moreover, this study is the starting point to obtain better material for DLW: exploring different mixtures in order to improve both resolution and mechanical responses of microstructures, remains one of our main goal.

With the results obtained with mixture **E_3** in our hands, we modified the composition to explore the effect on changing the crosslinking density and the crosslinker structure. More rigid networks, obtained by the use of higher percentage of crosslinker or by the use a trifuncional one, could give, in principle, better resolution in the DLW, with less shrinkage during the writing process and less modification after development. On the other hand, these systems present only small contractions limiting the applicability of the material. The optimal mixture is the one that allows the best compromise between these two opposite effects.

We tested a change in the percentage of **CL_2** from the reference mixtures (10% and 40% in respect to the 20% already used) and the use of the trifunctional molecule **CL_6** (**Scheme 32**) in the different percentages (10, 20 and 40%). Composition of the different mixtures is shown in **Table 9**.

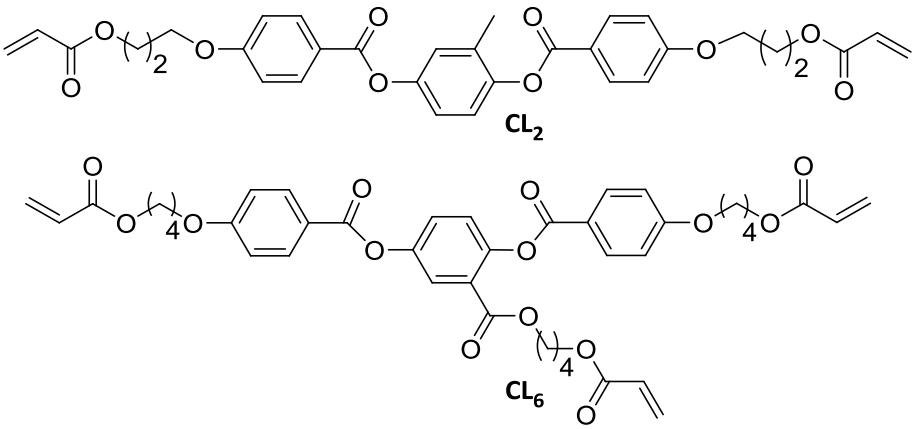

Scheme 32 Crosslinkers used for film preparation

Mixture	Monomer	Crosslinker	Dye	Initiator
E_3	**M_3** (78%)	**CL_2** (20%)	**D_3** (1%)	**IN_1** (1%)
E_4	**M_3** (88%)	**CL_2** (10%)	**D_3** (1%)	**IN_1** (1%)
E_5	**M_3** (58%)	**CL_2** (40%)	**D_3** (1%)	**IN_1** (1%)
E_6	**M_3** (88%)	**CL_6** (10%)	**D_3** (1%)	**IN_1** (1%)
E_7	**M_3** (78%)	**CL_6** (20%)	**D_3** (1%)	**IN_1** (1%)
E_8	**M_3** (58%)	**CL_6** (40%)	**D_3** (1%)	**IN_1** (1%)

Table 9 Different mixtures with CL_2 and CL_6. In bracket is reported the percentage in mol of each component.

We prepared films using the cells treated to obtain the splayed alignment of the LC mixture: a PI1311 coating was used on the bottom glass while, the top one was covered whit a rubbed PVA layer. Splayed films are able to generate bigger deformation than the uniaxial ones resulting the most efficient alignment for the bending of a structure.[79]

Polymerization was carried out with an UV lamp (385 nm): a suitable irradiation time was determined using the mixture **E_3**. It was infiltrated in different cells and then they were irradiated for different times (1, 2.5 and 5 minutes). The resulting films were removed and immersed in toluene for 8 h.

[79] M. Kondo, J. Mamiya, M. Kinoshita, T. Ikeda, Y. Yu, *Mol. Cryst. Liq. Cryst.* **2007***, 478*, 245.

At the end, the solvent was evaporated and the residue analyzed by ^{1}H-NMR: only if the polymerization was not completed we could observe signals of the non-polymerized monomers in the spectrum. For polymers prepared by irradiation for 1 or 2.5 minutes we observed a release of monomers in toluene while, after 5 minutes of irradiation, monomer signals were not detected demonstrating a complete polymerization.

Therefore, different films were prepared by irradiation for 5 minutes. Then the cells were opened and the samples directly removed from the glass surface and studied without further purifications. POM observation confirmed that alignment of the monomer mixtures was conserved in the final materials.
Thermal properties were evaluated by DSC measurements that should provide transition temperatures of the material. Film DSC traces on heating are reported in **Figure 48**. Unfortunately, the measurements show only T_g, reported in **Table 10**, while T_{NI} are not detected in the experiments.

Film	T_g [°C][b]
E_4 (10% CL_2)	13.6
E_3(20% CL_2)	21.4
E_5 (40% CL_2)	29.7
E_6 (10% CL_6)	16.9
E_7 (20% CL_6)	19.2
E_8 (40% CL_6)	45.7

Table 10 Glass transition temperature of some LCE films. [b]Determined from the midpoint of the baseline jump in second heating scan of the DSC trace.

As expected, a higher percentage of crosslinker results in the increase of T_g. The trifunctional molecule **CL_6** leads to comparable values of T_g that **CL_2** when used in the same percentage, despite **E_8** presents a strong increase of the temperature in respect to the other samples.

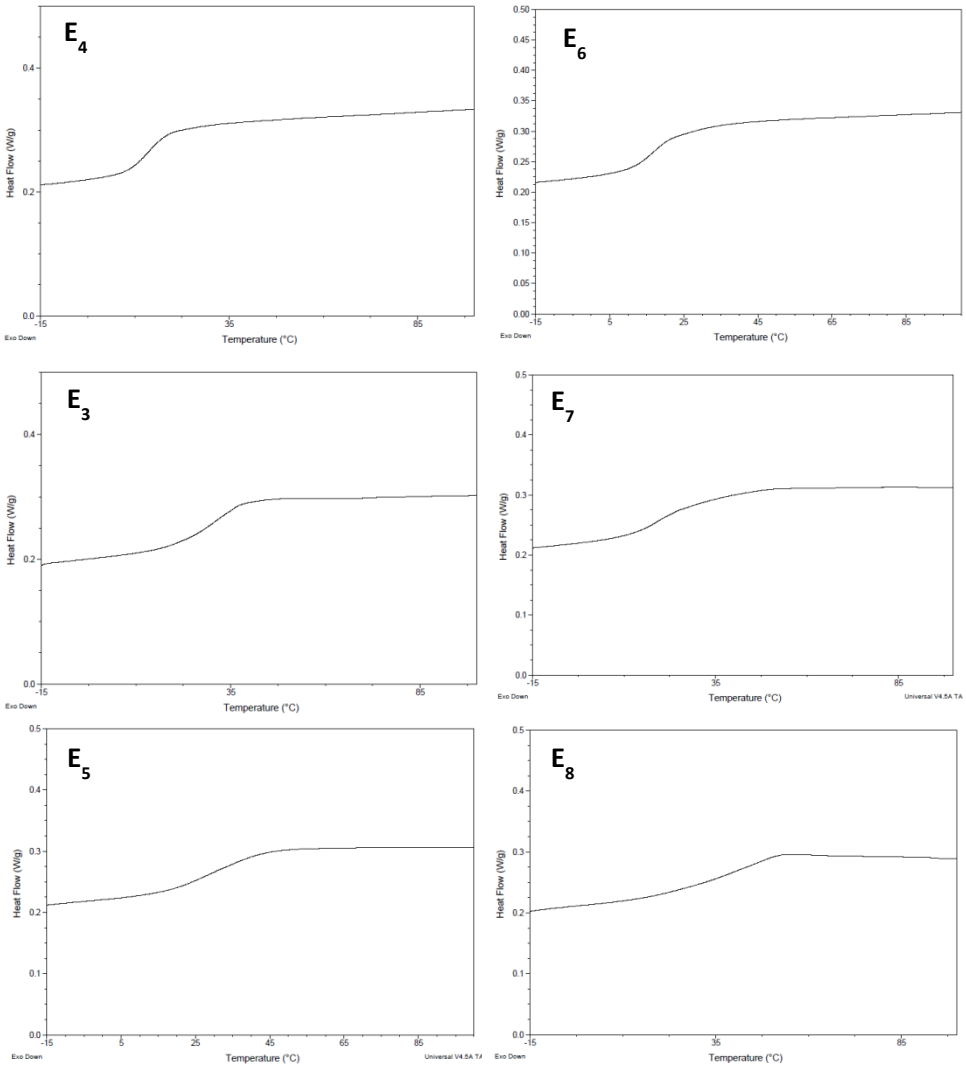

Figure 48 DSC traces (10 °C/min) corresponding to the second cycle of heating of films containing CL_2 or CL_6.

Film photoresponsivity was studied on samples with dimensions of 2x0.5 cm. Materials were cut to have the longest side of the film piece correspondent to alignment direction of the homogeneous surface. They were clamped on one side, with the other left free to move, and then irradiated with a 532 nm laser. Some pictures of response to irradiation of $\mathbf{E_3}$ are shown in **Figure 49**. As expected, irradiation on the homogeneous surface causes a bending towards the light sources, while irradiation on the homeotropic one causes the bending in the opposite direction.

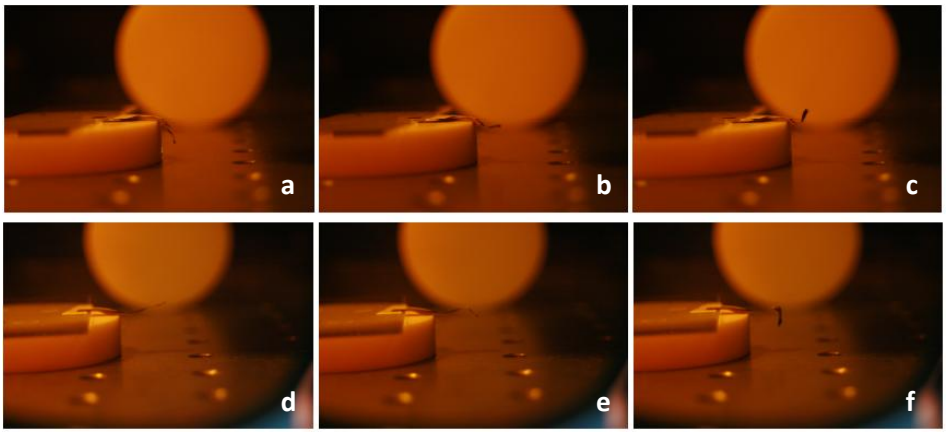

Figure 49 Photoinduced bending of a LCE stripe (E_3). The pictures were taken during the irradiation with light at 532 nm placed on the top of the sample. Wavelength was shined first on the homogeneous surface (**a**, **b** and **c**) and then on the homeotropic surface (**d**, **e** and **f**).

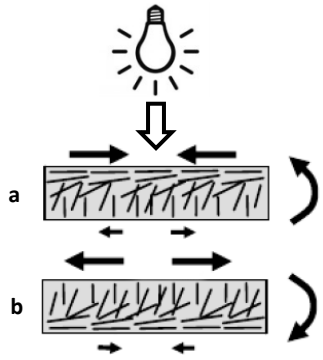

As result, the film bent always to the homogeneous side independently on the irradiated one (**Figure 50**) and then, bending speed can be enhanced by simultaneously irradiation on both surfaces.

Figure 50 Movement of a splayed sample irradiated on the homogeneous surface (a) or on the homeotropic one (b).

Comparing movement of films with **CL_6** (**Table 11**), we observe lower and slower deformation for more crosslinked samples, reflecting the increase of T_g and the hardness of the material. The same trend is observed for films containing **CL_2**.

Film	Angle $_{max}$ [°]	Time $_{max}$ [s]
E_6 (10% CL_6)	180	2.0
E_7 (20% CL_6)	110	2.0
E_8 (40% CL_6)	90	3.3

Table 11 Angle of maximum bending and time to reach this deformation in film with CL_6 under 532 nm irradiation. Data were obtained from images taken with a digital camera (3 frames/s).

Moreover, the higher crosslinking density obtained with the trifunctional crosslinker leads to smaller deformations: **Table 12** shows a comparison

between films containing 20% of different crosslinker demonstrating bigger deformation for the one containing **CL_2**.

Film	Angle $_{max}$ [°]	Time $_{max}$ [s]
E_3 (20% CL_2)	180	2.0
E_7 (20% CL_6)	110	2.0

Table 12 Comparison between bending in film with CL_2 and CL_6. Angle of maximum bending and time to reach the deformation under 532 nm irradiation were obtained from images taken with a digital camera (3 frames/s).

Shining off the irradiation, stripes recovered the initial position showing that movements were completely reversible even after many cycles of irradiation and relaxation. The complete bending-unbending sequence for a sample of **E_3** is shown in **Figure 51**. Recovery of the initial position was generally slower than the bending of about 0.7 s.

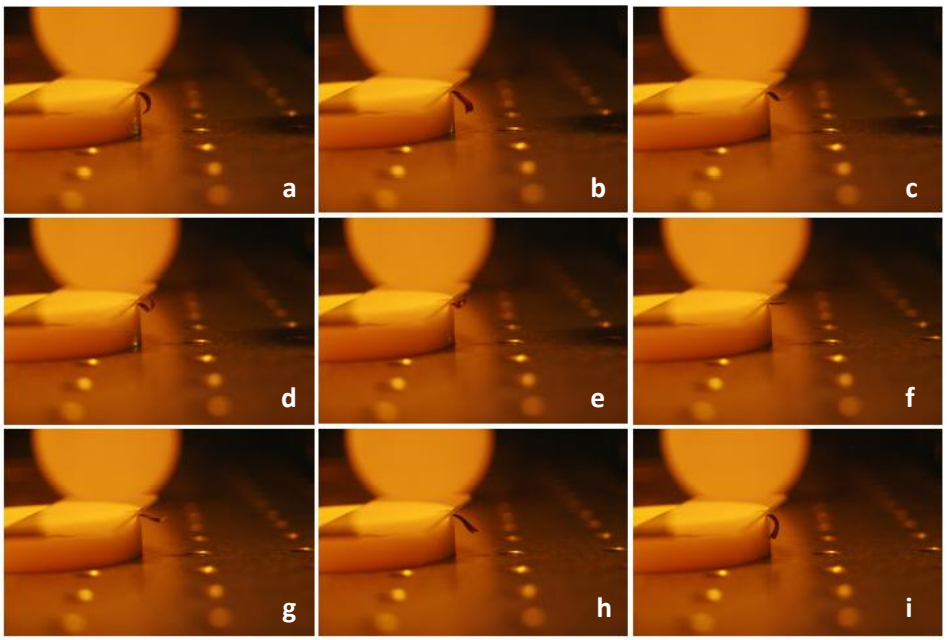

Figure 51 Reversible movement of a splayed E_3 film induced by a green laser: a-e) during the irradiation; f-i) after switching off the laser.

The results show that these mixtures have suitable properties to create microstructures with DLW. The use of the more hard **CL_6** based structures could improve the resolution of the technique conserving the possibility to deform them. In this case, we expect smaller shape-change during the

irradiation as just explained by the comparison between the different macroscopic sample.

Starting form **E_3** we evaluated also the opportunity to change the length of the flexible spacer on the monomer and on the crosslinker. We prepared different mixtures by substitution of the monomer with its analogues, **M_2** and **M_4**, or by the substitution of the crosslinker with its analogues, **CL_3** and **CL_4** (**Scheme 33**). Composition of the mixtures is shown in **Table 13**.

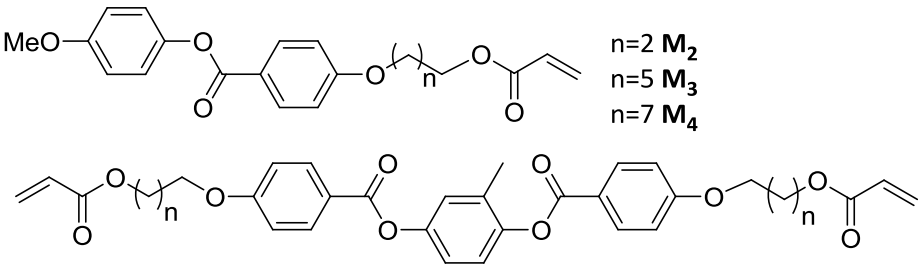

Scheme 33 Molecules with different flexible chains.

Mixture	Monomer	Crosslinker	Dye	Initiator	T_g [°C][b]
E_3	**M_3** (78%)	**CL_2** (20%)	**D_3** (1%)	**IN_1** (1%)	21.4
E_9	**M_2** (78%)	**CL_2** (20%)	**D_3** (1%)	**IN_1** (1%)	22.1
E_{10}	**M_4** (78%)	**CL_2** (20%)	**D_3** (1%)	**IN_1** (1%)	11.9
E_{11}	**M_3** (78%)	**CL_3** (20%)	**D_3** (1%)	**IN_1** (1%)	9.0
E_{12}	**M_3** (78%)	**CL_4** (20%)	**D_3** (1%)	**IN_1** (1%)	8.8

Table 13 Different mixtures containing M_{2-4} and CL_{2-4}: composition and T_g of the relative LCE film. In bracket is reported the percentage in mol of each component. [b]Determined from the midpoint of the baseline jump in second heating scan of the DSC trace.

We prepared films as previously described and their thermal properties were evaluated by DSC analysis. As in previous cases, DSC traces, reported in **Figure 52**, detected only the glass transitions. We observed a general decrease of T_g with the increase of flexibility of the molecules. Using **M_3**, which bears only 3 – CH_2- in the flexible chain, we obtain the highest T_g of the series and this value is comparable with that of **E_3** (22.1 and 21.4 °C respectively). A further increase of 2 –CH_2- in the monomer leads to a decrease of 10 °C in the T_g. The effect is more pronounced changing the crosslinker flexibility: starting from **CL_2** we obtained a decrease of more than 10 °C in the T_g by using **CL_3** or **CL_4**. These two samples present a similar T_g.

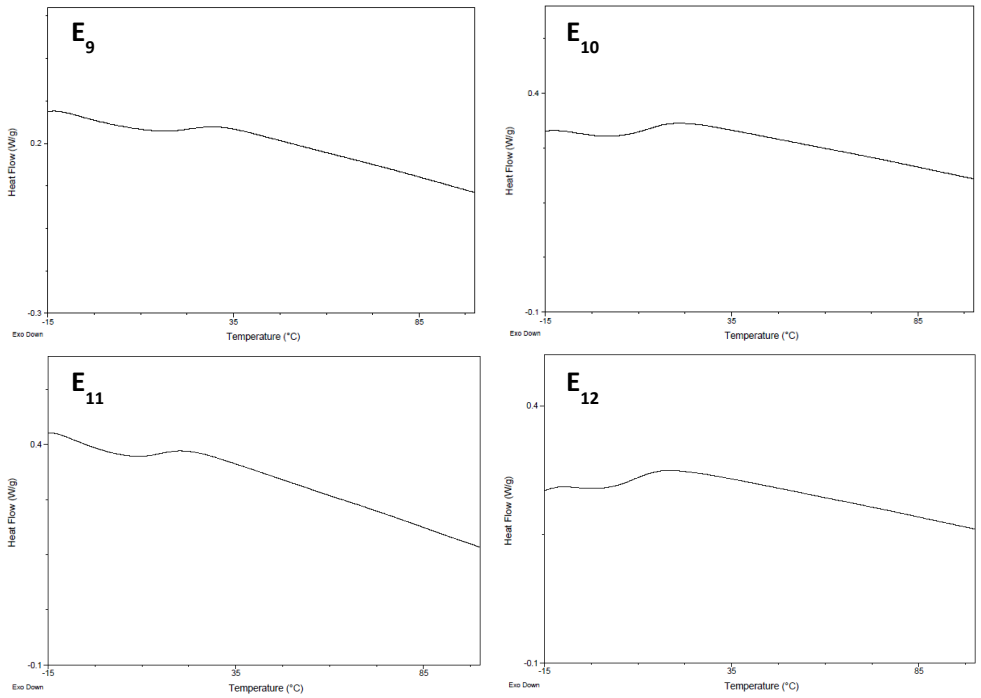

Figure 52 DSC traces (10 °C/min) corresponding to the second cycle of heating of films containing $M_{2\text{-}4}$ and $CL_{2\text{-}4}$.

Further studies on photoinduced movement of the films are under evaluation. As described in literature, increasing the flexible spacer on monomers could decrease the T_{NI} of the relative LCE.[55] We are undergoing measurements in order to verify this effect in the mixtures described above, and then the possibility to lead materials able to respond at different temperatures. Since thermal effect play an important role in the contraction of polymer containing **D_3**, we propose to study if such modifications reflect a lower power intensity needed for the activation. Moreover, the increase of the spacers length weakened the coupling between mesogens and backbone and it should lead to material with smaller contraction.[13] The same mixtures are under evaluation also by their use with DLW.

3.2.6. New challenges: multicolor structures and swimming

A hot research topic is to design artificial microstructures able to swim in a fluid: on this length scale, viscous forces dominate over the inertial ones with result that reciprocal motion cannot give rise to a net displacement or a suitable speed.[80] Using DLW of LCE structures, we believe that is possible to fabricate a microswimmer with design depicted in **Figure 53**.

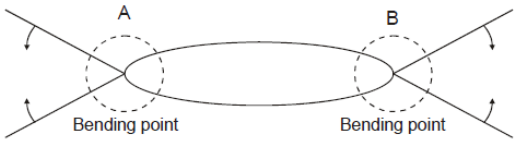

Figure 53 Example of structure able to perform non reciprocal movement.

The structure has to contain two light sensitive bending zone A and B and a central core. Non-reciprocal movements could be obtained if A and B bend with different response time, for example by using different material thickness, or by varying, over time, the light intensity over the actuator surface. Due to the small size, the second approach results difficult to realize in practice. A more advantageous strategy seems to be the fabrication of a "multicolor" structure with different spectral response of regions A and B.

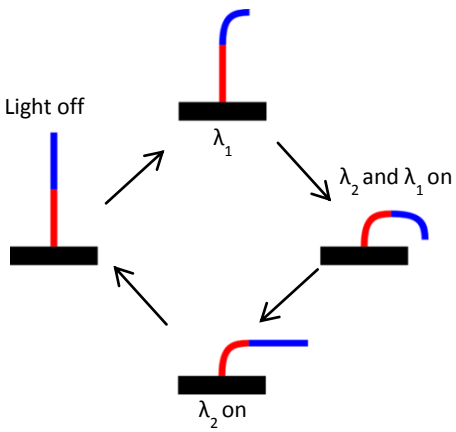

A "multicolor" structure can be realized including different dyes in different regions of this. Following **Scheme 34**, Broer et al. have developed a microactuator able to mimic the motion of natural cilia thought irradiation with UV and visible light: by selecting the color composition of the light the actuator position can be brought into four positions.[34]

Scheme 34 A "multicolor" structure.

"Multicolor" structures could be created with DLW through a multiple step writing process with different LC mixtures. This opportunity move us to study also materials containing dye with complementary absorption to that of **D_3**.

[80] E. M. Purcell, *Am. J. Phys.* **1977**, *45*, 3.

However, if dyes with strong absorption in the UV region are used in the mixtures, we have to change the laser wavelength of DLW workstation in order to integrate materials with different spectral responses in the same cell.

As preliminary work, we prepared a macroscopic film with mixture **E_{13}** (**Table 14**) and we studied its movement both in air and water.

Mixture	Monomer	Crosslinker	Dye	Initiator
E_{13}	**M_5** (50%)	**CL_2** (36%)	**D_7** (12%)	**IN_2** (2%)

Table 14 An example of mixture for film able to bend under UV irradiation. In bracket is reported the percentage in mol of each component.

D_7 (**Scheme 35**) is a commercial available dye with the same absorption spectrum of **D_1** and liquid crystalline properties: the molecule shows on cooling a Sm phase between 92 and 60 °C.[31] Using this dye, we have to avoid the use of UV light to polymerize the mixture. For this reason, we chose **IN_2** (**Irgacure 784**, **Scheme 35**) as photoinitiator since it allows to start the reaction by irradiation with visible light.

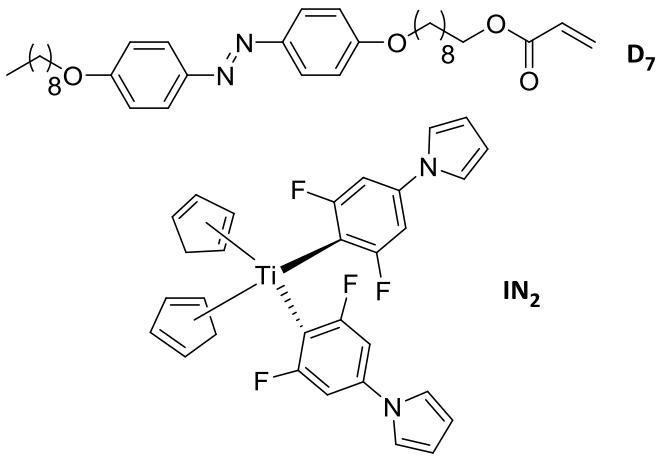

Scheme 35 Molecules used in the mixture E_{13}.

The mixture was infiltrated in a cell for splayed alignment and then temperature was cooled down until reaching the desired alignment. The mixture was polymerized for irradiation with a green lamp for 2 hours, according to examples reported in literature with this photoinitiator.[31] Once the film was taken out of the cell, it resulted bent, almost closed in a ring shape, instead of being flat. To test the mechanical properties, the film was clamped on one end and left free to move on the other side (**Figure 54a**).

Then, it was exposed to an UV irradiation (**Figure 54b**) in order to induce the *trans* to *cis* isomerization, and once it achieved the maximum deformation, the lamp was switched off. The dye presents a stable *cis* state and therefore the film did not return in the initial position. A visible light irradiation was required to bring it in the initial shape due to the reverse isomerization of the azobenzene (**Figure 54c-d**).

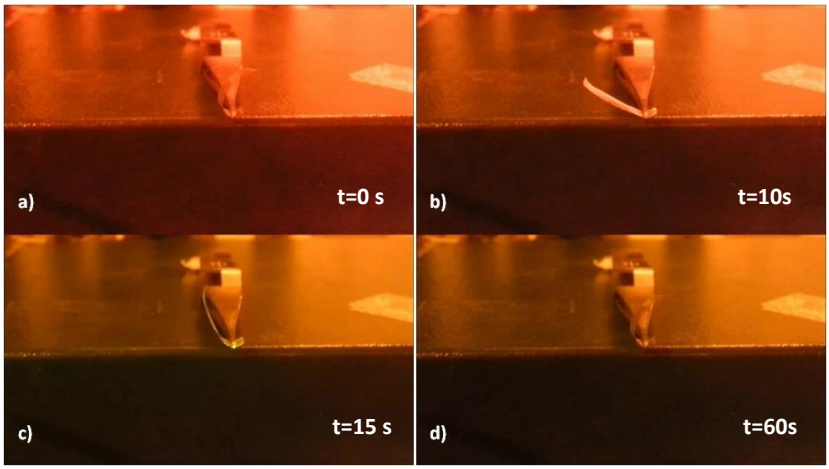

Figure 54 Photo-induced deformation of the cantilever in air. a) The film in its starting position; b) after irradiation with UV light (t=10 s); c) during irradiation with green light (t=15 s); d) after switching off the green lamp.

The light induced deformation of the LCE stripe is the result of two components: the dominant optical process due to the isomerization of the dye and a minor thermal effect linked to the raising of the internal temperature induced by the light radiation. Indeed, once the light is not incident on the sample the thermal component of deformation is recovered resulting in a tiny decrease of the total deformation. Furthermore, this effect is also responsible for the difference of time needed to undergo the two deformations: the relaxation back deformation is slower than the other one because the optical component has to overcome the thermal effect that acts in contraposition, tending to open the film.

In a second test, we repeated the irradiation when the material was immersed in a fluid. The film was clamped on one end and sunk in fresh water (18°C). As in the previous experiment the starting shape was not flat, but bent in a ring like shape (**Figure 55a**). When enlightened by a focused UV radiation the *trans* to *cis* isomerization caused the deformation of the film that became flat (**Figure 55b**). The time needed to undergo the complete deformation was

longer than the previous observed in air: when the stripe is sunk in a fluid, the thermal component of deformation is much less influent and this cause a slower deformation process. By irradiation with visible light, the stripe moved back to its initial configuration (**Figure 55c**).

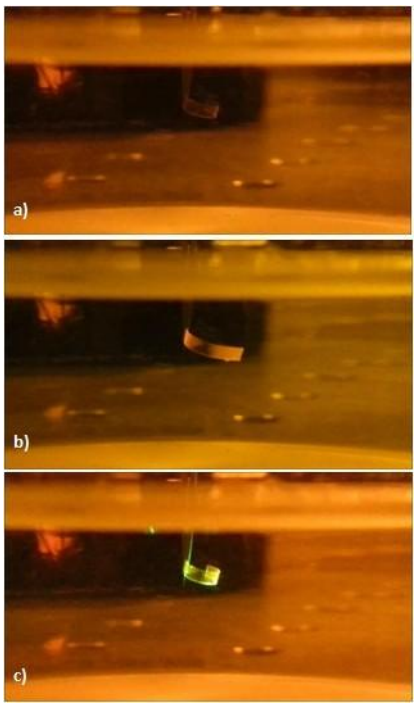

Figure 55 Photo-induced deformation of the cantilever in water. The film is sunk in fresh water (18 °C) inside a glass bowl. a) Initial shape of the film at t=0 s; b) deformed shape after UV exposition at t=35 s; c) final shape after irradiation with green light at t=75 s.

Meanwhile in the experiment carried out in air the times needed for the two isomerization were different (10 seconds for *trans* to *cis* and 45 seconds for *cis* to *trans*), in this second experiment they were pretty much the same (roughly 40 seconds). We believe that this is a direct proof that the thermal component is basically vanished in the second experiment, leaving only the optical component to drive the sample deformation process.

Since even after several weeks of test this material showed unchanged properties, hence it seems not to be affected neither by degradation due to UV exposure nor by the several load steps (deformation cycles).

The observed behavior could represent a breaking through for further research on light driven LCE devices able of “swimming” in fluids.

3.3 Experimental part

Materials: **IN_1** were purchased from Sigma-Aldrich, **IN_2** was purchased from Ciba Speciality Chemicals and dye **D_7** was purchased from Synthon Chemicals. Other molecules were prepared as described in Chapter 2.
The commercial photoresists IP-G and IP-L, purchased by Nanoscribe GmbH, contain molecules shown in **Scheme 36**.

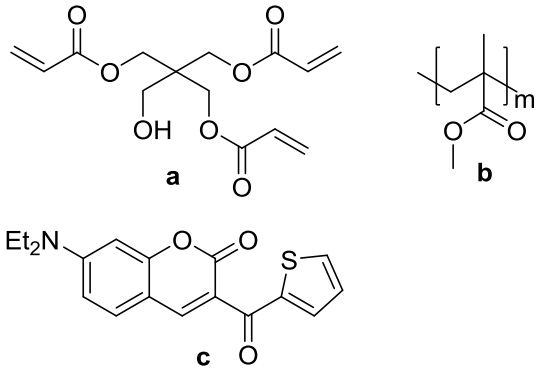

Scheme 36 Composition of IP-G and IP-L: a (less than 40%), **b** (less than 3%), **c** as photoinitiator (less than 5%) and butanone as solvent.

Cell preparation: glasses were washed with deionized water, dried and then spin coated with a PI-KEM LTD 6800 Spin coater (series SCS P6808P) instrument. For PVA coating, an aqueous solution of the polymer (M_w 13.000-23.000 87-89% hydrolyzed, purchased by Sigma Aldrich) 0.5% in weight was deposited on the glass and spin coated at 4000 rpm for 2 minutes. The glasses were then dried under the fume for 18 h. For
PI coating, the commercial solutions PI130 and PI1211 (Nissan Chemical Industries) were deposited directly on the glass and spin coated at 4000 rpm for 1 minutes. The glasses were heated at 90°C for 1 minute and then at 180°C for 30 minutes. PI130 and PVa coated glasses were rubbed unidirectionally with a cylinder covered by a velvet cloth.
To assemble the cell, one glass slide was placed with the polymeric layer upwards and glass microspheres (10, 20 or 50 μm, purchases by Duke Standards™-Thermo Scientific) were deposited above it as spacers. Then, the second glass was placed, with the polymer layer facing down, on the spacers and the cell was fixed with an adhesive.

For DLW fabrications, uniaxially rubbed PI130 coated glasses were used to make the cell with a 50 µm gap, if not otherwise specified. Macroscopic films were prepared using cells with a 20 µm gap and glasses coated with:

- PI 1211 on the bottom and PVA on the top for splayed samples;
- PVA on both surfaces for uniaxially homogeneous samples.

Infiltration of mixture and alignment in LC phase: monomer mixtures were infiltrated for capillarity into the cells on a hot plate at a temperature (T_{inf}) above the T_{LC-I} and then temperature was decreased until the polymerization temperature (T_{pol}) at 10 °C/min or 5 °C/min. T_{inf} and T_{pol} of mixtures are summarized in **Table 15**. For DLW fabrication the cell was installed directly onto a homemade heating stage fixed to the 3D piezo translation stage in the workstation.

Mixture	T_{inf} (°C)	T_{pol} (°C)
E_3	60	30
E_4	80	40
E_5	80	40
E_6	60	35
E_7	60	35
E_8	60	30
E_9	60	35
E_{10}	70	30
E_{11}	70	30
E_{12}	70	40
E_{13}[a]	100	120

Table 15 Temperature of infiltration and polymerization of different mixtures. a) The mixture is infiltrated in its LC phase to avoid the thermal polymerization that occurs above 120 °C. To obtain a good alignment, the mixture was quickly heated at 140 °C and then cooled at T_{pol}.

Direct Laser Writing system: two-photon absorption polymerization was induced by a focused laser beam from a 780 nm femtosecond laser in a commercial DLW workstation (Photonic Professional, Nanoscribe GmbH). The laser delivers 130 fs pulses with a 100 MHz repetition rate. Beam power was measured before the microscope objective. The laser beam was circularly polarized and focused with a 100×, 1.4 NA Oil Objective (Zeiss, Plan Apochromat). The sample position was controlled by a 3D piezo translation stage.

Fabrication of DLW structures with PI coated cells: LCE structures were written on the bottom inner surface of a glass cell. The laser power and the scan speed was 3 mW and 60 μms^{-1} for testing the swelling properties of LCEs (**Figure 32**), and 4 mW and 60 μms^{-1} for rings, woodpile and the other structures. After laser writing, the cell was opened and the structures were developed in two baths of toluene for 5 min. The structures were then dried in air for 10 min.

Fabrication of DLW structures on IP-L micro-grating: two glass coverslips were used to make the cell with a gap of 50 µm. IP-L resin was firstly infiltrated into the cell at room temperature. The IP-L micro-grating structures were written on both inner faces of the glass cell, using DLW workstation. The laser power and the scan speed for the IP-L gratings were 6 mW and 60 μms^{-1} respectively. After laser writing, the structure was developed in 2-propanol without opening the cell for 12 hours. The cell was dried in the air for 1 hour and then, LC monomer mixture was infiltrated into the cell. To fabricate the LCE structures a laser power of 4 mW (for microstructures) or 1.6 mW (for nanostructures) was used, while the scan speeds were 60 μms^{-1} for both. After laser writing, the cell was opened and the structure was developed in two baths of toluene for 5 min. The structure was then dried in air for 10 min.

Macroscopic film polymerization: samples aligned in LC phase were polymerized by irradiation with:

- an UV LED lamp (Thorlabs M385L2-C4, at 385 nm , I=1.8 $mWcm^{-2}$) for 5 minutes for mixtures containing $\mathbf{IN_1}$;
- a Green LED lamp (Thorlabs M505L3-C1, at 505nm, I=2.7 $mWcm^{-2}$) for 2 hours for mixtures containing $\mathbf{IN_2}$.

Characterization of the structures: an inverted microscope (Zeiss, Axio Observer A1) with cross polarisers was used to observe the alignment of LCE structures. A scanning electron microscope (PHENOM-World) was used to observe the LCE structures after sputter-coating them with 10 nm gold layer. Thermal transitions of material were measured using a DSC TA Instruments Q-2000 calorimeter under a nitrogen atmosphere (heating and cooling rate: 10 °C/min).

Light induced deformation observation: microstructures were illuminated with a DPSS 532 nm laser through a 10×, 0.25 NA (Plan Achromat, Olympus)

objective placed above the sample structure and the movement movies were recorded by a CMOS camera (frame rate 25.8 fps). Macroscopic films containing **D_3** were irradiated with a Dreamlasers SDL-532-600T at 532 nm laser (I= 140 $mWcm^{-2}$). Macroscopic film containing **D_7** was irradiated with a 385 nm (Thorlabs M385L2-C4, I=1.8 $mWcm^{-2}$) and a 505 nm (Thorlabs M505L3-C1, I=2.7 $mWcm^{-2}$) LED lamps.

Chapter 4

New LCE architectures by thiol-yne click chemistry

4.1 Introduction

The concept of Click Chemistry was introduced in 2001 by Sharpless et al. by the pioneering use of copper catalyst in Huisgen alkyne-azide reaction.[81] Afterwards, the concept has been applied by many groups for the synthesis of biomedical libraries, dendrimers, functional block copolymers, hydrogels, derivatization of cellular surfaces and many others. Characteristics of click reactions include high yields with byproducts absent or removable by non–chromatographic processes, insensitivity to oxygen or water, mild and solventless (or aqueous) conditions and orthogonality with other common organic synthetic reactions.[82]

Click chemistry has been seldom employed for LCE preparation. Grubbs et al. described the formation of a LC network by "click" crosslinking azide terminal groups in a preformed LC linear polymer with a crosslinker bearing three terminal alkynes (**Scheme 37**). [15]

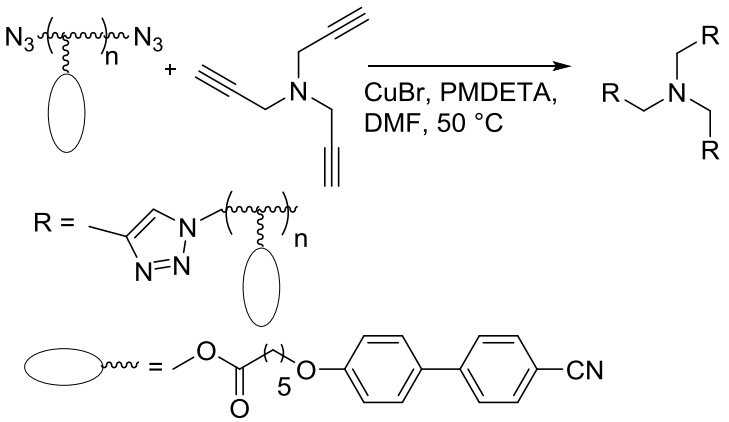

Scheme 37 Crosslinking of a LC network by alkyne-azide-click chemistry.

Recently, thiol-ene click chemistry emerged as a suitable reaction for assembling LC networks: a series of different side-chain LCEs with polysiloxane backbone have been prepared by grating mesogenic monomers with an alkene terminal group to the poly(3-mercaptopropylmethylsiloxane) (**Scheme 38**). This synthetic strategy does not require noble metal platinum catalyst, used in

[81] H. C. Kolb, M.G. Finn, K. B. Sharpless, *Angew. Chem. Int. Ed.* **2001**, *40*, 2004.
[82] C. E. Hoyle, C. N. Bowman, *Angew. Chem. Int. Ed.* **2010**, *49*, 1540.

the traditional hydrosilylation method, which is very expensive and difficult to be removed from the final material.[83]

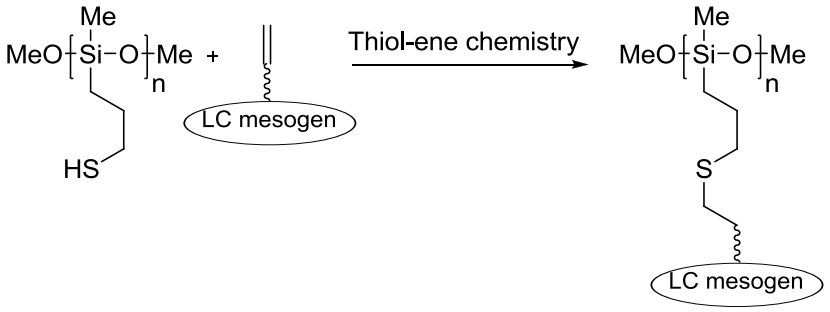

Scheme 38 Polisiloxane-based LC polymers prepared by thiol-ene click chemistry.

Light mediated thiol-ene radical reactions have proved to be a good alternative to classical acrylate photopolymerization that is plagued by several problems, as the inhibition by oxygen, complex kinetics and the formation of highly heterogeneous polymers. Keller et al. described the preparation of a main-chain LCE by thiol-ene radical polymerization using monomers shown in **Scheme 39**.[84] They developed the first micrometer main-chain LCE actuator exceeding the limitation of the strategies previously reported, which normally required a two-step crosslinking procedure as originally described by Finkelmann.[85]

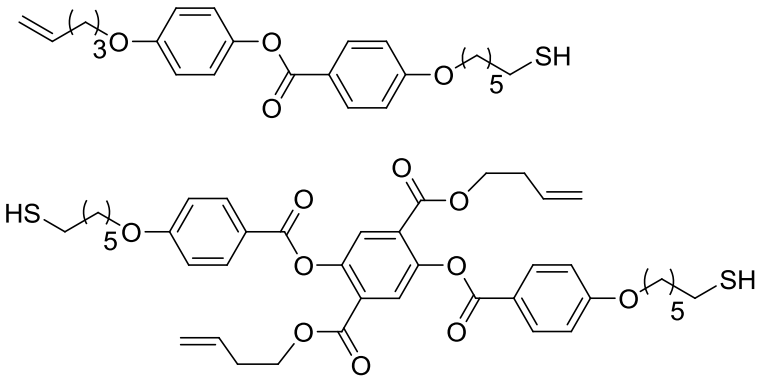

Scheme 39 Monomers for LCE preparation by thol-ene polymerization.

[83] H. Yang, M.-X. Liu, Y.-W. Yao, P.-Y. Tao, B.-P. Lin, P. Keller, X.-Q- Zhang, Y. Sun, L.-X. Guo, *Macromolecules* **2013**, *46*, 3406.
[84] H. Yang, A. Buguin, J.-M.Taulemesse, K. Kaneko, S. Méry, A. Bergeret, P. Keller, *J. Am. Chem. Soc.* **2009**, *131*, 15000.
[85] J. Küpfer, H. Finkelmann, *Macromol. Chem. Phys.* **1994**, *195*, 1353.

This approach is very attractive to prepare materials able to perform lager deformation than those reported in Chapter 3: contraction of LCEs increase with the coupling between the mesogenic units and the polymeric backbone and main-chain architecture results in the strongest possible coupling for these materials.

Liquid Crystals and Polymers research group at the University of Zaragoza has recently used DLW to prepare a biomaterial by thiol-yne click chemistry. In this reaction, two molecules of a thiol react with an alkyne to yield a 1,2 dithiosubstituted adduct (**Scheme 40**).[86]

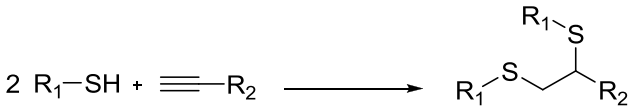

Scheme 40 Thyol-yne click chemistry.

The use of alkynes instead of alkenes allows to enhance the maximum of crosslinking density and the substitution degree of the final polymer.

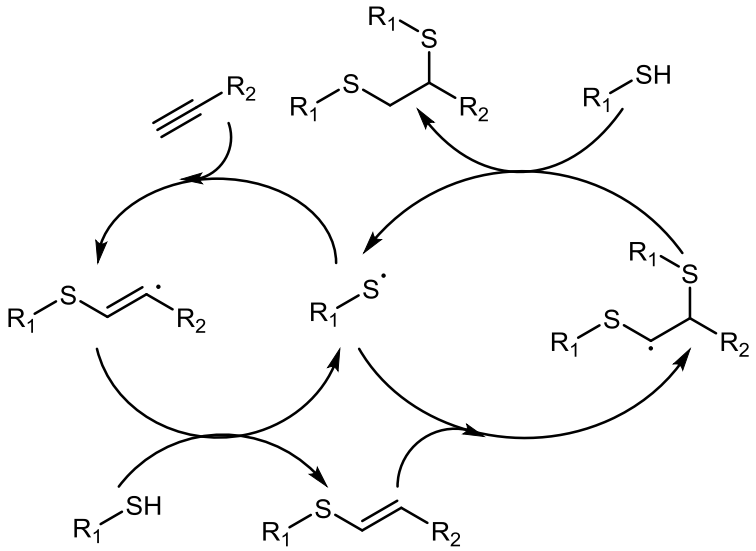

Scheme 41 Mechanism of thiol-yne click chemistry.

[86] M. Lomba, L. Oriol, R. Alcalá, C. Sánchez, M. Moros, V. Grazú , J. L. Serrano, J. M. De La Fuente, *Macromol. Biosci.* **2011**, *11*, 1505.

The mechanism of thiol-yne polymerization, shown in **Scheme 41**, proceeds by addition of a thiyl radical to an alkyne with the resulting carbon-centered radical able to abstract a hydrogen from another thiol, generating a vinyl sulfide moiety and regenerating a thiyl radical. The vinyl sulfide is capable of undergoing further reaction through addition of a second thiyl radical and kinetic studies showed that this second addition proceeds three time faster than the first one.[87]

Fascinated by the possibility to create LCEs with new architectures, we started to explore the use of thyol-yne click reaction. In collaboration with the Liquid Crystals and Polymers group of Zaragoza, suitable liquid crystalline monomers have been prepared and photopolymerized using different crosslinkers. Thermal properties and contractions of the resulting films have been studied and compared.

[87] B. D. Fairbanks, T. F. Scott, C. J. Kloxin,K. S. Anseth, C. N. Bowman, *Macromolecules* **2009**, *42*, 211.

4.2 Results and discussion

In order to obtain liquid crystalline polymers by thiol-yne click chemistry, we designed two LC monomers, one functionalized with two thiol groups and the other bearing an alkyne: their polymerization gives a mixed main-chain/side-chain LC polymer (**Scheme 42**). Morever, we designed and prepared various molecules containing two alkyne groups as crosslinkers able to connect different polymeric chains.

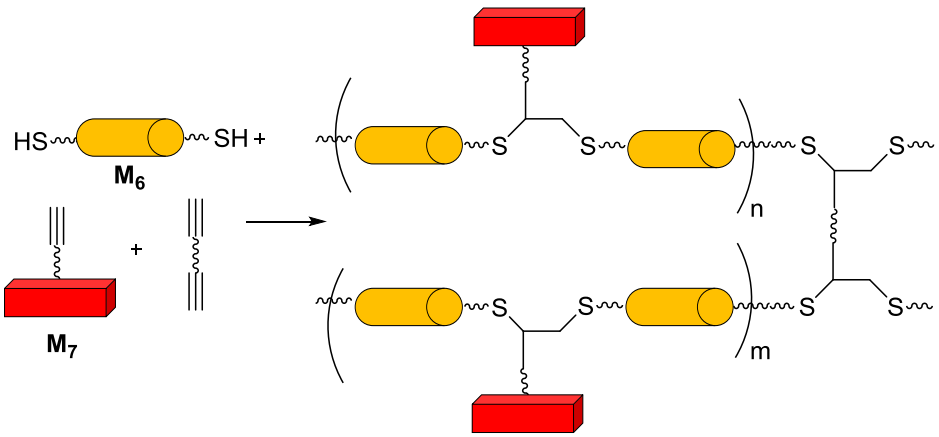

Scheme 42 Structure of LCEs based on thiol-yne click chemistry.

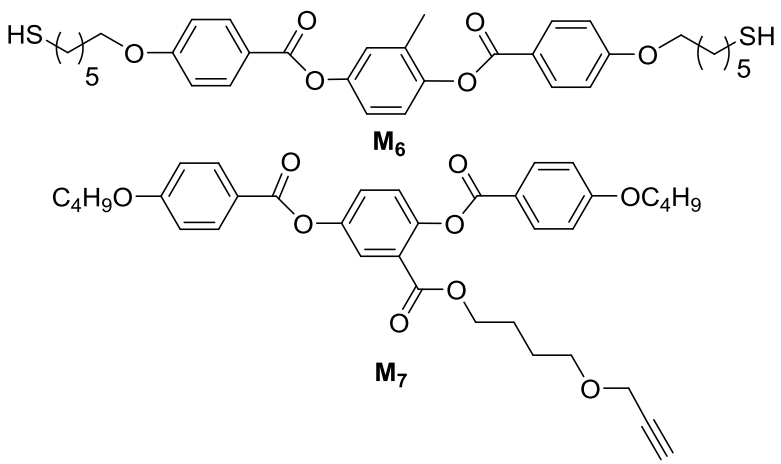

Scheme 43 Monomers for LCEs preparation by thiol-yne click chemistry.

The monomer structures have been chosen based on our expertise on acrylate based materials. Firstly, we decided to prepare the dithiol **M_6** modifying the structure of **CL_3**, which shows a broad nematic phase temperature range, by introduction of thiol groups at the end of the alkyl chains. The second monomer, which has to bear an alkyne group, is present in the side-chain of the final material. For this reason, we chose to use a "side-on" monomer able to maximise the coupling with the polymer backbone: starting from the structure of **M_1**, we designed **M_7** by replacing the terminal acrylate group with a propargyl moiety (**Scheme 43**).

4.2.1 Synthesis and mesomorphic properties of monomers

Monomer **M_6** was prepared following the synthetic route shown in **Scheme 44.** Benzyl 4-hydroxybenzoate (**51**) was subjected to a Williamson reaction with 1,6-dibromohexane to give **52**. Five equivalents of 1,6-dibromohexane, used in excess in order to minimize the amount of the disubstituted product, afforded a very high yield (86% yield). The benzyl ester **52** was hydrogenated to remove the benzyl group with $Pd(OH)_2/C$ as catalyst in a mixture of cyclohexene and THF at reflux affording **53** in 92% yield. The conditions resulted a safer alternative to the common procedure based on the use of the more dangerous molecular H_2. In such reaction, the catalyst acts as a transfer hydrogenation medium from a donor molecule (in our case cyclohexene) to the reactant. The stability of the oxided donor molecule (1,3-cyclohexadiene) drives the reaction.

The acid **53** was esterified with methyl hydroquinone in order to obtain **54**. The reaction is not trivial and different conditions were attempted in order to gain the desired product with high yields. As first try, we used a standard procedure with DCC as coupling agent but large amount of byproducts was formed. We then decided to interconvert **54** to acyl chloride and then perform the reaction with methylhydroquinone, but we had no success in the purification of the final product. At the end, we modified the first approach using EDC instead of DCC to form the active ester, finally obtaining **54** in 64% yield.

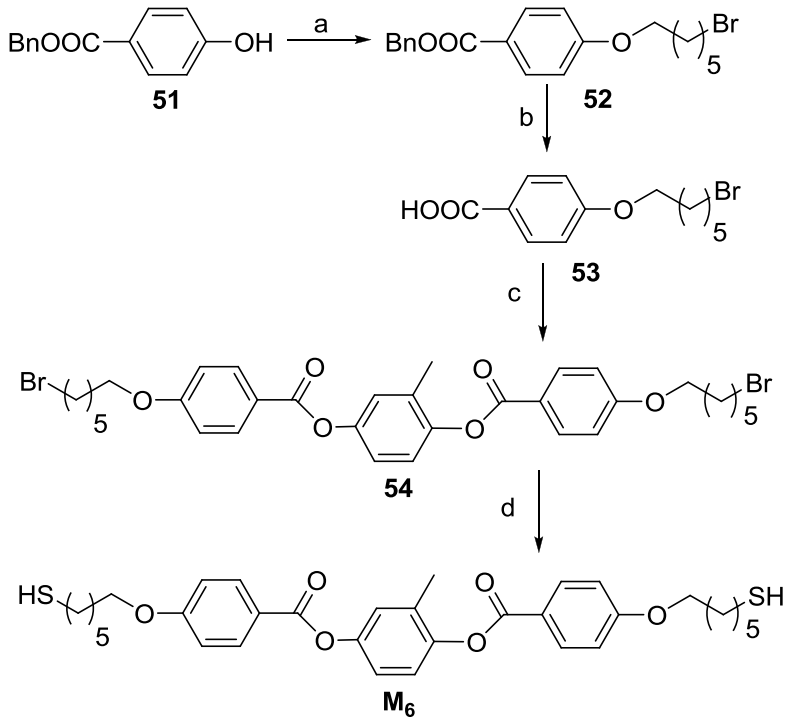

Scheme 44 Synthesis of M_6. Reagents and conditions: a) 1,6-dibromohexane, K_2CO_3, acetone, reflux, 4 h, 86%; b) $Pd(OH)_2/C$, cyclohexene, THF, reflux, 18 h, 92%; c) methylhydroquinone, EDC, DMAP, THF, rt, 48 h, 64%; d) $(TMSi)_2S$, TBAF, THF, -10 °C then rt, 30', then H_2O, 85%.

M_6 was obtained through a trimethylsilylthioxy-dehalogenation reaction on the dibromide precursor **54** in 85% yield. In this reaction the tetrabutylammonium trimethylsilylthiolate, generated in situ by addition of a solution of TBAF to hexamethyldisilathiane in THF, reacts rapidly with a variety of alkyl bromides and chlorides at room temperature. Upon aqueous workup or filtration through a silica gel column, the corresponding thiols are released in the organic medium (**Scheme 45**). Due to neutral condition and short reaction time, this procedure can be used for the preparation of many functionalized thiols avoiding the autoxidation products usually formed with other methods.[88]

Purification of **M_6** by FCC with different mixtures of solvents was unsuccessful and recrystallization from ethanol afforded the pure monomer only when the starting material was very pure. For these reasons, accurate purification of **54** resulted very important.

[88] J. Hu, M. A. Fox, *J. Org. Chem.* **1999**, *64*, 4959.

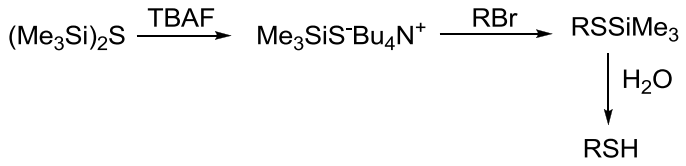

Scheme 45 Mechanism of trimethylsilylthioxy-dehalogenation reaction.

Monomer **M_7** was prepared by esterification between the mesogenic unit **4** and alkyne **56** (**Scheme 46**). Synthesis of **4** was already described in Chapter 2 while **56** was prepared by monopropargylation of the 1,4 butanediol (**55**).[89] The reaction started with deprotonation of the hydroxyl groups of **55** by dropwise addition of a solution of NaH, then proceeds with the addition of propargyl bromide. Four equivalents of **55** wiht respect to the alkyne were required to avoid the formation of the disubstituted product affording **56** in 71% yield.

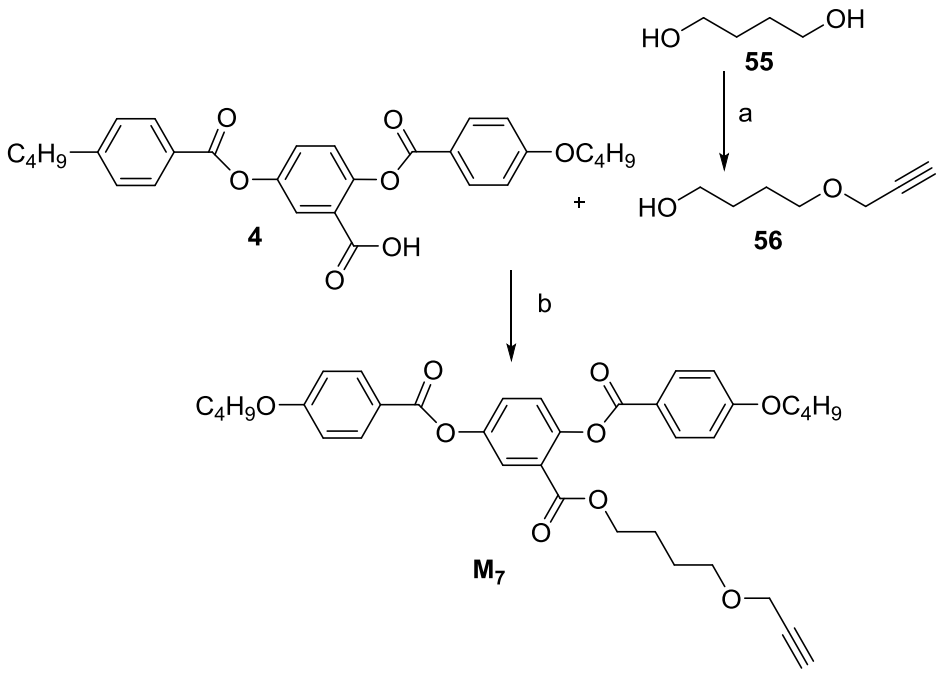

Scheme 46 Synthesis of M_7. Reagents and conditions: a) NaH, DMF, O °C, 30' then propargyl bromide, rt, 18 h, 71%; b) DCC, DMAP, CH_2Cl_2, rt, 18 h, 75%.

[89] Y. Yamamoto, K. Kurihara, A. Yamada, M. Takahashi, Y. Takahashi, N. Miyaura, *Tetrahedron* **2003**, *59*, 537.

In order to investigate the influence of flexibility of the crosslinker on the final polymers, we prepared three different derivatives containing two alkyne groups (**CL_7**, **CL_8** and **CL_9**) with structure shown in **Scheme 47**. Propargyl alcohol was used in the esterification with adipic acid to obtain **CL_7** and with terephthalic acid to obtain **CL_9**. **CL_8** was obtained by coupling 4-pentynoic acid with 1,10-decandiol.

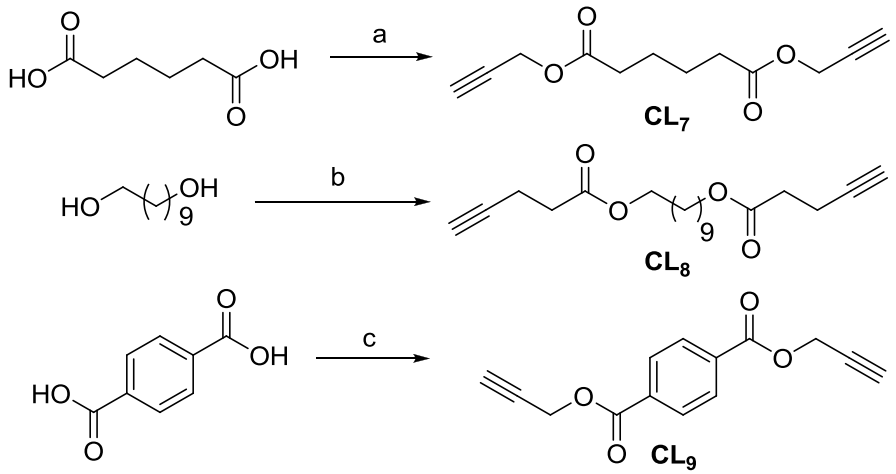

Scheme 47 Synthesis of crosslinkers. Reagents and conditions: a) propargyl alcohol, DCC, DMAP, CH_2Cl_2,rt, 18 h, 79%; b) 4-pentynoic acid, DCC, DMAP, CH_2Cl_2, rt, 18 h, 79%; c) propargyl alcohol, DCC, DMAP, CH_2Cl_2, rt, 18 h, 35%.

The mesomorphic properties of **M_6**, its dibromide precursor **54** and **M_7** were studied using DSC and POM and transition temperatures are summarized in **Table 16**. The three compounds presented enantiotropic nematic phases. **54** and **M_6** show a broad nematic phase (approximately from 85 °C to 160 °C) with a strong tendency to the homeotropic alignment as observed by POM: the substitution of the bromide with the thiol group does not affect the liquid crystalline properties of the structure. **M_7** presents a smaller range of temperature for the nematic phase on heating and the crystallization is not observed during the cooling stage. Formation of the crystalline phase in the sample is observed only on standing it at room temperature for at least 30 minutes.

Molecule	Phase transition temperatures [°C] [a]	T_g [°C] [b]
54	h: Cr 83.9 N 158.7 (1.84) I c: I 157.2 (1.94) N 53.8 Cr	-
M_6	h: Cr 80.9 N 162.3 (2.12) I c: I 162.6 (2.12) N 44.6 Cr	-
M_7	h: Cr 68.9 N 87.2 (1.15) I c: I 86.5 (1.37) N[c]	-20.4

Table 16 Thermal properties of monomers obtained during the second heating (h)–cooling (c) cycle of DSC experiments. [a]Determined from the onset of the transition peak. In bracket is reported the enthalpy of the transition (kJ/mol) determined from the integration of peak. [b]Determined from the midpoint of the baseline jump.[c] Crystallization was not observed on cooling down until -50 °C.

4.2.2 Preparation and characterization of LCE films

Mixtures containing **M_6**, **M_7** and different crosslinkers were prepared. We chose to use different percentages of crosslinker: quantities of the other components resulted from the stoichiometry of the reaction. An UV photoinitiator, **Irgacure 651** (**Figure 56**), was added in 4% w/w according to previous studies on thiol-yne photopolymerization performed in our laboratory.

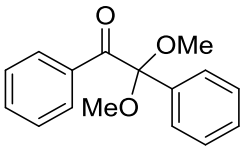

Figure 56 Structure of Irgacure 651

Mixtures and the relative polymers are noted according to the following nomenclature:

E_CL$_a$b

where

- *a* is the number of crosslinker;
- *b* is the percentage in mol of the crosslinker;

In order to study the dynamic of the polymerization process, a photo-DSC was performed on the mixture **E-CL$_7$20**. In this experiment, the sample and the reference are heated at 85 °C (the same temperature used later for film preparation) and then they are irradiated with UV light for 10 minutes. The DSC trace, reported in **Figure 57**, shows an intense exothermic peak right after the starting of irradiation and the recovery of the baseline only 2 minutes after. The exothermic peak is due to the photoinduced reaction and the

measure shows that polymerization takes place in the first few minutes of irradiation.

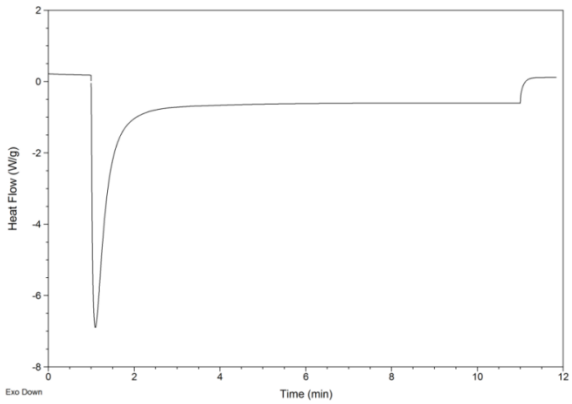

Figure 57 Photo-DCS trace at 85 °C of the mixture E-CL$_1$20.

Based on this study, we chose 10 minute as polymerization time to be sure that all the mixture in the cell was converted into the polymer. Preparation of the films was performed by infiltration of the mixtures in their isotropic phase in a rubbed cell followed by a slow cool down in order to reach the nematic phase. All samples show formation of the nematic phase around 110 °C and crystallization occurs only after several hours (more than 1 h) at room temperature. After polymerization by irradiation with an UV lamp, films were removed from the cell and their alignment was checked by POM. Their thermal properties were studied with TGA and DSC analysis and results are summarized in **Table 17**. DSC traces are shown in **Figure 58** and TGA traces are reported in Appendix.

Film	T_d [°C][a]	T_g [°C][b]	T_{NI} [°C][c]	ΔH_{NI} [J/g][d]
E-CL$_7$20	301.9	8.5	146.5	2.12
E-CL$_7$10	294.4	11.8	148.9	2.14
E-CL$_8$20	318.8	0.8	127.3	1.24
E-CL$_9$20	274.6	16.0	147.2	2.16

Table 17 Thermal properties of LCE films. [a] Decomposition temperature determined by the TGA curve by the 5% weight loss of the sample. [b] Determined from the midpoint of the baseline jump in DSC trace. [c] and [d] determined respectively from the maximum and the area of the transition peak in the DSC trace.

TGA analysis show that all the films are stable at least until 270 °C and only above this temperature decomposition is observed. T_{NI} and ΔH_{NI} are very similar for the two films containing **CL$_7$** and **CL$_9$** and these parameters decrease

using the more longer, and then more flexible, crosslinker **CL_8**. Using the more rigid **CL_9** an increase of the T_g is observed**.**

E-$CL_7$20 is the stronger and better handling film, while **E-$CL_7$10** and **E-$CL_8$20** are more sticky and, during the removal from the cell, it is easy to break these samples. Dissolving the PVA sacrificial layers in water helps to remove the whole film. **E-$CL_9$20** has properties intermediate between the two mentioned above. Based on these data we decided not to prepare the films containing 10% of **CL_8** and **CL_9**.

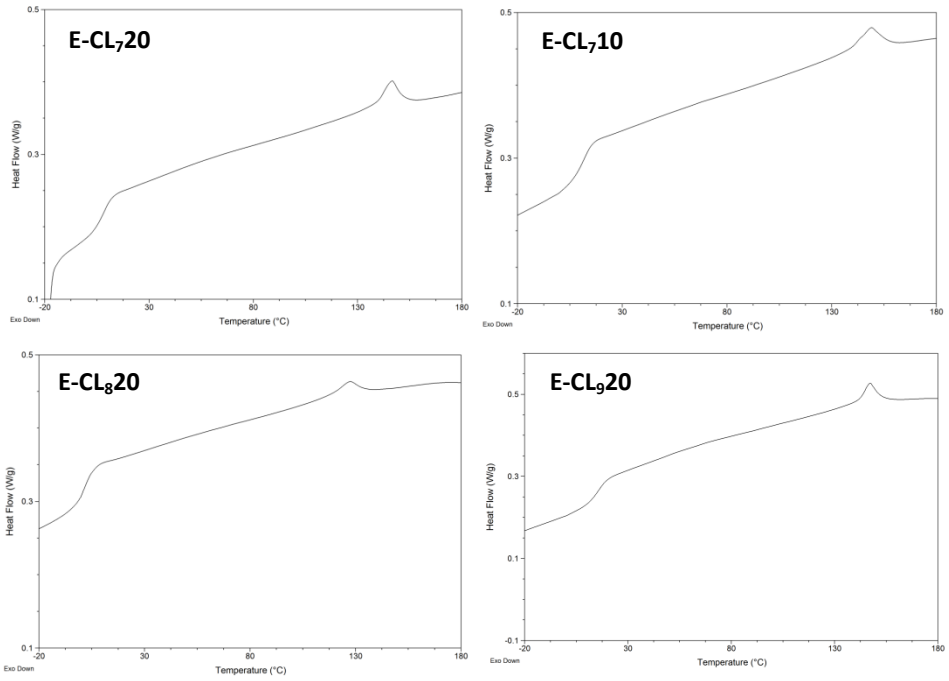

Figure 58 DSC traces (10 °C/min) corresponding to the second cycle of heating of LCE films.

Contractions of the films were then investigated: a piece of each film was put on a silicone oil drop on the top of a glass plate, then was heat to induce the isotropic phase (170 °C for all samples) and cooled down to room temperature. Contractions are reported in **Table 18** and quantify as $(L_{rt}- L_{170})/L_{rt}$ where L_{rt} and L_{170} are respectively the length of sample at room temperature and at 170 °C along the alignment direction. Materials were cut to have the longest side of the film piece correspondent to alignment direction.

Sample	Contraction
E-CL$_7$20	48%
E-CL$_7$10	41%
E-CL$_8$20	48%
E-CL$_9$20	35%

Table 18 Effect of N to I transition on films length.

All samples are able to undergo big deformations, bigger than contractions previously reported for side-chain LCEs prepared by acrylate polymerization and described in literature[13] and in Chapter 3.

For **E-CL$_8$20** also a relevant increase in the direction perpendicular to the contraction direction is observed (188% of the original length). By cooling down the samples, only the polymers containing **CL$_7$** recover their original shape (**Figure 59**) while the other two samples do not show a total reversible contraction and they recover only the 87% for **E-CL$_8$20** and 94% **E-CL$_9$20** of their original length after the first heating cycle. In subsequent heating and cooling cycles, these two films do not show new loss in the recovery step, suggesting that an irreversible change occurs in their structure only during the first heating process.

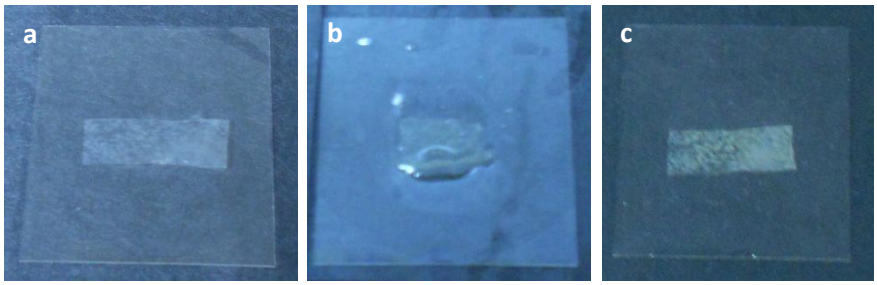

Figure 59 A piece of E-CL$_7$20 at room temperature (a), at 170 °C (b) and again to room temperature (c).

E-CL$_7$20 was then selected, due to its best properties, as reference for further modifications and we decided to use as dithiol also a more flexible spacer as **57** or a more rigid one as **58**. Mixtures in which **M$_6$** is totally replaced with **57** or **58** do not show liquid crystalline phase. Then we prepared mixtures containing as dithiol **M$_6$:57** (1:1) or **M$_6$:58** (1:1): unfortunately POM observations show in all cases that nematic phase was present only on cooling and only in some region of the sample. Nematic regions increased cooling the samples until room temperature but they were always mixed with isotropic regions and leaving the samples at this temperature also crystalline regions

appeared (**Figure 60**). For these problems, we decided that the new mixtures were not useful for films preparation.

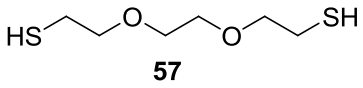

57

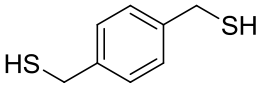

58

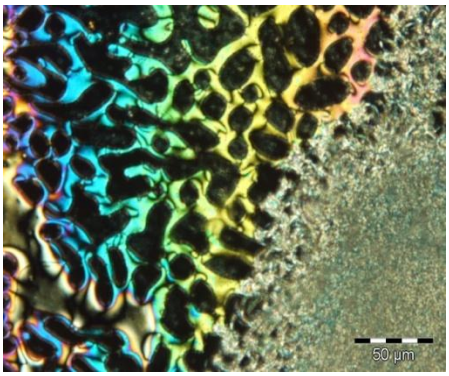

Figure 60 Other dithiols used and a POM images of one mixture at room temperature.

However, this stop do not affect the impression that the material described in this chapter are very interesting for the development of micrometer actuator able to undergo big deformations: we are working on development of such material to obtain photoactive LCEs to be use in DLW microfabrication.

4.3 Experimental part

General methods. Commercial reagents were used as received. All reactions were magnetically stirred and monitored by TLC on 0.25 mm silica gel plates (Merck F_{254}) and column chromatography was carried out on Silica Gel 60 (32-63 μm). IR spectra were obtained on a Nicolet Avatar 360-FT-IR spectrometer using KBr pellets. NMR spectra were recorded on a Bruker AV-400 spectrometer. Elemental analysis was performed using a Perkin-Elmer 2400 Series II analyzer. MALDI-TOF MS was performed on an Autoflex mass spectrometer (Bruker Daltonics) using DCTB as matrix. Thermal stability was characterized using a Q-5000 TA thermogravimetric analyzer at 10 °C/min under a nitrogen atmosphere up to 600 °C. Thermal transitions were measured using a DSC TA Instruments Q-20 calorimeter under a nitrogen atmosphere (heating and cooling rate: 10 °C/min). The light source was a photocalorimetry accessory from TA Instruments composed by a 200 W high pressure Hg source provided with a 250–450 nm filter. Light was transmitted to the sample through an extended range dual-quartz light guide. Polarized optical microscopy (POM) was performed using an Olympus BH-2 polarizing microscope fitted with a Linkam THMS600 hot stage.

Benzyl4-[(6-bromohexyl)oxy]benzoate (**52**). A mixture of benzyl 4-hydroxybenzoate (5 g, 21.9 mmol), 1,6-dibromohexane (26.7 g, 109.06 mol), K_2CO_3 (4.6 g, 32.9 mmol) and acetone (75 ml) was stirred at reflux for 4 h. After cooling, the mixture was filtered and the filtrate was evaporated under reduced pressure. The crude product was purified by FCC (hexane:AcOEt 10:1, R_f=0.2) affording the desired product in 86% yield (7.4 g, 18.9 mmol) as a white solid. ^{1}H-NMR (400 MHz, $CDCl_3$) δ 8.03-8.01 (m, 2H, Ar), 7.46-7.33 (m, 5H, Ar), 6.91-6.88 (m, 2H, Ar), 5.34 (s, 2H, Bn), 4.01 (t, *J* = 6.4 Hz, 2H , ArO-CH_2), 3.43 (t, *J* = 6.8 Hz, 2H, A-CH_2Br), 1.93-1.86 (m, 2H, ArO-CH_2CH_2), 1.84-1.79 (m, 2H, A-CH_2CH_2Br), 1.52-1.46 (m, 4H, aliphatic –CH_2-) ppm.

4-[(6-Bromohexyl)oxy]benzoic acid (**53**). To a solution of **52** (14.63 g, 37.39 mmol) in THF (200 mL) and cyclohexene (200 mL), 20% $Pd(OH)_2$/C (1.4 g) was added. The mixture was stirred on reflux for 18 h, filtered through a Celite pad and the filtrate was evaporated under reduced pressure. The crude product was purified by recrystallization from methanol affording **53** in 92% yield (10.40 g, 34.53 mmol) as white solid. ^{1}H NMR (400 MHz, $CDCl_3$) δ 8.06-8.04 (m,

2H, Ar), 6.94-6.92 (m, 2H, Ar), 4.05 (t, *J* = 6.4 Hz, 2H, ArO-CH_2), 3.44 (t, *J* = 6.8 Hz, 2H, A-CH_2Br), 1.96-1.90 (m, 2H, ArO-CH_2CH_2), 1.86-1.82 (m, 2H, A-CH_2CH_2Br), 1.54-1.53 (m, 4H, aliphatic –CH_2-) ppm.

2-Methyl-1,4-phenylene bis{4-[(6-bromohexyl)oxy]benzoate} (**54**). A solution of **53** (5.56 g, 18.46 mmol), methylhydroquinone (1.14 g, 9.23 mmol), EDC (3.89 g, 20.31 mmol) and DMAP (338 mg, 2.77 mmol) in 100 mL of dry THF was stirred at room temperature under Ar atmosphere for 48 h. The mixture was poured into a solution of NH_4Cl (3 g in 200 mL of water) and extracted 2 times with CH_2Cl_2. The combined organic layers were washed with water, dried over $MgSO_4$, filtered and evaporated under reduced pressure. The crude product was purified by FCC (hexane:AcOEt:CH_2Cl_2 8:1:1, R_f=0.22) and then recrystallized from ethanol affording the desired product in 64% yield (4.08 g, 5.91 mmol) as a white solid. ^{1}H-NMR (400 MHz, $CDCl_3$) δ 8.18-8.13 (m, 4H, Ar), 7.17 (d, *J* = 8.6 Hz, 1H, Ar), 7.13 (d, *J* = 2.7 Hz, 1H, Ar), 7.09 (dd, *J* = 8.6, 2.7 Hz, 1H, Ar), 6.99-6.96 (m, 4H, Ar), 4.08-4.04 (m, 4H, ArO-CH_2), 3.44 (t, *J* = 6.7 Hz, 4H, A-CH_2Br), 2.25 (s, 3H, Me), 1.95-1.90 (m, 4H, ArO-CH_2CH_2), 1.88-1.84 (m, 4H, A-CH_2CH_2Br), 1.56-1.52 (m, 8H, aliphatic –CH_2-) ppm; ^{13}C NMR (100 MHz, $CDCl_3$) δ 165.0 (s, C=0), 164.6 (s, C=0), 163.6 (s, Ar), 163.5 (s, Ar), 148.6 (s, Ar), 147.2 (s, Ar), 132.4(d, 4C, Ar), 131.9 (s, Ar), 124.2 (d, Ar), 123.0 (d, Ar), 121.8 (s, Ar), 121.6 (s, Ar), 120.1 (d, Ar), 114.5, 114.4, (d, 4C, Ar), 68.2, 68.1 (t, 2C, ArO-CH_2), 33.8 (t, 2C, A-CH_2Br), 32.76, 29.06, 28.01, 25.37 (t, 8C, aliphatic –CH_2-), 16.56 (q, Me) ppm; IR (KBr): 2963, 2863, 1728, 1602, 1576, 1509 cm^{-1};MS (MALDI-TOF) *m/z*: 713.1 ([M+Na]$^+$; 100); Anal. Calcd for $C_{33}H_{38}Br_2O_6$ (690.46): C 57.40, H 5.55; found C 57.69, H 5.84.

2-Methyl-1,4-phenylene bis{4-[(6-mercaptohexyl)oxy]benzoate} (**M_6**). A solution of compound **54** (1.06 g, 1.53 mmol) in 30 mL dry THF was cooled to -10 °C under Ar atmosphere. Bis(trimethylsilyl)silane (840 µL, 4 mmol) and TBAF (1M solution in THF, 3.65 mL, 3.65 mmol) were added respectively. The mixture was stirred for 30' at room temperature and then poured into a saturated ammonium chloride solution (60 mL). The resulting solution was extracted by AcOEt (3x50 mL). The combined organic layers were washed with water, dried over $MgSO_4$, filtered, and evaporated under reduced pressure. The crude product was purified by recrystallization from ethanol affording **M_6** in 85% yield (773 mg, 1.30 mmol) as a white solid. ^{1}H-NMR (400 MHz, $CDCl_3$) δ 8.17-8.15 (m, 2H, Ar), 8.15-8.13 (m, 2H, Ar), 7.17 (d, *J* = 8.6 Hz, 1H, Ar), 7.13 (d,

J = 2.7 Hz, 1H, Ar), 7.08 (dd, *J* = 8.6, 2.7 Hz, 1H, Ar), 6.92-6.88 (m, 4H, Ar), 4.06 (t, *J* = 6.4 Hz, 2H, ArO-C*H*$_2$), 4.05 (t, J = 6.4 Hz, 2H, ArO-C*H*$_2$), 2.54 (pseudo q, *J* = 7.4 Hz, 4H, A-C*H*$_2$SH), 2.24 (s, 3H, Me), 1.87-1.80 (m, 4H, ArO-CH$_2$*CH*$_2$), 1.70-1.63 (m, 4H, A-C*H*$_2$CH$_2$SH), 1.51-1.49 (m, 8H, aliphatic –CH$_2$-), 1.35 (t, *J* = 7.7, 2H, SH) ppm. ^{13}C NMR (100 MHz, $CDCl_3$) δ 164.9 (s, C=0), 164.5 (s, C=0), 163.5 (s, 2C, Ar), 148.4 (s, Ar), 147.1 (s, Ar), 132.3 (d, 4C, Ar), 131.8 (s, Ar), 124.1 (d, Ar), 122.9 (d, Ar), 121.6 (s, Ar), 121.5 (d, Ar), 120.0 (s, Ar), 114.4, 114.3, (d, 4C, Ar), 68.1 (t, 2C, ArO-*C*H$_2$), 33.9, 29.0, 28.1, 25.5 (t, 8C, aliphatic –CH$_2$-), 24.5 (t, 2C, A-*C*H$_2$Br), 16.4 (q, Me). IR (KBr): 2938, 2856, 1730, 1603, 1510, 1182 cm^{-1}; MS (MALDI-TOF) *m/z*: 619.3 ([M+Na]$^+$; 100); Anal. Calcd for $C_{33}H_{40}O_6S_2$ (596.80): C 66.41, H 6.76, S 10.75; found C 66.25, H 6.99, S 10.99.

4-(Prop-2-ynyloxy)butan-1-ol (**56**). A solution of 1,4-butanediol (25 g, 278 mmol) in DMF (40 mL) was added dropwise into a suspension of sodium hydride (60% w/w in mineral oil, 10.3 g, 257 mmol) in DMF (70 mL) at 0 °C. After being stirred for 30' at 0 °C, a solution of propargyl bromide (80% w/w in toluene, 10.33 g, 69.5 mmol) in DMF (25 mL) was added. The mixture was stirred for 18 h at room temperature then water was added (400 mL) and the product was extracted with AcOEt (300 mL). The organic phase was washed twice with water, dried over $MgSO_4$, filtered and concentrated under reduced pressure. The crude product was purified by FCC (hexane:AcOEt 1:1, R_f=0.35) affording the desired product in 71% yield (6.3 g, 49.2mmol) as a yellow liquid.^{1}H-NMR (400 MHz, $CDCl_3$) δ 4.13 (d, *J* = 2.4 Hz, 2H, OC*H*$_2$-C≡CH), 3.64 (t, *J* = 5.8 Hz, 2H, C*H*$_2$OCH$_2$-C≡CH), 3.55 (t, *J* = 5.8 Hz, 2H, C*H*$_2$OH), 2.56 (broad s, 1H, OH), 2.42 (t, *J* = 2.4 Hz, 1H, OCH$_2$≡C*H*), 1.70-1.62 (m, 4H, aliphatic –CH$_2$-) ppm.

4-(Prop-2-yn-1-yloxy)butyl 2,5-bis[(4-butoxybenzoyl)oxy]benzoate (**M$_7$**). A solution of **4** (2 g, 3.95 mmol), **56** (506 mg, 3.95 mmol), DCC (896 mg, 4.34 mmol) and DMAP (53 mg, 0.43 mmol) in 100 mL of dry CH_2Cl_2 was stirred at room temperature under Ar atmosphere for 18 h. The *N,N*-dicyclohexylurea was filtered and the filtrate was washed with water (100 mL), 5% acetic acid solution (100 mL) and water (100 mL). The organic layers were dried over $MgSO_4$, filtered and evaporated under reduced pressure. The crude material was purified by FCC (hexane:AcOEt 8:1, R_f=0.14) affording the desired product in 75% yield (1.82 g, 2.96 mmol) as a white solid. If the product contains impurities it can be recrystallized from ethanol. ^{1}H-NMR (400 MHz, $CDCl_3$) δ 8.17-8.14 (m, 4H, Ar), 7.89 (d, *J* = 2.8 Hz, 1H, Ar), 7.46 (dd, *J* = 8.7, 2.8 Hz, 1H,

Ar), 7.26 (d, *J* = 8.7 Hz, 1H, Ar), 7.00-6.97 (m, 4H, Ar), 4.21-4.18 (m, 2H, OC*H*$_2$-C≡CH), 4.07-4.05 (m, 6H, ArO-C*H*$_2$-A, C*H*$_2$CO), 5.40 (t, *J* = 6.0 Hz, 2H, C*H*$_2$OCH$_2$-C≡CH), 2.39 (t, *J* = 2.4 Hz, 1H, OCH$_2$-C≡C*H*), 1.85-1.78 (m, 4H, aliphatic –CH$_2$-), 1.60-1.50 (m, 8H, aliphatic –CH$_2$-), 1.00 (t, *J* = 7.4 Hz, 6H, Me) ppm; ^{13}C NMR (100 MHz, $CDCl_3$) δ 165.0, 164.7, 164.2, 163.9, 163.7, 148.5, 148.3 (s, 7C, 3C=0, 4Ar), 132.6 (d, 2C,Ar), 132.5 (d, 2C,Ar), 127.3, 125.1, 125.0 (d, 3C, Ar), 124.9, 121.6, 121.2 (s, 3C, Ar), 114.5 (d, 4C, Ar), 79.9 (s, OCH$_2$-*C*≡CH), 74.3 (d, OCH$_2$-C≡*C*H), 69.4 (t, *C*H$_2$OCH$_2$-C≡CH), 68.2, 68.1 (t, 2C, ArO-*C*H$_2$-A), 65.3 (t, O*C*H$_2$-C≡CH), 58.1 (t, *C*H$_2$CO), 31.3 (t, 2C, aliphatic –CH$_2$-), 26.0, 25.3, 19.3 (t, 4C, aliphatic –CH$_2$-), 13.9 (q, 2C, Me) ppm; IR (KBr): 3265, 2958, 2873, 2124, 1713, 1699, 1512, 1421, 1252, 1162 cm^{-1}; MS (ESI) *m/z*: 639.0 ([M+Na]$^+$; 100); Anal. Calcd for $C_{36}H_{40}O_9$ (616.70): C 70.11, H 6.54; found C 69.88, H 6.82.

Dipropargyladipate (**CL$_7$**). A solution of adipic acid (4 g, 27.37 mmol), propargyl alcohol (3.56 mL, 20.22 mmol), DCC (12.43 g, 60.22 mmol) and DMAP (735 mg, 6.02 mmol) in 200 mL of dry CH_2Cl_2 was stirred at room temperature for 18 h. The *N,N*-dicyclohexylurea was filtered and the filtrate was washed with water (200 mL), 5% acetic acid solution (200 mL) and water (200 mL). The organic layers were dried over $MgSO_4$, filtered and evaporated under reduced pressure. The crude material was purified by FCC (hexane:AcOEt 8:1, R_f=0.22) affording the desired product in 79% yield (4.8 g, 6.83 mmol) as a yellow solid. ^{1}H-NMR (400 MHz, $CDCl_3$) δ 4.68 (d, *J* = 2.5 Hz, 4H, C*H*$_2$C≡CH), 2.47 (t, *J* = 2.5 Hz, 2H, C≡C*H*), 2.40-2.37 (m, 4H, C*H*$_2$COO), 1.71-1.68 (m, 4H, aliphatic –CH$_2$-) ppm.

Decane-1,10-diyl bispent-4-ynoate (**CL$_8$**). A solution of 1,10-decandiol (114 mg, 0.66 mmol), 4-pentynoic acid (129 mg, 1.31 mmol), DCC (298 mg, 1.44 mmol) and DMAP (24 mg, 0.19 mmol) in 5 mL of dry CH_2Cl_2 was stirred at room temperature for 18 h. The *N,N*-dicyclohexylurea was filtered and the filtrate was washed with water (10 mL), 5% acetic acid solution (10 mL) and water (10 mL). The organic layers were dried over $MgSO_4$, filtered and evaporated under reduced pressure. The crude material was purified by FCC (hexane:AcOEt 8:1, R_f=0.31) affording the desired product in 79% yield (174 mg, 0.52 mmol) as a yellow liquid.^{1}H-NMR (400 MHz, $CDCl_3$) δ 4.09 (d, *J* = 6.72 Hz, 4H, C*H*$_2$COO), 2.57-2.48 (m, 8H, HC≡CC*H*$_2$, COOC*H*$_2$), 1.97 (t, *J* = 2.5 Hz, 2H, C≡C*H*), 1.66-1.59 (m, 4H, aliphatic –CH$_2$-), 1.35-1.25 (m, 12H, aliphatic –CH$_2$-) ppm.

Diprop-2-yn-1-yl terephthalate (**CL_9**). A solution of terephthalic acid (1 g, 6.02 mmol), propargyl alcohol (0.78 mL, 13.25 mmol), DCC (2.73 g, 13.25 mmol) and DMAP (161 mg, 1.32 mmol) in 50 mL of dry CH_2Cl_2 was stirred at room temperature for 18 h. The *N,N*-dicyclohexylurea was filtered and the filtrate was washed with water (100 mL), 5% acetic acid solution (100 mL) and water (100 mL). The organic layers were dried over $MgSO_4$, filtered and evaporated under reduced pressure. The crude material was purified by FCC (hexane:AcOEt 9:1, R_f=0.28) affording the desired product in 35% yield (518 mg, 2.13 mmol) as a white solid. ^{1}H-NMR (400 MHz, $CDCl_3$) δ 8.15 (s, 4H, Ar), 4.96 (d, *J* = 2.46 Hz, 4H, HC≡CCH_2), 2.54 (t, *J* = 2.46 Hz, 2H, HC≡CCH_2).

Preparation of LCE Films. Mixture of **M_6**, **M_7**, one of the crosslinker and **Irgacure 651** (4% w/w in respect to the other monomers) were infiltrated in a glass rubbed cell with a 20 µm gap at 140 °C (isotropic phase of the mixtures). The inner surfaces of the cell were spin-coated with a PVA solution (5% in water), dried on vacuum 18 h and rubbed with a velvet cloth. After infiltration the cell was cooled down 5 °C/min to a temperature in which the mixture reaches the homogeneous alignment (85 °C for **E-CL_7(20)** and **E-CL_7(10)**, 45 °C for **E-CL_8(20)** and **E-CL_9(20)**) and then irradiated 10 minutes with a UV lamp (Philips 9W, 350-400 nm). After polymerization cell was open and film removed; dissolving the coating of PVA with water can help to remove the whole film.

Chapter 5

Conclusions

This work shows how to combine the mechanical properties of Liquid Crystalline Elastomers with Direct Laser Writing to create 3D microstructures that:

- possess a determined liquid crystalline alignment;
- are patterned in a desired shape;
- are able to deform under irradiation.

Regarding the chemistry involved in the system, two light activated reactions have been explored in order to create elastomeric networks. Acrylate free radical polymerization has been successfully used for DLW fabrication of LCE microstructures. A small library of acrylate based LCE components has been prepared allowing to screen different mixtures and to identify a suitable material for DLW.
The synthetic strategies were mainly based on esterification reactions, to create and to extend the aromatic rigid cores, and on Williamson reactions to introduce the desired flexible spacers. Different conditions were screened and optimized to obtain various molecules. Such procedures could be easily applied also to the prepare different polymerizable or LC compounds by the simple change of alkyl halide or substituted phenols used in the different steps. Also the synthesis of different azobenzenes were addressed showing different conditions needed with different substitution pattern on the aniline electrophiles. An example of oxidation procedure to prepare azobenzenes was discussed.
All the prepared molecules keep our interest by offering the possibility to prepare new mixtures and then study and optimize the material properties.

The second reaction employed to prepare LC networks is the thiol-yne click chemistry, applied for the first time to the field of LCE. Suitable monomers were prepared and polymerized using different no LC crosslinker. Substitution of the acrylate based backbone leads to new material with less glassy character. Moreover these LCEs, which incorporate mesogens also in the main-chain of the network, are able to undergo larger deformation (until 48%). These promising results gave the way to further studies on click-reactions to prepare new materials for DLW fabrications.
Regarding the 3D printing process, we demonstrated that two-photon DLW is a suitable technique for preparing 1D, 2D, and 3D LCE structures with sub-

micrometer resolution. Suitable compounds were chosen so that conventional DLW setup could be used.
The high power of laser used to achieve the two-photon absorption is compatible with the LC mixture used and the final structures maintain the liquid crystalline properties and the possibility of light activated deformations.
We demonstrated that DLW can be used to integrate microstructures based on different materials on the same surface as well as a free form design of 3D LCE structures.
Moreover, we used DLW to fabricate micro-gratings on the inner surfaces of a glass cell, thus controlling the liquid crystalline orientation with designed desired patterns. Such orientation grating pattern allowed to fabricate micrometer scale LCE structures and, at the same time, locally select different molecular orientation orders. Due to light excitation, these structures deform along different directions, perpendicular to the micro-grating orientations. At the end, LCE nano-structures embedded into the grating network were found to have remarkable resistance to wet lithography development.
A further improvement of the LCE microactuators properties prompted us to prepare different monomer mixtures: starting from a reference one, we tested the change of percentage and structure of the crosslinker, as well as the change of the length of the different flexible spacers on the molecule. These mixtures, used only to prepare macroscopic films, are under evaluation for DLW fabrication. The ultimate goal of obtaining a material able to enhanced movement, or which can be activated by lower power of the excitation wavelength is a major challenge in the project, which will be faced in further studies

We believe that the work reported in this PhD thesis, both concerning the obtained materials and preparation technique, can play an important role in future research and applications in micro/nanorobotics. We have defined a versatile tool to accomplish microrobotic structures that can be optically driven and controlled. Also, application in micro/nanophotonics will be addressed, where the optical induced deformation of microphotonic structures can be used to modify and tune their photonic responses.

Appendix

DSC traces and POM images of compounds

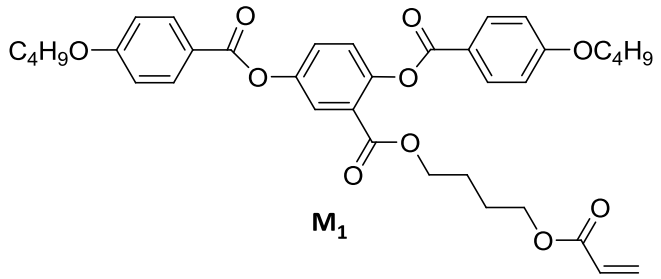

M_1

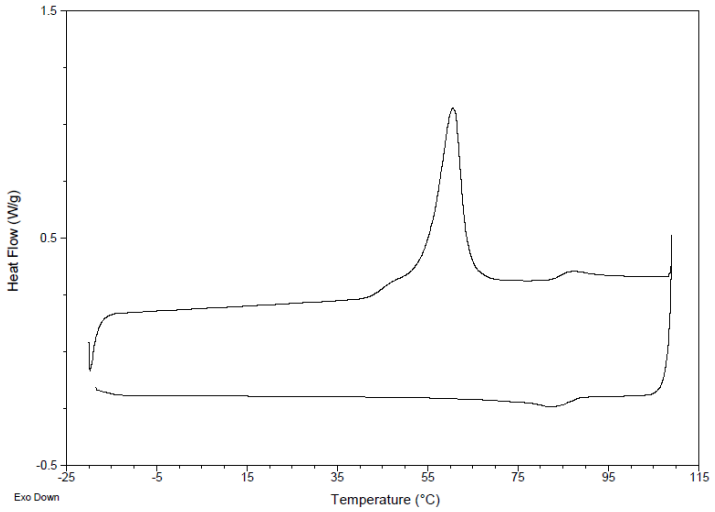

Figure 61 DSC trace corresponding to the first cycle of heating and cooling of M_1.

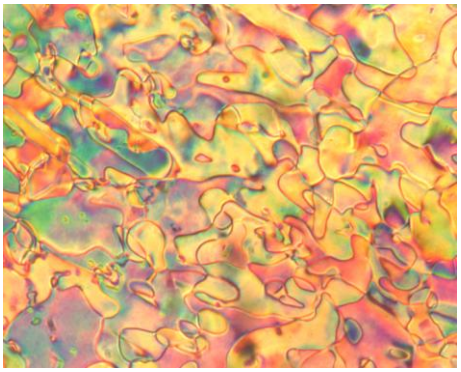

Figure 62 POM image of M_1 at 50 °C on cooling.

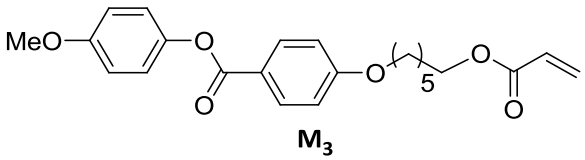

M_3

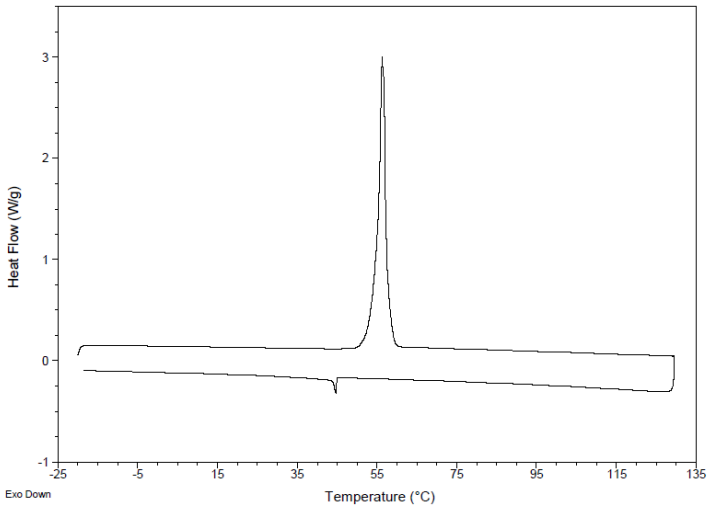

Figure 63 DSC trace corresponding to the first cycle of heating and cooling of M_3.

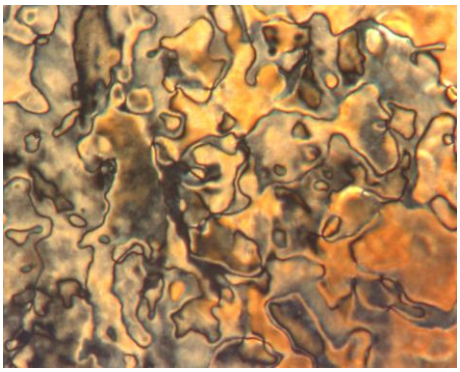

Figure 64 POM image of M_3 at 35 °C on cooling.

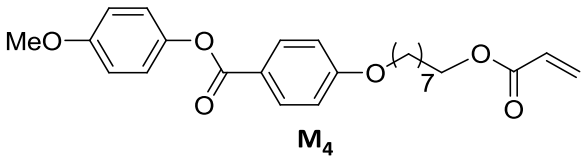

M_4

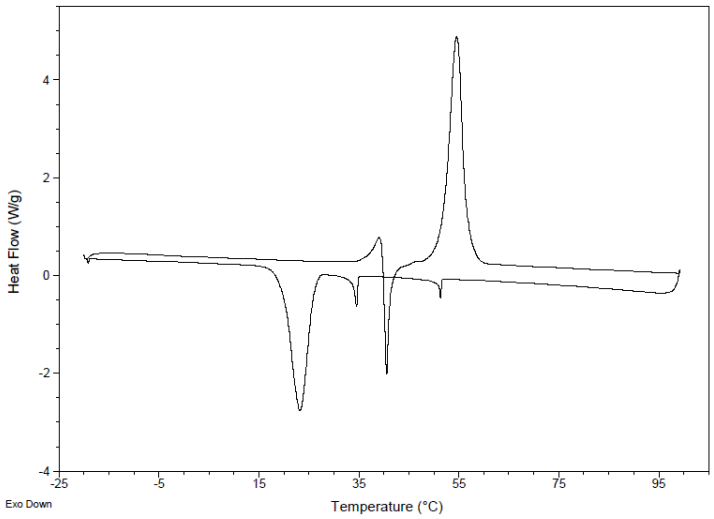

Figure 65 DSC trace corresponding to the second cycle of heating and cooling of M_3.

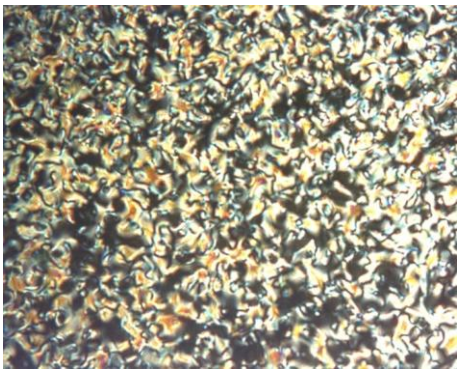

Figure 66 POM image of M_4 at 50 °C on cooling.

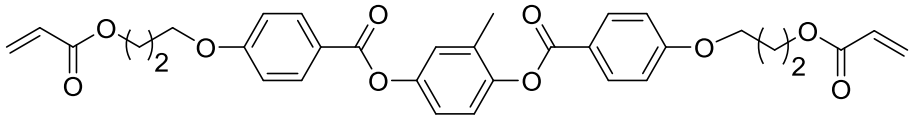

CL_2

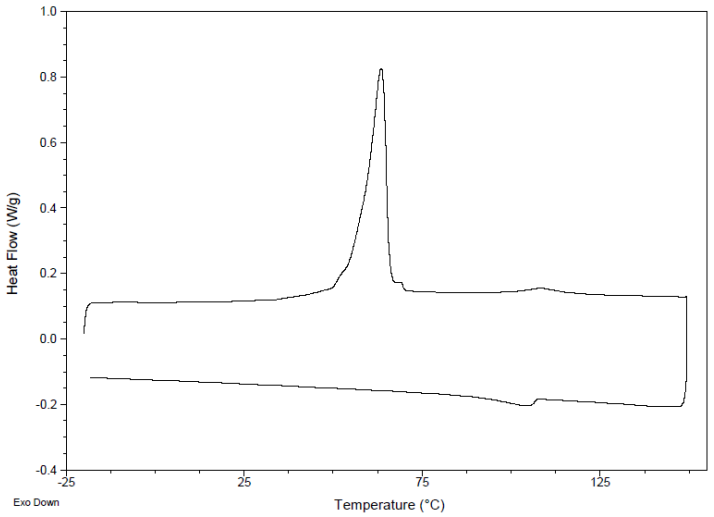

Figure 67 DSC trace corresponding to the first cycle of heating and cooling of CL_2.

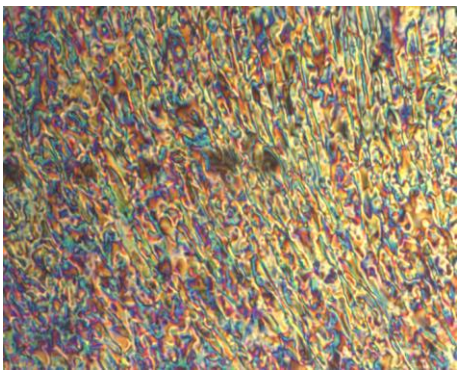

Figure 68 POM image of CL_2 at 100 °C on cooling.

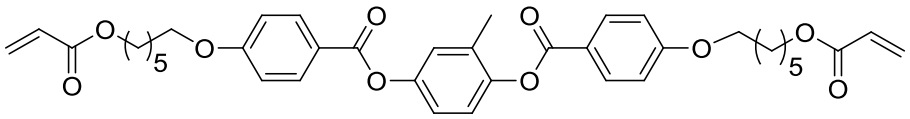

CL_3

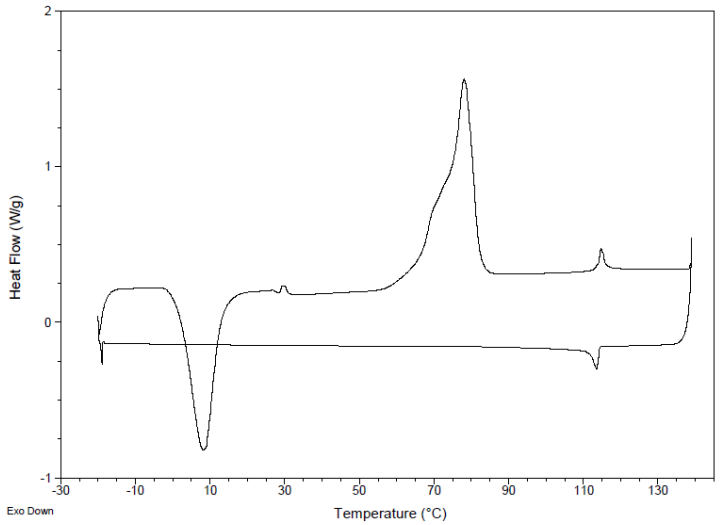

Figure 69 DSC trace corresponding to the second cycle of heating and cooling of CL_3.

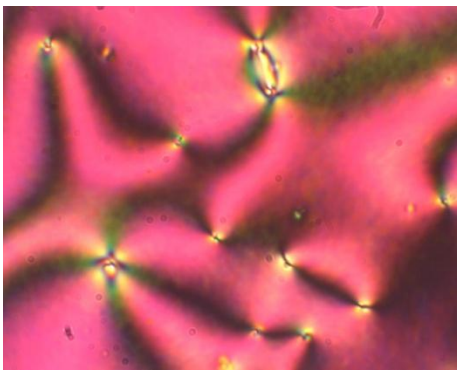

Figure 70 POM image of CL_3 at 90 °C on cooling.

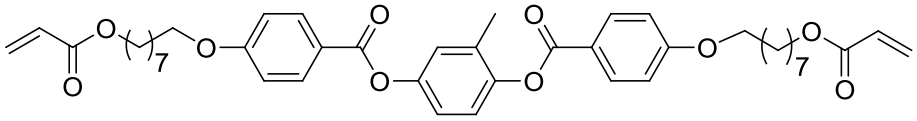

CL_4

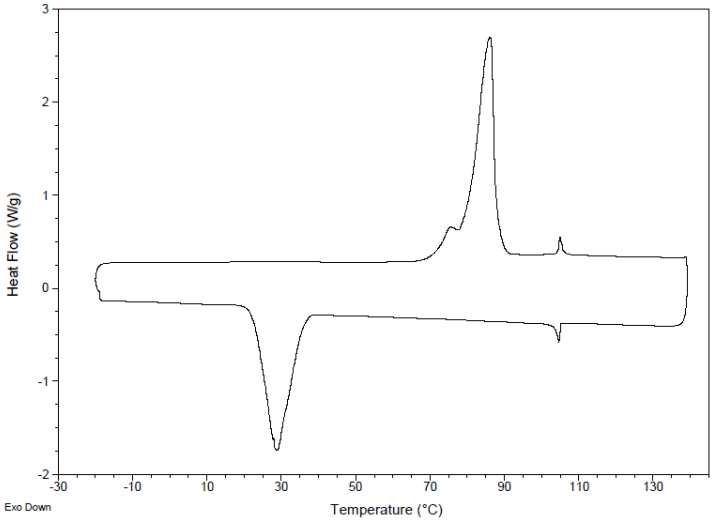

Figure 71 DSC trace corresponding to the second cycle of heating and cooling of CL_4.

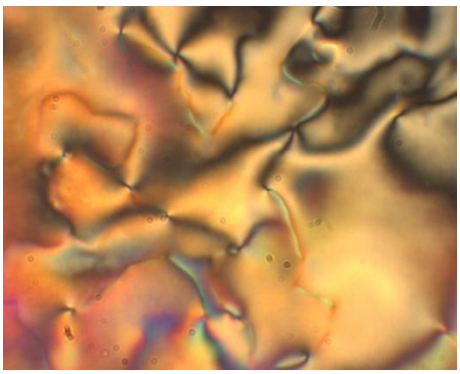

Figure 72 POM image of CL_4 at 100 °C on cooling.

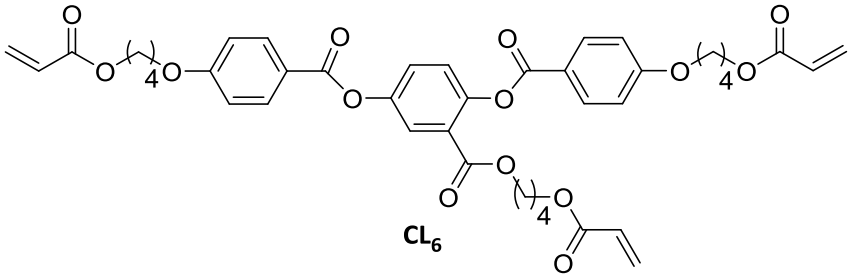

CL_6

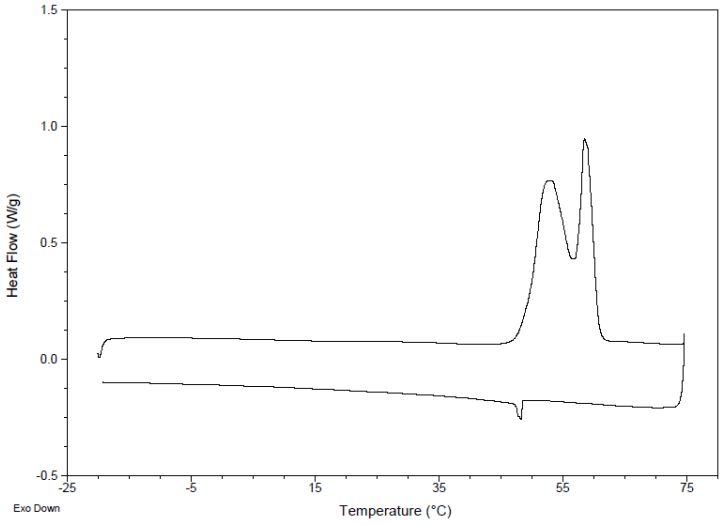

Figure 73 DSC trace corresponding to the second cycle of heating and cooling of CL_6.

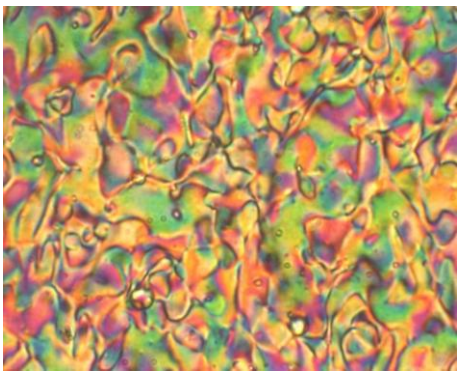

Figure 74 POM image of CL_6 at 35 °C on cooling.

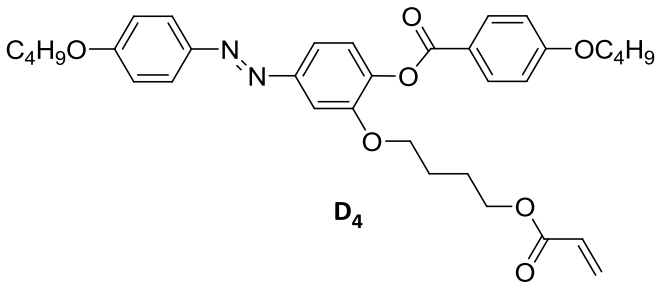

D_4

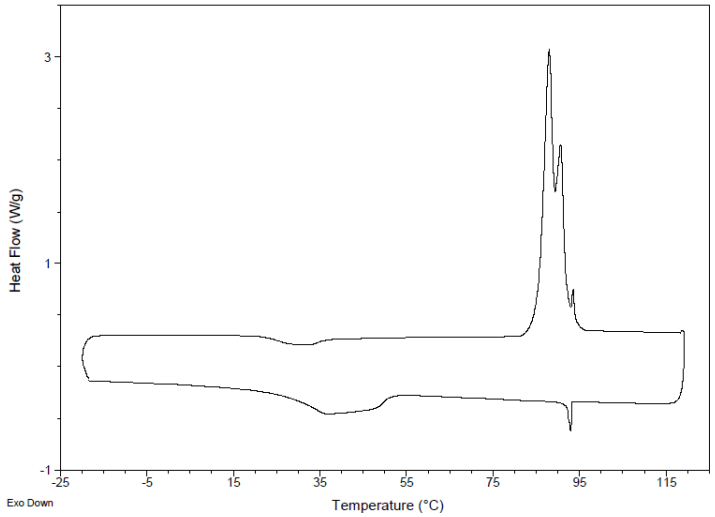

Figure 75 DSC trace corresponding to the second cycle of heating and cooling of D_4.

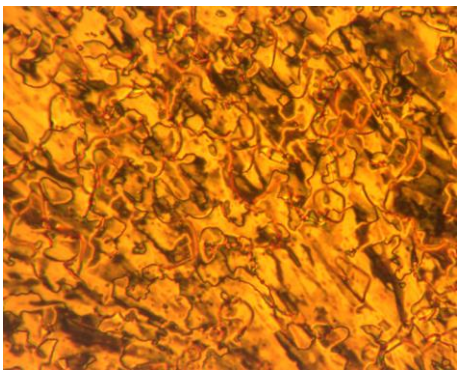

Figure 76 POM image of D_4 at 68 °C on cooling.

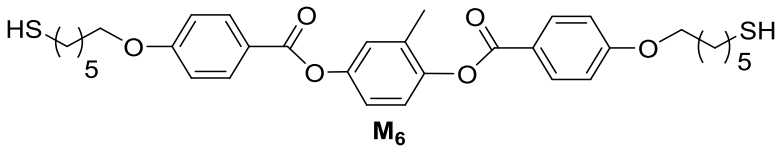

M_6

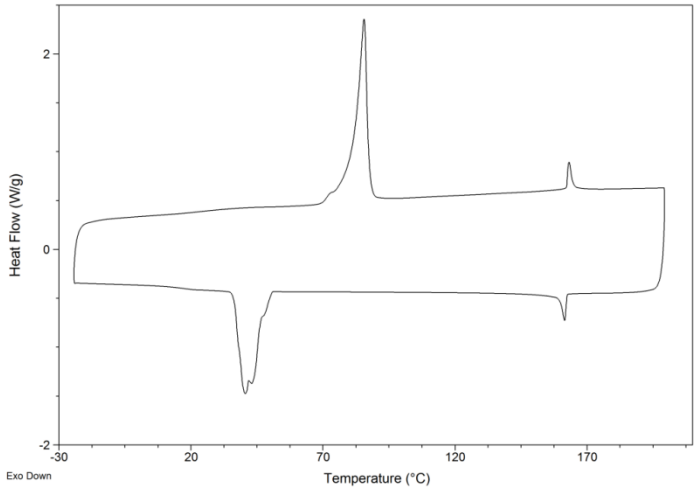

Figure 77 DSC trace corresponding to the second cycle of heating and cooling of M_6.

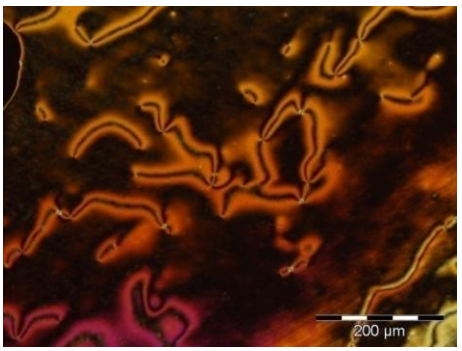

Figure 78 POM image of M_6 at 130 °C on cooling.

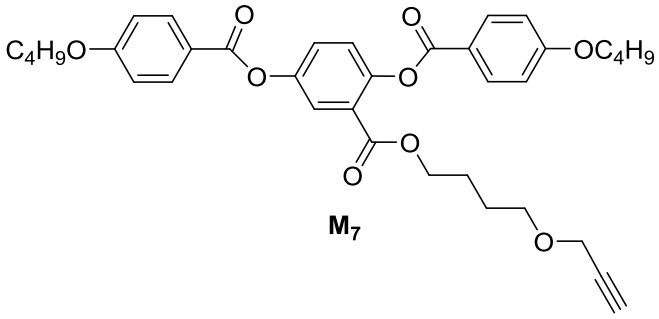

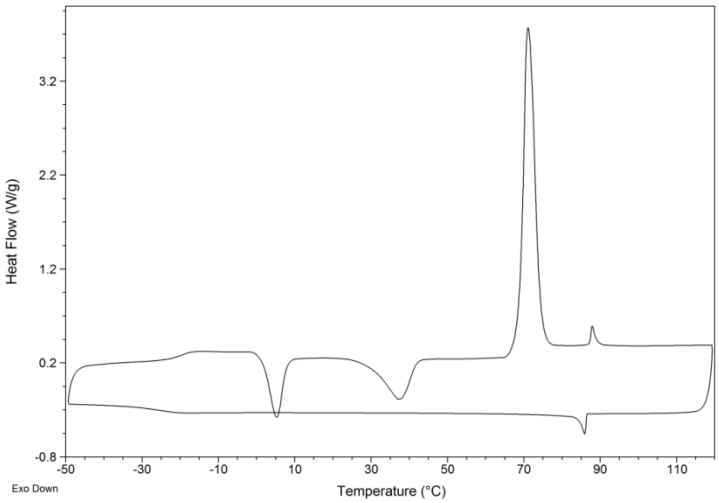

Figure 79 DSC trace corresponding to the second cycle of heating and cooling of M_7.

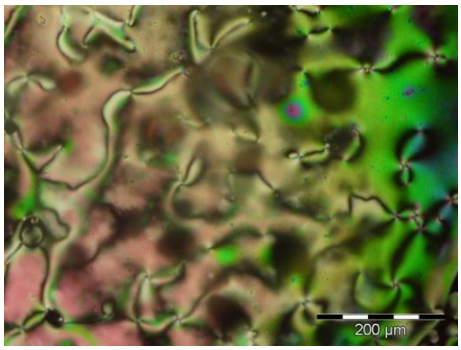

Figure 80 POM image of M_7 at 24 °C on cooling.

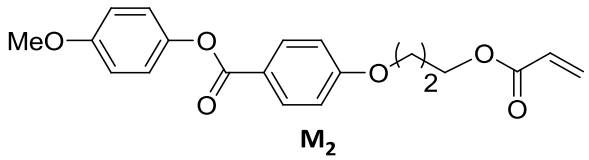

M_2

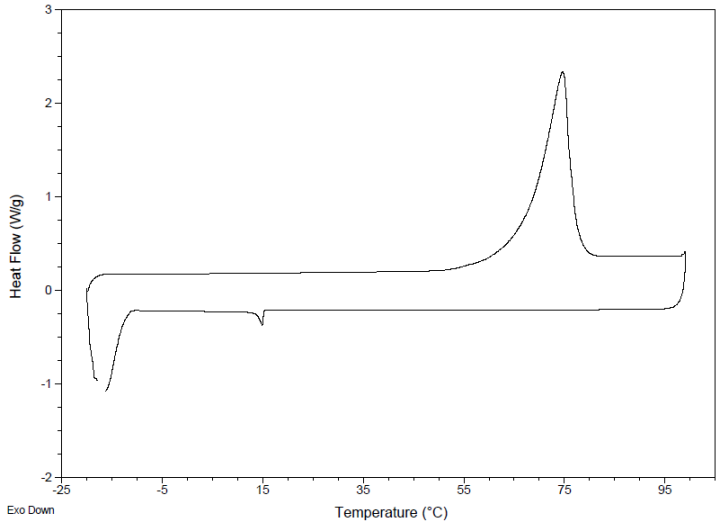

Figure 81 DSC trace corresponding to the second cycle of heating and cooling of M_2.

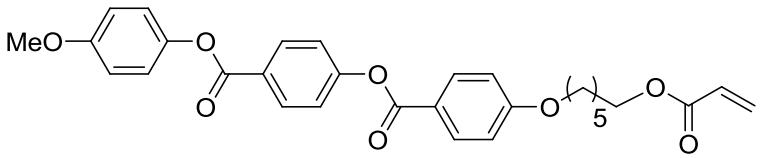

M_5

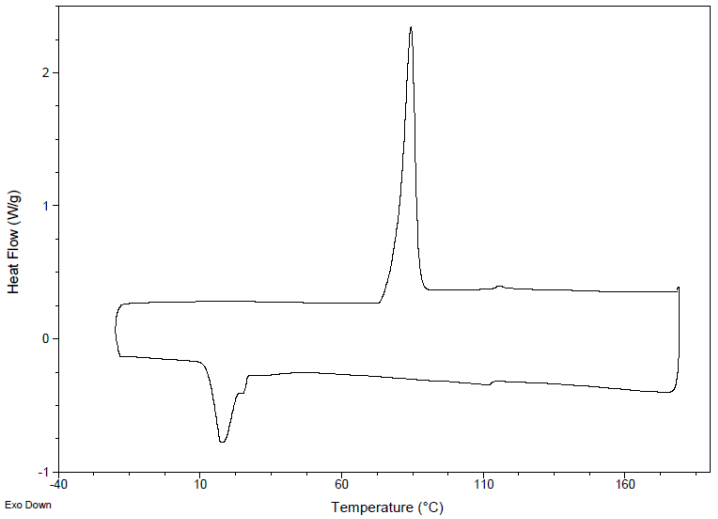

Figure 82 DSC trace corresponding to the second cycle of heating and cooling of M_5.

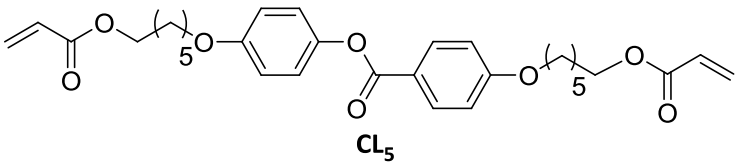

CL_5

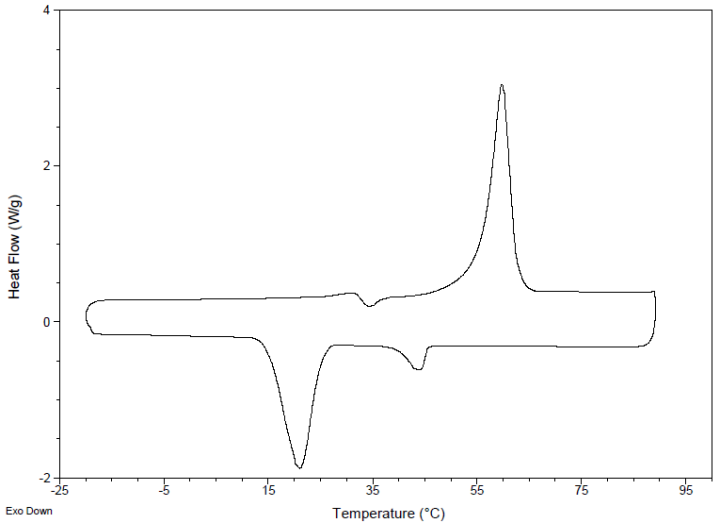

Figure 83 DSC trace corresponding to the second cycle of heating and cooling of CL_5.

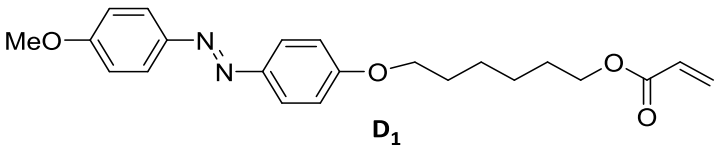

D_1

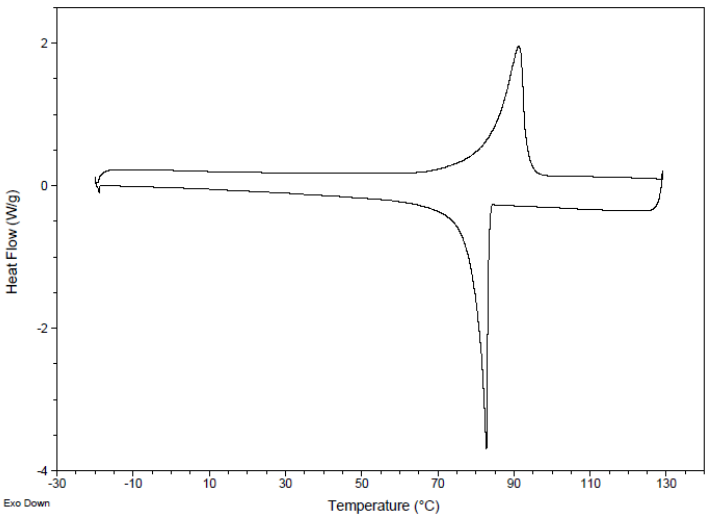

Figure 84 DSC trace corresponding to the second cycle of heating and cooling of D_1.

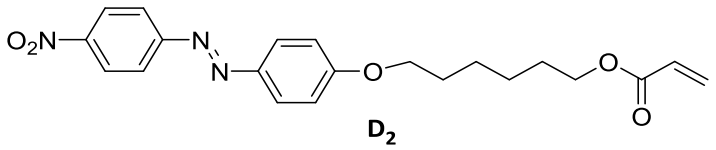

D_2

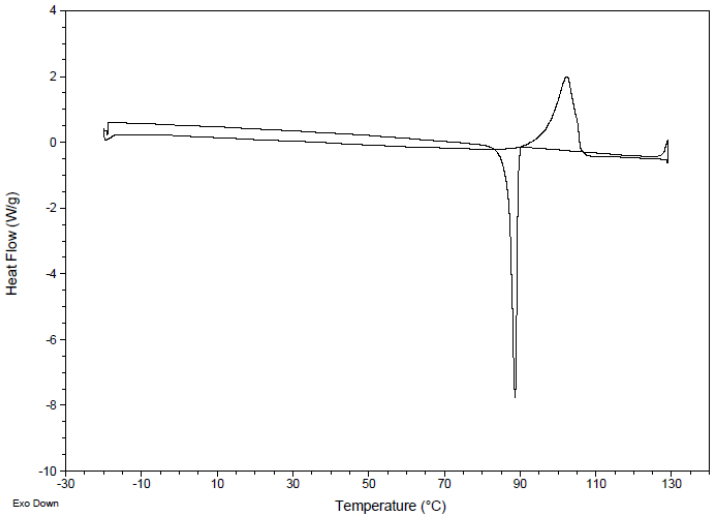

Figure 85 DSC trace corresponding to the second cycle of heating and cooling of D_2.

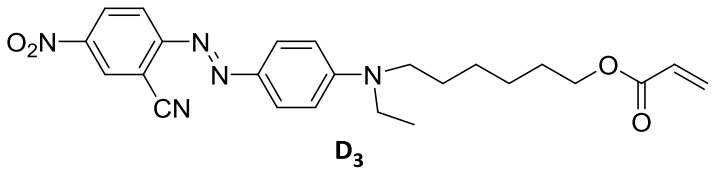

D_3

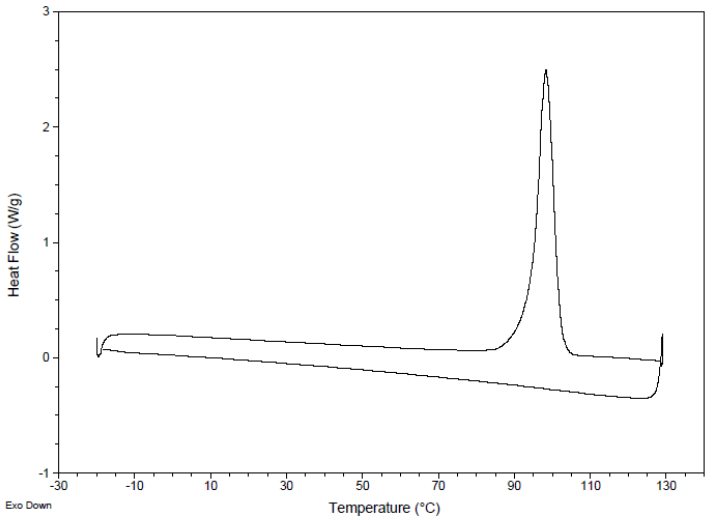

Figure 86 DSC trace corresponding to the first cycle of heating and cooling of D_3.

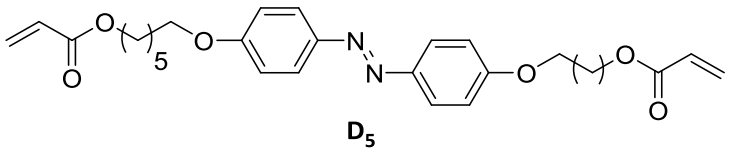

D_5

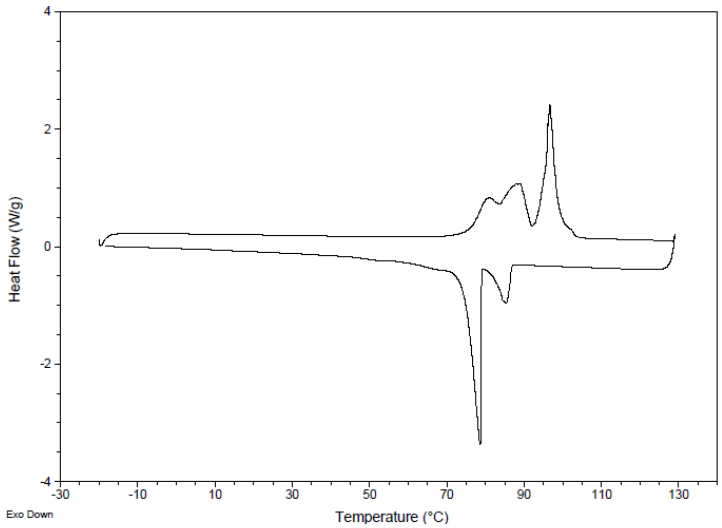

Figure 87 DSC trace corresponding to the second cycle of heating and cooling of D_5.

Thermogravimetric analysis of LCE films based on thiol-yne click chemistry

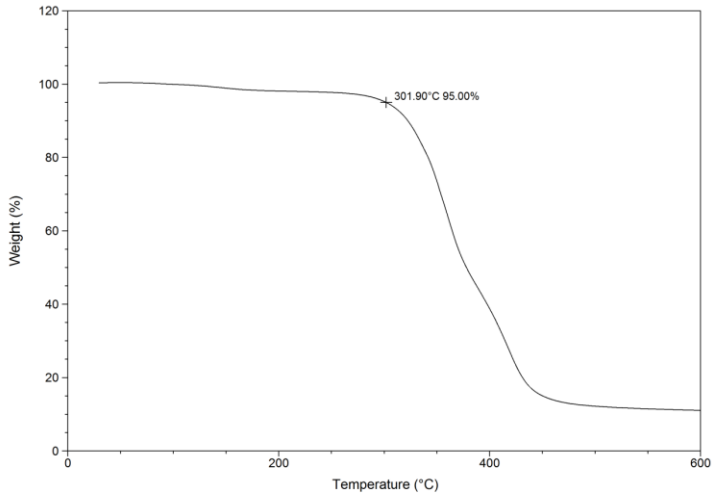

Figure 88 TGA trace of E-CL$_7$20.

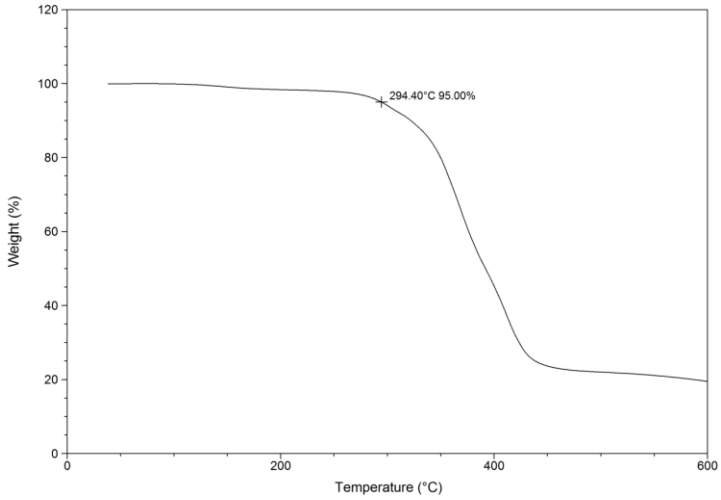

Figure 89 TGA trace of E-CL$_7$10.

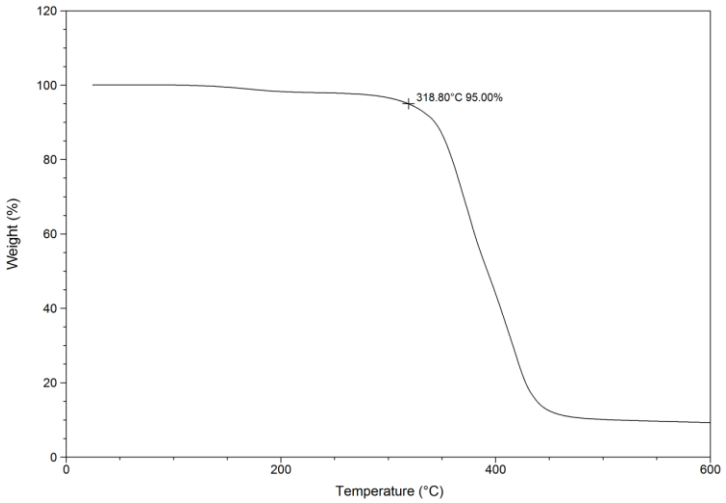

Figure 90 TGA trace of E-$CL_8$20.

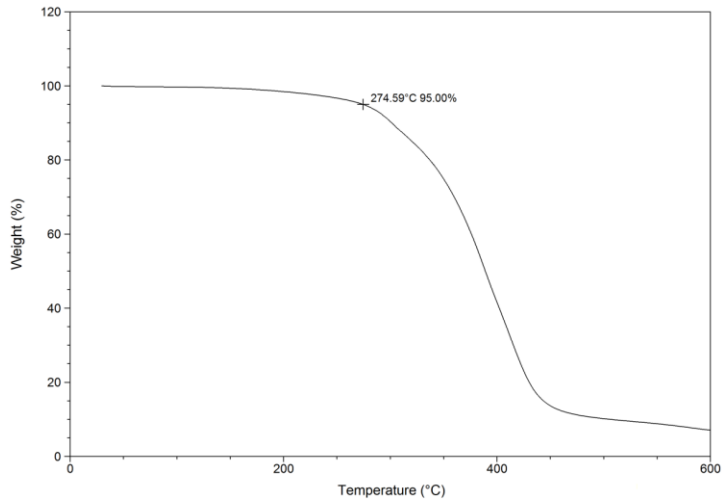

Figure 91 TGA trace of E-$CL_9$20.

Abbreviations

Cr: crystalline phase
DCC: dicyclohexylcarbodiimide
DIAD: diisopropyl azodicarboxylate
DIAD: diisopropylazodicarboxylate
DMAP: 4-*N*,*N*-dimethylaminopyridine
DMEAD: di-2-methoxyethyl azodicarboxylate
DMF: *N*,*N*-dimethylformamide
DSC: differential scanning calorimetry
EDC: 1-ethyl-3(3-dimethylaminopropyl) carbodiimide
FCC: flash column chromatography
I: isotropic phase
LC: liquid crystal
LCE: liquid crystalline elastomers
N*: cholesteric phase
N: nematic phase
NA: numerical aperture
NMP: *N*-methyl-2-pyrrolidone
PI: polyimides
POM: polarized optical microscopy
PVA: polyvinyl alcohol
SEM: scanning electron microscope
Sm: smectic phase
TBAF: tetrabutylammonium fluoride
T_d: decomposition temperature
TEA: triethylamine
T_g: glass transition temperature
TGA: thermogravimetric analysis
TLC: thin layer chromatography
T_{LC-I}: clearing temperature (LC to isotropic phase transition temperature)
T_m: melting temperature
T_{N-I}: nematic to isotropic phase transition temperature